Crystallographic Texture of the Arthropod Cuticle Using Synchrotron Wide Angle X-ray Diffraction

Von der Fakultät für Georessourcen und Materialtechnik
der Rheinisch-Westfälischen Technischen Hochschule Aachen

zur Erlangung des akademischen Grades eines

Doktors der Naturwissenschaften

genehmigte Dissertation

vorgelegt von **Master of Science**

Ali Al-Sawalmih
aus Irjan, Jordanien

Berichter: Professor Dr.-Ing. D. RAABE
Universitätsprofessor Dr. rer. nat. G. GOTTSTEIN

Tag der mündlichen Prüfung: 26 October 2007

For my parents for their support and real love

Acknowledgements

I would like to thank Prof. Dierk Raabe, my supervisor, for his many suggestions and constant support during this research. I am also thankful to Dr. Helge Fabritius and Dr. Patricia Romano for their support through sample preparation and microstructure imaging.

Dr. Sangbong Yi expressed his interest in my work and supplied me with some of his analysis programs, which gave me a better perspective on my own results. Also I am thankful to Dr. Stefan Zaefferer for his kind suggestions and the fruitful discussion which optimized this work.

I had the pleasure of meeting the group members; they are wonderful people and their support makes research like this possible. A scholarship of the *German Research Foundation (DFG)* under the framework of the Gottfried Wilhelm Leibniz Award, which was awarded to me for the period 2004–2006 to cover my life expenses, was crucial to the successful completion of this study.

X-ray measurements were carried out in the BL9-beamline at the DELTA synchrotron facility - Dortmund and in the SCD-beamline at the ANKA synchrotron facility - Karlsruhe. So, extensive thanks are given to Dr. Gernot Buth (SCD-beamline at ANKA), Dr. Christian Sternemann (BL9-beamline at DELTA) for their valuable help and technical support.

Of course, I am grateful to my parents for their encouragement and praying. I am also proud of my wife Carolin Pukallus for her *love* and help. Finally, I wish to thank Nader Zaafarani for the nice and the friendly moments we spent in the same office together for almost three years. Without them this work would never have come into existence (literally).

Düsseldorf, Germany December 4, 2006 Ali Al-Sawalmih

Abstract

Arthropods, which include the crustaceans (e.g. crabs, lobsters, isopods), insects, arachnids (e.g. spiders, scorpions, ticks, mites), and several lesser groups, account for approximately 80 percent of all known animal species. The outer covering of these animals is referred to as exoskeleton or cuticle, and it covers the entire body of the animal. It has a remarkable mechanical properties which provide structural support to the body, armor against loads that are externally imposed by predators. It also enables mobility through the formation of joints and attachment sites for muscles.

Crustacean cuticle contains α-chitin-protein organic fibers associated with crystallites of calcite and considerable amounts of amorphous calcium carbonate (ACC). However, the cuticle of the horseshoe crab *Limulus polyphemus* contains mainly α-chitin-protein fibers, but no crystalline biominerals. In this study, X-ray pole figure analysis was performed to investigate the preferred orientation (crystallographic texture) of calcite and α-chitin, in the crustaceans, edible crab *Cancer pagurus* and american lobster *Homarus americanus* cuticles, with respect to their orientation relationship firstly, and their alignment with respect to the cuticle geometry secondly. The preferred orientation of α-chitin in the cuticle of horseshoe crab was also determined. Synchrotron wide-angle X-ray diffraction (XRD) was employed in studying the texture of samples from different parts of the exoskeleton. The importance of the crystallographic textures in biological materials lies in its direct relationship with its possible role of the contained macromolecules in controlling the epitaxy of the minerals during the biomineralization process. Furthermore, it reveals informations about the topological texture, which is represented by the fibers' arrangements in the cuticle.

This study shows that crab and lobster cuticles reveal a strong crystallographic texture and preferred orientation correlation between

the orientation distribution of calcite and α-chitin. It was observed that the c-axis of the hexagonal calcite and the b-axis of the orthorhombic α-chitin are firstly preferentially aligned parallel to each other and secondly oriented along the surface normal, whereas the other axes are co-aligned with respect to each other throughout the cuticle plane. The observed spatial rotational freedom of the c-axis of α-chitin (fiber axis) represents the twisted plywood structure of the α-chitin fibers as observed in scanning electron microscopy (SEM). Additionally, a smaller fraction of the α-chitin unit cells in lobster and crab cuticle is oriented with their fiber axis toward the cuticle surface, which was also observed in the SEM images of the cuticle.

The texture of the horseshoe crab contains two strong fiber texture components perpendicular to each other. The first one is characterized by a very strong crystallographic orientation of b-axis parallel to the surface normal, whereas the other axes are co-aligned through the cuticle surface plan, which is similar to the observed strong fiber texture component in crustacean cuticle. The second fiber texture component is characterized by a strong crystallographic orientation of c-axis (α-chitin fiber direction) with a preferred alignment pointing parallel to the cuticle plane.

The synchrotron X-ray crystallographic texture results gave for the first time a statistical description of the orientation relationship between the organic and inorganic components in arthropod cuticle, consistent with the morphological texture determined by SEM. This result strongly suggests that the fibrous structure of α-chitin assists the growth of calcite crystals in crustacean cuticle by functioning directly or indirectly as a template for nucleation and subsequent growth of calcite on the basis of oriented nucleation and epitaxial growth of calcite.

Zusammenfassung

Die Kutikula der Krebstiere [Crustaceae] enthält organische α-Chitin-Protein Fasern in Verbindung mit Kalzitkristallen und einem beträchtlichen Anteil an amorphem Kalziumcarbonat (ACC). Die Kutikula des Pfeilschwanzkrebses Limulus polyphemus hingegen enthält überwiegend α-Chitin-Protein Fasern, jedoch keine kristallinen Biomineralien.

In der vorliegenden Studie wurden die Orientierungen (Kristallographische Textur) des Kalzits und der α-Chitin Fasern mittels Röntgen-Weitwinkelpolfiguranalyse untersucht, sowohl ihr Verhältnis zueinander als auch zur Geometrie der Kutikula. Untersucht wurde die Kutikula der Krebstiere Cancer pagurus (eine essbare Krabbe) und des amerikanischen Hummers Homarus americanus. An der Kutikula des Pfeilschwanzkrebses wurde die Orientierung der α-Chitin Fasern untersucht. Mittels Synchrotron Röntgen-Weitwinkelexperimenten konnte gezielt die Textur an verschiedenen Stellen des Exoskelettes untersucht werden. Die mögliche Funktion der organischen Makromoleküle bei einer Kontrolle der Epitaxie der Minerale bei der Biomineralisation und ihr Verhältnis zur topologischen Textur bedingen das spezielle Interesse an der kristallographischen Textur biologischer Materialien.

Die vorliegende Studie zeigt die ausgeprägte kristallographische Textur der Krabben- und Hummerkutikeln und die deutliche Korrelation der Vorzugsorientierungen der Kalzitkristalle und der α-Chitin Fasern. Es wurde gezeigt, dass die kristallographische c-Achse des hexagonalen Kalzits und die b-Achse des orthorhombischen α-Chitins vorzugsweise parallel zu einander und normal zur Oberfläche der Kutikula orientiert sind, wobei die anderen Achsen parallel zur Oberfläche angeordnet sind. Die beobachtete Orientierungsverteilung der c-Achse (Faserachse) der α-Chitin Fasern entspricht einer “twisted plywood structure” die auch auf SEM Aufnahmen beobachtet werden

konnte. Weiters ist ein kleinerer Teil des α-Chitin mit der Faserachse zur Oberfläche hin orientiert, was ebenfalls durch SEM Aufnahmen beobachtet werden konnte.

Die Textur der Pfeilschwanzkrebskutikula enthält zwei starke Fasertexturkomponenten die normal zu einander orientiert sind. Die Erste ist durch eine starke Orientierung der kristallographischen b-Achse parallel zur Oberflächennormale gekennzeichnet, wobei die anderen Achsen parallel zur Oberfläche angeordnet sind, vergleichbar der starken Fasertexturkomponente bei den untersuchten Krebstieren. Die zweite Texturkomponente ist durch eine starke Orientierung der c-Achse (Faserachse) der α-Chitin Fasern mit bevorzugter Anordnung parallel zur Oberfläche gekennzeichnet.

Die Ergebnisse der Synchrotronexperimente ermöglichten erstmals eine statistische Beschreibung der Orientierungsverhältnisse der organischen und anorganischen Komponenten von Artropodenkutikeln und den Vergleich mit der morphologischen Textur, die mittels SEM-Aufnahmen bestimmt wurde. Die Resultate deuten darauf hin, dass die Faserstruktur des α-Chitins direkt oder indirekt als Template für die orientierte Nukleation und das epitaktische Wachstum der Kalzitkristalle fungieren.

Contents

Chapter 1

Introduction

Lobsters and crabs are large arthropods (joint-limb animals), which belong to the class of crustacea and the order of decapoda (Vernberg and Vernberg, 1983; Horst and Freeman, 1993). Their body is divided into three main parts: the head (cephalon), the thorax bearing the walking legs, and the tail (abdomen) which ends with the telson. The physical characteristics of decapod crustaceans may vary widely between the different species of this group. On the other hand, horseshoe crab is an arthropods but it belongs to the class of chelicerata. The outer covering of these animals is referred to as exoskeleton or cuticle, and it covers the entire body of the animal and provides mechanical support to the body, armor against loads that are externally imposed by predators, and enables mobility through the formation of joints and attachment sites for muscles. A functional role also lies in protecting the inner organs from swelling which is essential since the marine crustaceans are slightly hyperosmotic to seawater (Vernberg and Vernberg, 1983; Horst and Freeman, 1993).

The cuticle is secreted by a single-layered epithelium, and consists – like that of most related crustaceans and the arthropods in general– of several layers with specific structural and functional properties. In order to grow, the animals have to replace their old exoskeleton periodically by a new, larger one in a process called molt. Before the old cuticle is shed a new, thin and yet unmineralized cuticle is secreted by the epidermal cells. After the molt the animals grow very quickly and the new soft cuticle is completed and mineralized in order to regain its protective function as fast as possible.

Arthropod cuticle is a nanocomposite material composed mainly of α-chitin-protein fibers, structured hierarchically from the nano- to the millimeter level. Crustaceans, like lobster and crab, add calcite to their cuticle, and considerable amounts of amorphous calcium carbonate (ACC) may exist as calcium storage or for mechanical isotropy enhancement. α-Chitin-protein fibers contain bundles of nanofibrils which are basically 10-20 anti-parallel chains of chitin (α-chitin) covered by a sheath of proteins.

Chitin is a crystalline biopolymer. It is an insoluble linear polymer of β-1,4-linked N-acetylglucosamine residues. Chitin occurs in three different polymorphic forms that differ in the polarity of the molecular chains in the crystal cell. In α-chitin, which is the most abundant crystalline variant, the chains are arranged in an anti-parallel fashion. In β-chitin the chains are parallel. It is a crystalline hydrate and water can penetrate between the chains of the β-chitin lattice. γ-Chitin is a mixture of α- and β-chitin with two parallel chains in one direction and the third one in the opposite direction. The three forms can be found in parts of the same organism. Calcite is a crystalline mineral, and the most stable polymorph of calcium carbonate. It exists as biomineral content in the shells of many organisms as well as sedimentary rocks.

Quantitative microstructure and crystallographic texture studies of the exoskeleton of crustaceans are important because of the strong relationship which exists between the crystallographic and morphological directionality of the microscopic ingredients of biological tissues. It also reveals the possible role of the contained macromolecules in controlling the epitaxy of the minerals during the biomineralization process. Furthermore, basic crystallographic and orientational issues associated with the nucleation, epitaxial growth, and phase transformation of the minerals in chitin-protein tissue can be tackled on a quantitative basis by the use of modern crystallographic texture analysis.

Part I

Basic Concepts

Chapter 2

Chitin

2.1 Chitin Biopolymers

Biological skeletal systems in general exist to support the body of the organism. Most of these systems are built up mainly from one of the three principal organic fibrous materials: cellulose, chitin, or collagen. All these organic materials are biopolymers and associated with proteins composing fibers. Cellulose, for example, is predominate in plant kingdom (with a notable exception being fungi in which it is replaced by chitin), while chitin and collagen, are the main successful candidates for the support of the "body" in multicellular organisms.

Chitin is usually organized as a cuticle at one surface of an epithelium, like in arthropods and other invertebrates, since they produce chitin in limited amounts (Rudall and Kenchington, 1973). Collagen, together with apatites crystallites, exists widely as permeation connective tissues (e.g bone) forming an internal framework and supporting complex organs like human and other vertebrates.

Chitin is a linear polysaccharide biopolymer, having a similar chemical structure to cellulose and occurring widely in nature; in crustacean, insects, mushrooms, mollusks, and in the cell walls of bacteria. It can be regarded as analogue of cellulose, with an aminoacetyl group ($NHCOCH_3$) instead of the hydroxyl group (OH) as indicated in dash-lined boxes in Fig. 2.1. It is chemically expressed by *(1→4)-linked 2-acetamido-2-deoxy-beta-D-glucan* and composed of *N-acetyl-glucosamine* repeat unit through *β-1, 4 glucosidic* linkages, Fig. 2.2.

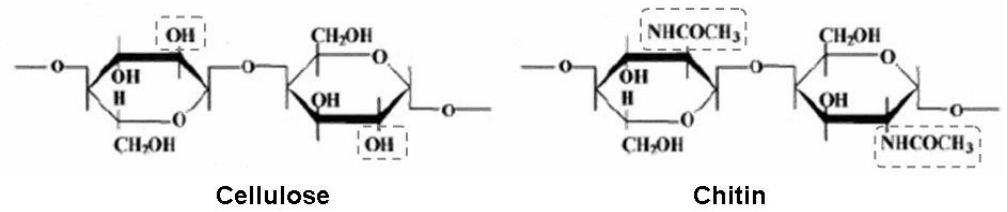

Fig. 2.1: Chitin can be regarded as analogue of cellulose with an amino-acetyl group ($NHCOCH_3$) instead of the C_2 hydroxyl group (OH) which is indicated by the dash-lined boxes. Adapted from Ref. (Jang et al., 2004).

The chemical properties of chitin are completely different from those of cellulose in spite of their similar structures, which is due to the strong hydrogen bonding between the aminoacetyl and hydroxyl groups. Thus chitin is not so far regarded as a useful resource compared to other polysaccharides such as cellulose and starch. Structurally, chitin is a derivative of cellulose in which the hydroxyl group at C_2 is replaced by an acetamido group , and it is stabilized by $C_3OH\cdots C_5$ intramolecular and $NH\cdots OCC$ and $C_6O\cdots OC$ intermolecular hydrogen bonds, giving it th same structural stability as cellulose (Minke and Blackwell, 1978).

Recently, chitin and its derivatives have been reported to have some useful medical applications (Mattheus, 1997). It is produced commercially from crab and shrimp shells by treatment with dilute NAOH solution for deproteinization, followed by treatment with dilute HCl solution for demineralization. Chitosan is a derivative of chitin, which is produced by treatment of chitin with concentrated NaOH at elevated temperature (Mattheus, 1997).

In addition of being naturally abundant in the sea shells and biologically reproducible on the earth, chitin possesses a remarkable characteristics: it is biodegradable, non antigenic in animal tissues and organs, nontoxic in oral and implant administration. Chitin is able to be processed with several casting products including flakes, fine powders, beads, membranes, sponges, cotton, fibers, and gels (Mattheus, 1997).

The name chitin was proposed by Odier in 1823 for a substance which were isolated from the *elytra* of May beetles (Odier, 1823),

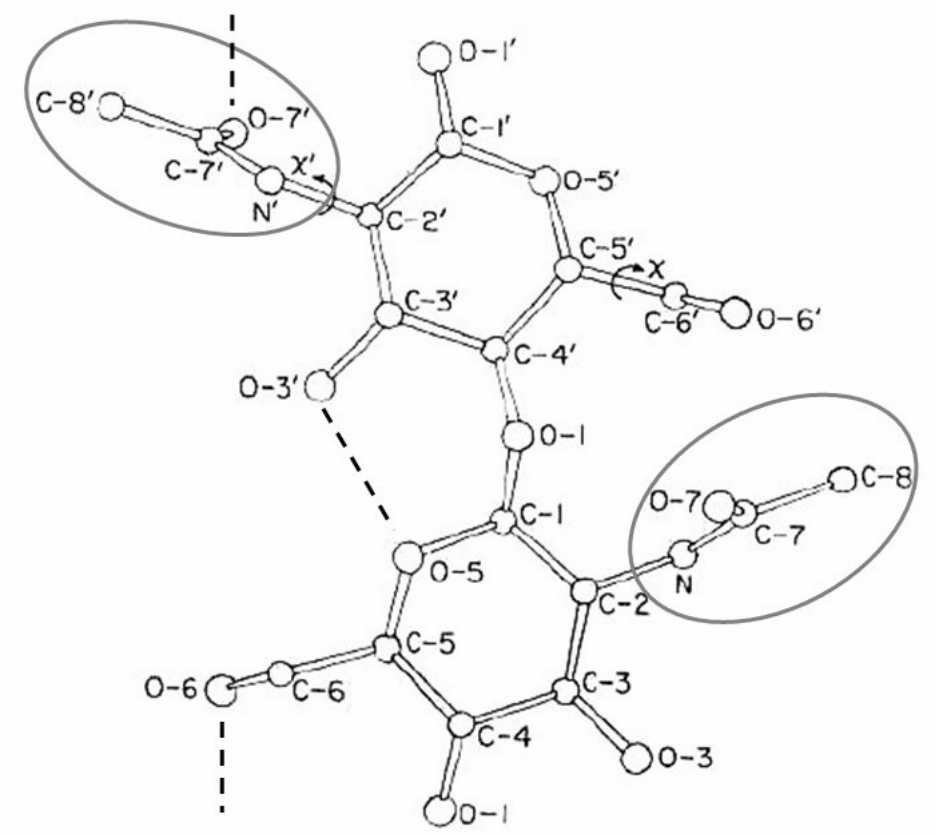

Fig. 2.2: Molecular model for chitin monomer, showing the numbering of the atoms and intramolecular hydrogen bonds (dashed lines) which stabilize its structure. The amino-acetyl group is indicated. Adapted from Ref. (Minke and Blackwell, 1978).

after being discovered in 1811, when Braconnot (Braconnot, 1811) obtained an alkali-resistant fraction from higher fungi.

Chitin is crystalline, and exists in nature as fibers associated with proteins in the organism exoskeleton. It occurs in three different polymorphic forms, namely, α-chitin, β-chitin, and γ-chitin, depending upon the chain polarity in its crystalline structure, Fig. 2.3. α-Chitin is the most abundant and stable polymorphic form, on the other hand, β-chitin is rare in nature and is a metastable form, transforming into α-form during the dissolving process (Saito et al., 2000).

The chains in α-chitin have antiparallel arrangement (Minke and Blackwell, 1978), while the β-form has parallel chains (Akhtar and Haleem, 1990), Fig. 2.3. It occurs in the shells of crustaceans (crabs, shrimp, lobsters, etc.), in the shells and skeletons of mollusks and insects, etc. and in the cell walls of fungi (mushrooms, yeast, etc.) (Gardner and Blackwell, 1975). β-Chitin occurs in squid pens, in the extracellular spines of the euryhaline diatom (Herth and Barthlott, 1979), and in pogonophore tubes (Blackwell, 1969) and many others.

The γ-Form has a mixture of antiparallel and parallel chains, occurs in the cocoons of insects (Rudall and Kenchington, 1973). It is very rare in nature and its structure is still not fully understood (Jolles and Muzzarelli., 1999).

2.2 α-Chitin

α-Chitin exists in the exoskeleton and connective membranes of arthropods as fibers which is composed of nanofibrils (few chains of chitin surrounded helically by proteins subunits). These fibers are distributed in many directions through the surface (see chapter 4).

Arthropods exoskeletons, in general, are largely composed of α-chitin-protein complexes, whereas crustacean shells usually contain additionally calcium carbonate. The occur

2.2.1 Structure of α-Chitin

α-chitin is the most common form, and its structure has been the subject of several crystallographic investigations, dating back to the

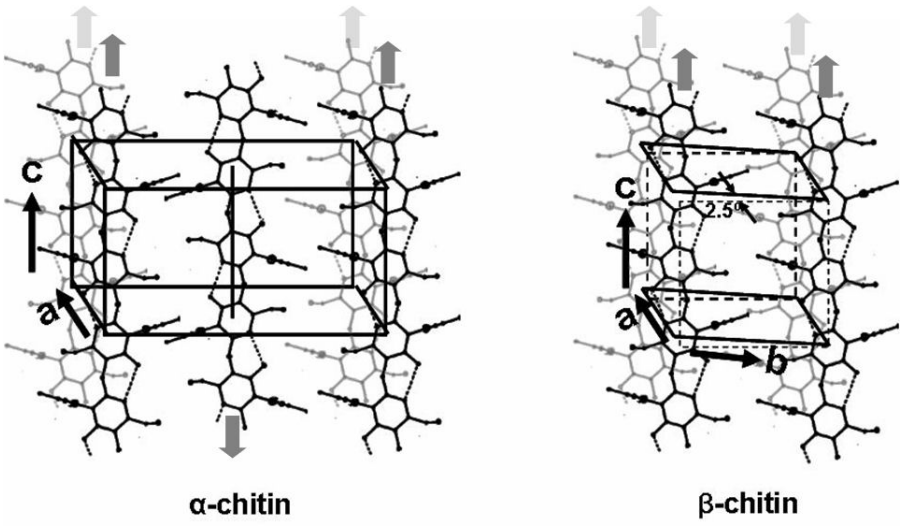

Fig. 2.3: α-chitin antiparallel chains (left) and β-chitin parallel chains (right).

1920s. Carlström was the first who identified the unit cell dimension and the probable space group of α-chitin in 1957 (Carlström, 1957), which was based on structure refinement using optical diffraction analogs. The proposed structure had an orthorhombic unit cell with dimensions a = 4.76 Å, b = 18.85 Å, and c = 10.28 Å (chain axis), and space group $P2_12_12_1$, Fig. 2.4.

An X-ray diffraction analysis of α-chitin from deproteinized lobster tendon by Minke and Blackwell in 1978 (Minke and Blackwell, 1978) gave the unit cell dimensions a= 4.74 ±0.001 Å, b= 18.86 ±0.002 Å and c= 10.32 ±0.002 Å (chain axis). These results were in accordance with the unit cell data determined later using electron diffraction analysis of α-chitin, which gave the unit cell dimensions a = 4.74 Å, b =10.32 Å, and c =18.86 Å (Paralikar and Balasubramanya, 1984). The latter was adopted by the *Crystallographica Database* under the PDF-file number 35-1974. Among these unit-cell determinations, the most recent one has been given by Chanzy in 1996 using a microbeam diffraction experiments on highly crystalline chitin specimens from Sagitta gazellae (a gigantic Antarctic arrow worm) (Saito et al., 1998). Measurements gave for the orthorhombic unit cell of chitin the parameters a= 4.75 Å, b= 18.91 Å, c= 10.41 Å.

Calculations by Marchessault & Sarko in 1967 (Marchessault and

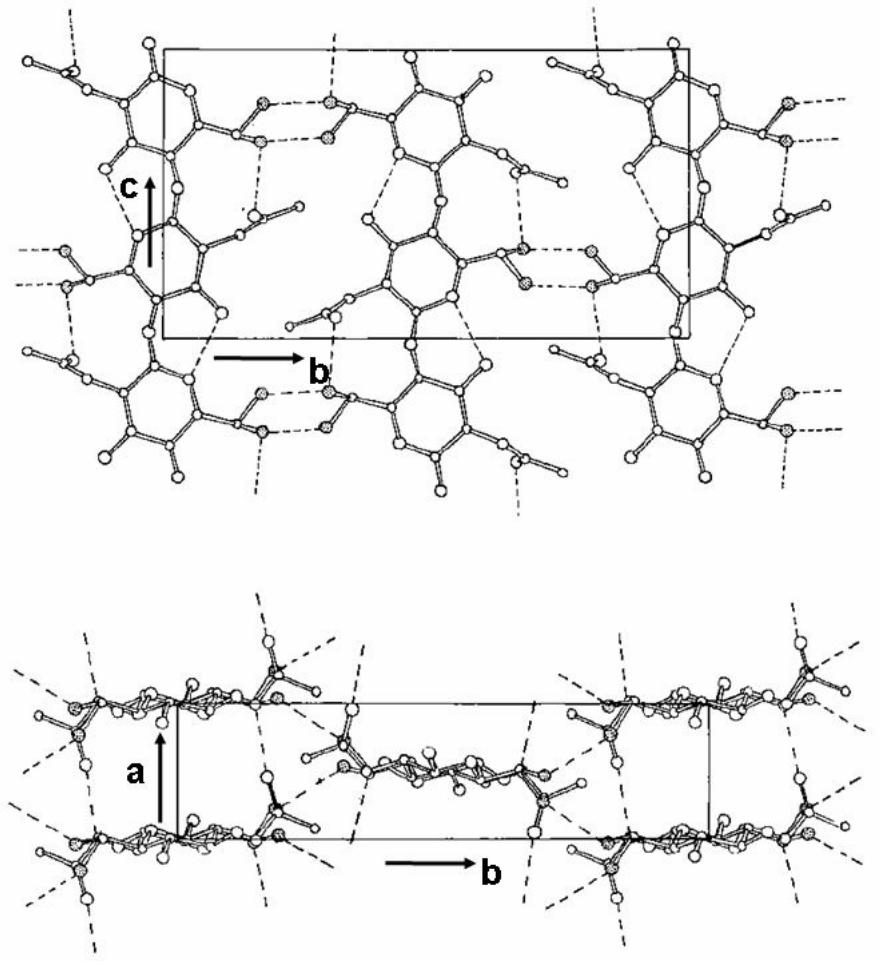

Fig. 2.4: Proposed structure of α-chitin from two different projections. Adapted from Ref. (Minke and Blackwell, 1978).

Sarko, 1967) showed that the Carlström structure gave reasonable agreement with their calculated X-ray intensities. The structure proposed by Carlström extended and refined later by Abdul-Haleem (Haleem and Parker, 1976). Nevertheless, the structure is generally considered to be the true structure, although it was subject to a number of criticisms (Minke and Blackwell, 1978).

These studies point toward a two chain unit cell and a $P2_12_12_1$ space group that implies an anti-parallel packing of the chains in the α-chitin crystals. The X-ray fiber diagram of lobster tendon chitin and the electron diffraction of crab chitin microfibrils show clearly the presence of meridional odd reflections (Minke and Blackwell, 1978; Paralikar and Balasubramanya, 1984) that are not consistent with $P2_12_12_1$.

Fig. 2.5 shows the X-ray diffraction patterns of alpha chitin isolated from six references and from different arthropods in the range of 5-30°. It is a typical powder pattern of alpha-chitin crystal structure determined by Blackwell *et al.* (Minke and Blackwell, 1978), where (020) and (110) are the predominate reflections. The X-ray diffractograms exhibit differences in intensity and distances of different planes, which implies a slight difference in the structure of the α-chitin in different organisms (Cardenas et al., 2004). Since α-chitin is organic biopolymer and has a large unit cell, it diffracts poorly and only at relatively low 2θ angles.

2.2.2 Crystallinity of α-Chitin

α-Chitin, as other crystalline polymers, is not a fully crystalline biopolymer. Zhang *et al.* (Zhang et al., 2000) and Cardenas *et al.* (Cardenas et al., 2004) determined the crystallinity of α-chitin for different organisms. The former has calculated the degree of crystallinity of chitin prepared from beetles, silkworms, and shrimp after pretreatment with 2N HCl at 100 °C, whereas Cardenas *et al.* determined the crystallinity for chitin from shrimp, lobster, crab and king crab, based on the X-ray diffraction. In their studies, samples from different sources are showing almost the same diffraction feature, i.e. the extremely similar 2θ can be assigned to the reported corresponding diffraction planes (020), (110), and (101) of the α-chitin orthorhombic crystal structure (Fig. 2.5).

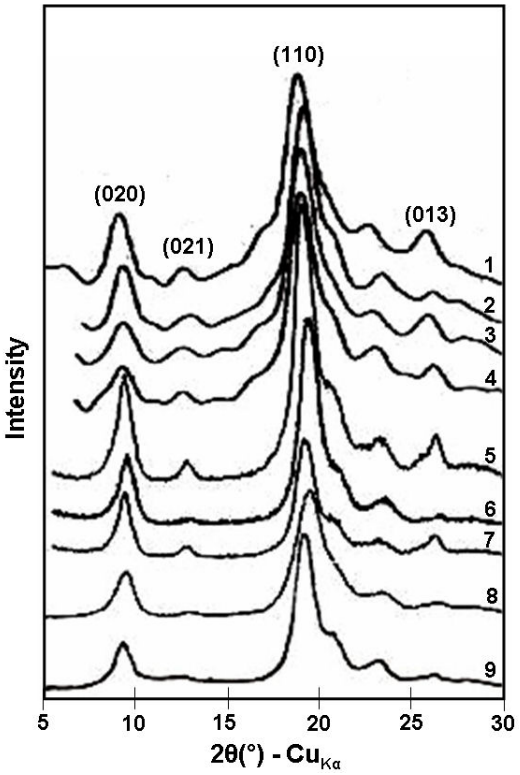

Fig. 2.5: X-ray diffraction patterns of alpha chitin isolated from six references and from different arthropods. 1) shrimp, 2) prawn, 3) lobster, 4) king crab (Cardenas et al., 2004), 5) beetle larva cuticles, 6) silkworm pupa exuvia, 7) shrimp (Zhang et al., 2000), 8) shrimp (Andrade et al., 2002), 9) crab (Takai et al., 1992).

The degree of crystallinity of the semi-crystalline samples is estimated using the Hermans–Weidinger equation: $X_c\% = \{K \cdot I_c/(I_c + I_a)\} \times 100\%$, where X_c, I_c, and I_a represent the degree of crystallinity, diffraction intensity in the crystalline region, and diffraction intensity in the amorphous region, respectively. K is a modulus having a value ranging from 1.1–0.8.

Fig. 2.6 shows the results of the crystallinities calculated for α-chitin from different shells, keeping in mind that the crystallinity of β-chitin is less than that of α-chitin because of its parallel structure of the chains.

Chitin isolated from	Crystallinitiy (%)	
Silkworm pupa exuviae	54	
Beetle larva cuticles	58	(a)
Shrimp shells	56	
Shrimp chitin	76.2	
Lobster chitin	82.7	(b)
Crab chitin	81.9	
King crab chitin	80.6	

Fig. 2.6: The results of the crystallinities calculated for chitin extracted from arthropods shells after treatment with 2 N HCl at room temperature. (a) from ref. (Zhang et al., 2000) and (b) from ref. (Cardenas et al., 2004).

Recently, Heredia *et al.* have reported an amorphous α-chitin in the brown shrimp *Penaeus aztecus* shell coupling with calcite forming spherulites (Heredia et al., 2006). However, dried white spot material has previously been shown to consist of $CaCO_3$ in the form of calcite, incorporated into a matrix of amorphous α-chitin (Walton and Blackwell, 1973).

2.3 β-Chitin

β-Chitin was first recognized by Picken in 1949 (Picken, 1949), and Lotmar and Picken (Lotmar and Picken, 1950) in 1950. It was also studied by various workers (Rudall, 1955; Dweltz, 1961; Carlström,

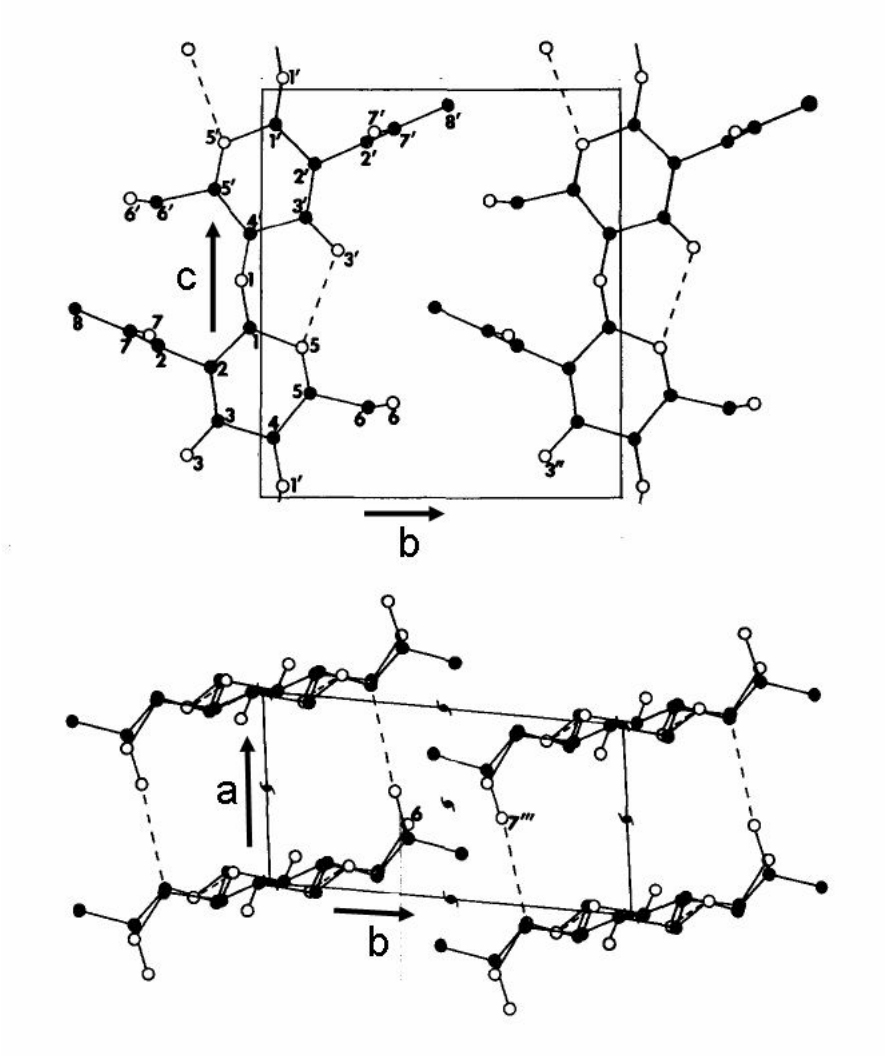

Fig. 2.7: The structure of β-chitin. Adapted from (Akhtar and Haleem, 1990).

1962; Ramachandran and Ramakrishnan, 1962; Dweltz and Colvin, 1968; Blackwell, 1969; Pervaiz and Haleem, 1975).

The refined structure of β-chitin was proposed by Gardner and Blackwell (Gardner and Blackwell, 1975) with monoclinic unit cell of dimensions a=4.85 Å, b=9.26 Å, c=10.38 Å (chain axis), γ=97.5° and space group $P2_1$. The parallel structure was refined later by Akhtar and Haleem in 1989 (Akhtar and Haleem, 1990).

β-Chitin as metastable polymorph can transform into stable α-chitin because it possesses the unique property of accepting small molecules as intercalates within its lattice to yield a series of crystallosolvates. These crystallosolvates keep the fibrillar morphology of the parent chitin and on drying, they revert normally to the anhydrous structure, without any apparent modification of morphology and crystallinity. β-Chitin hydrates are the best known examples of these crystallosolvates (Saito et al., 2000).

Upon hydration, the unit cell of β-chitin expands along its b parameter, which increases from 9.17 Å in the anhydrous case to 11.2 Å when the samples are immersed in water, yielding what is known as the β-chitin dehydrate (Gardner and Blackwell, 1975). This is a part of the process in which β-chitin converts totally into α-chitin (Saito et al., 2000).

Chapter 3

Biogenic Calcium Carbonate

3.1 Biominerals in Nature

Biominerals are diverse in nature and occur in the skeletal materials of the animals as well as in some plants. However, most of biominerals are compounds, and made up from a limited number of anions, namely, carbonates CO_3^{-2}, phosphate PO_3^{-2}, oxides, and oxalate $(C_2O_4)^{-2}$. Carbonates and phosphates are usually combined with calcium in the form of calcium carbonate and calcium phosphate. The former occurs mainly in the arthropod exoskeleton associated with fibers of chitin while the latter occurs as a main component of bone and teeth in the vertebrates.

Calcium carbonates are the most abundant biominerals in nature and occurs mostly in the exoskeleton of the invertebrates (mainly arthropods and mollusks), associated with organic fibers of α- or β-chitin embedded in protein filling matrix. Calcium phosphate occurs in the endoskeleton (bones or teeth) of vertebrates with collagen organic matrix. There are two main types of biogenic oxides in nature: amorphous silicon oxide (opal) which exists in macroscopic organisms like diatoms and plant phytoliths, and iron oxide (magnetite Fe_2O_3) which exists in some bacteria and the brain of the bee. Calcium oxalate is found in fungi and some plants.

Biominerals organization in organisms Biological materials can be classified into three groups based on the organization of their

mineral constituents (Weiner and Addadi, 1997). The first type is composed of crystalline biominerals, which are aligned at least in one direction with respect to the tissue geometry. This type of biological materials are most common one. The best known examples of such materials are bones, teeth, arthropods and mollusks shells of various types. In the second type, a single crystal or constitutes the entire structure. The echinoderms and sea urchin are the best known for forming such large single crystal skeletal structures of calcite. The third group produce biological materials containing an amorphous mineral, the most common being amorphous silica (Weiner and Addadi, 1997).

Characteristics of Biominerals There are three characteristics that distinguish biogenic minerals from geological ones. The first one is that biogenic minerals have unusual external morphologies, Fig. 3.1. A second characteristic of biominerals is that many are actually composites or agglomerations of crystals associated with organic material (such as collagen or chitin) (Weiner and Dove, 2003). The third one is its distorted structure, which resulted from being incorporated with organic matrix, like the case of aragonite (Pokroy et al., 2004, 2006a) and calcite (Pokroy et al., 2006b).

Carbonates are common constituents of the earth's near-surface crust, and few of them form biological skeletal materials. The carbonate rocks make up 10 to 15% of sedimentary rocks. They largely consist of two types of rocks: Limestones which are composed mostly of calcite ($CaCO_3$) or high Mg calcite ($Ca,Mg)CO_3$, and Dolostones which are composed mostly of dolomite $CaMg(CO_3)_2$.

Hydrous and Anhydrated Carbonates In general, carbonates are divided based on their hydration and crystal structure into the following groups (Gaines et al., 1997): anhydrous carbonates and hydrated carbonates.

Anhydrous carbonates include calcite group (Trigonal), aragonite group (orthorhombic), and Dolomite compound group (Trigonal). Calcite group like calcite $CaCO_3$, Magnesite $MgCO_3$, Siderite $FeCO_3$, Rhodochrosite $MnCO_3$, Sphaerocobaltite $CoCO_3$, Smithsonite $ZnCO_3$, Otavite $CdCO_3$, Gaspeite $(Ni,Mg,Fe^{2+})CO_3$, Vaterite $CaCO_3$, and Gregoryite $(Na_2,K_2,Ca)CO_3$. Aragonite group (Orthorhombic) like Aragonite $CaCO_3$, Witherite $BaCO_3$, Strontianite

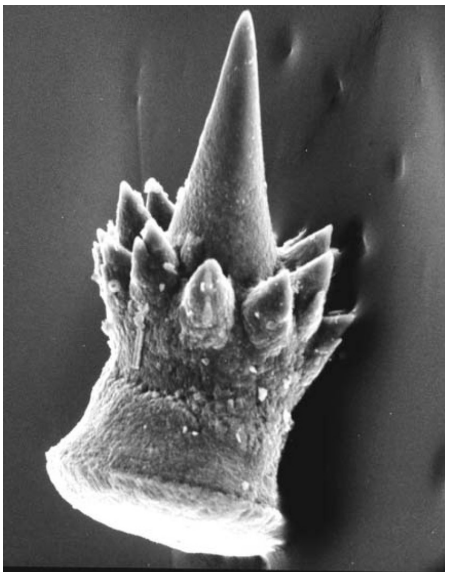

Fig. 3.1: Calcitic spicule formed by the ascidia which have unusual external morphologies which is a characteristic that distinguish minerals in Biology from the geologically ones. Adapted from (Weiner and Dove, 2003).

$SrCO_3$, Cerussite $PbCO_3$, Rutherfordine $UO_2(CO_3)$, Widenmannite $Pb_2(UO_2)(CO_3)_3$, Natrite Na_2CO_3, Zabuyelite Li_2CO_3. Dolomite compound group includes Dolomite $CaMg(CO_3)$ and other Minerals.

Hydrated carbonates includes many minerals like Thermonatrite $Na_2CO_3{\cdot}(H_2O)$ Natron $Na_2CO_3{\cdot}10(H_2O)$ CaCO3-monohydrate $CaCO_3{\cdot}(H_2O)$, Ikaite $CaCO_3{\cdot}6(H_2O)$, Barringtonite $MgCO_3{\cdot}2(H_2O)$, Lansfordite $MgCO_3{\cdot}5(H_2O)$, and Hellyerite $NiCO_3{\cdot}6(H_2O)$. Carbonates can come also with Hydroxyl(OH) or Halogen(Cl or F).

3.2 Biogenic Calcium Carbonate

Calcium is the only candidate for crustaceans and mollusks for mineralizing their exoskeleton. The calcium-bearing minerals comprise about 50% of all known biominerals, whereas about 25% of the biominerals are amorphous, in that they do not diffract X-rays (see section 3.7) (Weiner and Dove, 2003).

Mineral	Formula	Organism	Location	Function
Calcite	$CaCO_3$	Coccolithophores	Cell wall scales	Exoskeleton
		Foraminifera	Shell	Exoskeleton
		Mollusks	Shell	Exoskeleton
		Crustaceans	Crab cuticle	Mechanical strength
		Birds	Eggshells	Protection
		Echinoderms	Lens	Optical imaging
		Mammals	Inner ear	Gravity receptor
Mg–calcite	$(Mg,Ca)CO_3$	Octocorals	Spicules	Mechanical strength
		Echinoderms	Shell/spines	Strength/protection
Aragonite	$CaCO_3$	Scleratinian corals	Cell wall	Exoskeleton
		Mollusks	Shell	Exoskeleton
		Gastropods	Love dart	Reproduction
		Cephalopods	Shell	Buoyancy device
		Fish	Head	Gravity receptor
Vaterite	$CaCO_3$	Gastropods	Shell	Exoskeleton
		Ascidians	Spicules	Protection
Amorphous	$CaCO_3.nH_2O$	Crustaceans	Crab cuticle	Mechanical strength
		Echinoids	Larval spicules	Precursor phase
		Porifera	Spicules	Strength/protection
		Ascidiacea	Spicules	Mechanical strength
		Plants	Leaves	Calcium store

Fig. 3.2: Occurrence of calcium carbonate in biology: adapted from Ref. (Mann, 2001)

Calcium carbonate ($CaCO_3$) is one of the most abundant biominerals. It occurs mostly in invertebrate skeletal materials, especially, crustaceans and mollusks exoskeleton, as composites associated with organic fibers embedded in organic matrix. It exists naturally in six polymorphic phases, which varies in their thermodynamic stability under standard condition, in hydration and in crystallinity. Polymorphism of minerals implies the same chemical composition but distinct crystal structure. All of them exist in crystalline form except amorphous calcium carbonate ACC ($CaCO_3 \cdot 1.5H_2O$), which is rare in nature, although it has been found in the exoskeleton of many crustaceans (Raabe et al., 2006; Raz et al., 2002; Becker et al., 2005). Crystalline $CaCO_3$ exists in three anhydrous forms, namely, calcite, aragonite, and vaterite. The other two hydrated forms are: calcium carbonate hexahydrate $CaCO_6 \cdot 3H_2O$ and calcium carbonate monohydrate $CaCO_3 \cdot H_2O$, Fig. 3.2.

Calcium carbonate composites are common in the exoskeleton of invertebrates. It is rare in vertebrates, with exception being the otolith

in the ear, which is responsible for the balance of the body. The otolith organs sense gravity and linear acceleration for the initiation of movement in a straight line. Four crystalline morphs occur in fish otoliths, namely, aragonite, vaterite, calcite and carbonate monohydrate (Gauldie, 1993). Teleost fishes have three pairs of otoliths; sagitta, lapillus and asteriscus. Otoliths are crystalline structures composed of calcium carbonate contained in the endolymphatic sac in the inner ear of fish. The sizes of both sagittae and lapilli at hatching showed large variations even when the most asymmetrical otoliths were excluded from analysis. Otoliths arise by fusion of primary granules, the first calcified structures to appear during development, and they grow by deposition of calcium carbonate and protein matrix (Gauldie and Nelson, 1990; Neilson et al., 1985). Calcium carbonates have received remarkable interest from many branches of science, since its structures and its composites have exceptional mechanical properties (Ashby et al., 1995).

3.3 Calcite

Calcite is the most abundant carbonate mineral on the face of the earth, being the most stable polymorph of $CaCO_3$ and somewhat more stable than aragonite under ambient conditions (Lippmann, 1973) (Reeder, 1983). Calcite (and aragonite as well) occur in biological and geological materials like exoskeleton of crustaceans and sedimentary, igneous, and metamorphic rocks (like limestones, marbles, chalks which are a common cement in clastic sedimentary rocks), and as gangue in hydrothermal veins (like alkalic to mafic igneous rocks which are common as speleothems in caves) (Mann, 2001).

Calcite crystallizes in the hexagonal/rhombohedral space group, $R\bar{3}c$, and has a hexagonal unit cell, which contains six $CaCO_3$ units, Fig. 3.3, with the following parameters: a=4.989 Å and c= 17.062 Å (Maslen et al., 1993). It was studied before and gave a slightly different unit cell parameters: 4.978 Å, 17.3540 Å, for a, and c, respectively (Markgraf and Reeder, 1985). Calcium ions Ca^{2+} and CO_3^{-2} are located in alternate layers, perpendicular to the c-axis, and spaced at intervals of $c/12$. The CO_3 groups are identically oriented within a layer, which reverse alternatively between adjacent layers, breaking up the traditional analogy of calcite structure to

NaCl (when the Na^+ and the Cl^- ions is replaced by Ca and CO_3 groups, respectively).

The isostructural calcite group consists of several minerals with the following elements in place of calcium: magnesium, iron, manganese, cobalt, zinc, cadmium, and nickel. All these mineral carbonates have different names and are considered end-members in the series with an ideal composition expressed, e.g., as $MgCO_3$, for the mineral magnesite. These are the elements most likely to be incorporated in calcite whether formed strictly inorganically or precipitated when the elements are bio-accumulated. It should be pointed out that there is virtually no substitution for the carbonate group in calcite group structures (Reeder, 1983). Figure 3.4 is the result of a calculation that illustrates the possible cations which can fit into sixfold coordination position in the calcite group structures.

The formation of any biomineral indicates the composition of the ions available in the surrounding media and habitat with the specific mineral species and form dictated by an input of energy, to overcome the nucleation barrier. The continued availability of ions is essential for growth of the mineral species consistent with the biological needs.

Calcite can undergo a phase transitions at high pressure. Applying high pressures on calcite deduces a slightly denser phase (Calcite II) at 1.44-1.5 GPa, and and a transition to a significantly denser phase (Calcite III) at 1.74-2.2 GPa (Smyth, 1997).

Moreover, It was found that the lattice of biogenic calcite is anisotropically distorted as compared to geological calcite. Porkoy *et al.* reported a lattice distortions which are most probably induced by the control macromolecules [1] (Pokroy et al., 2006b).

3.4 Aragonite

Aragonite is described by an orthorhombic unit cell. Aragonite is common and close to calcite in stability. The limiting value for the transition from the rhombohedral calcitic structure to that of the orthorhombic aragonite structure is very close to the radius of the calcium ion , Fig. 3.5. Like in calcite, the Ca and CO_3 groups in

[1] control macromolecules play a crucial role in the nucleation, growth and morphological modifications of biogenic crystals, see 4.1.

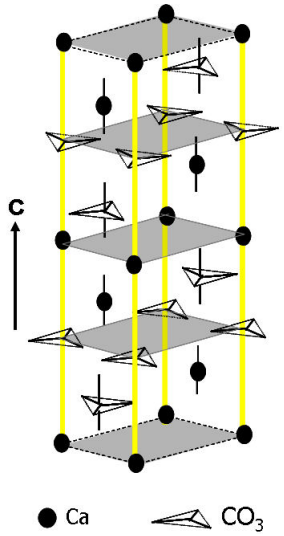

Fig. 3.3: Schematic diagrams of hexagonal unit cell of calcite where calcite is the shaded balls and the triangles are $CaCO_3$ group: reprinted from Ref. (Lippmann, 1973).

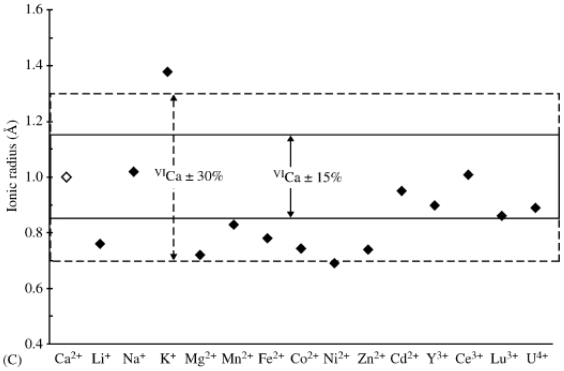

Fig. 3.4: Plot of the possible *best fit* 15%, and next *best fit*, 30%, of cations that could take the place of Ca in sixfold coordination in the calcite structure (courtesy of Stefan Nicolescu, Department of Geology and Geophysics, Yale University).

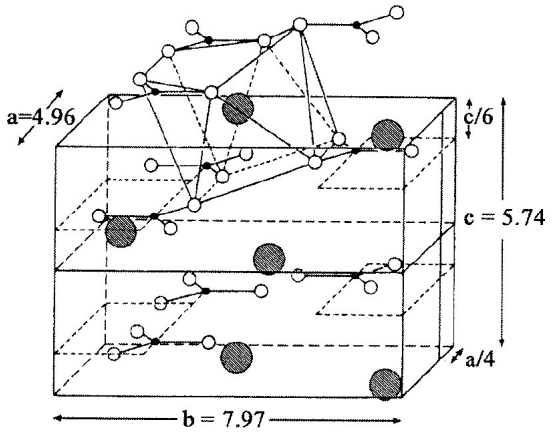

Fig. 3.5: Schematic diagrams of unit cell of aragonite, with additional CO_3^2 groups outside cell shown to demonstrate coordination of Ca ion: reprinted from Ref. (Lippmann, 1973).

aragonite are arranged in alternate layers perpendicular to the c axis (Lippmann, 1973; Speer, 1983). Differences between the structure of calcite and aragonite, however, exists in the splitting of the CO_3 layers into two layers parallel to the a-axis such that they appear corrugated. Another differences also exists in the Ca coordination between calcite and aragonite is that each Ca in the aragonite structure is also surrounded by six CO_3 groups, three CO_3 groups are bonded via two oxygens, while the remaining three are bonded by one oxygen each, leading to nine immediate oxygen neighbors. In aragonite however, all of the Ca–O distances are substantially greater than in calcite.

According to the updated diffraction database (JCPDS file 41-1475), aragonite has an orthorhombic unit cell (space group $Pmcn(62)$) with lattice parameters a=4.9623 Å, b=7.968 Å and c=5.7439 Å. This structure was clarified and confirmed recently by Caspi (Caspi et al., 2005). These lattice parameters are slightly different for the biogenic aragonite where incorporation of aragonite within macromolecules in skeletal materials creates anisotropic lattice distortions relative to the geological aragonite, being max. 0.1% along the c axis of the orthorhombic unit cell (Pokroy et al., 2004, 2006a).

The aragonite structure has alternate layers of carbonate groups and cations with the triangular CO_3 pointing in opposite directions along the c-axis, but the cations are in ninefold coordination catering to

larger size elements such as strontium, barium, and lead. Aragonite is one of the members of an isostructural group that includes these other cations.

In biology, aragonite and calcite occur widely in polycrystalline form, and the choice of the selected polymorph is almost always under strict genetic control. both have a feature that one polymorph offers some advantages over the other, even though both have very similar lattice energies and the same composition. Aragonite has the advantage of not having cleavage planes[2] (Han et al., 1991), but has the disadvantage of its small size and needle-like morphology. It also has a strong tendency to form spherulitic clusters of crystals with high porosity. Calcite, on the other hand, tends to form larger crystals, but these are very brittle. The calcite crystal cleaves easily along its {10.4} planes, called "cleavage rhombo-hedron" planes (Lawn, 1993).

3.5 Vaterite

Vaterite is a metastable form of the anhydrated calcium carbonate. It crystallizes in the hexagonal/rhombohedral space group $P6_3/mmc$, and the calcium is in sixfold coordination (Gaines et al., 1997). The Ca and CO_3 groups are again organised in alternating layers parallel to the c axis, but in contrast to aragonite and calcite, the plane of the CO_3 groups is parallel to the c axis (Lippmann, 1973), Fig. 3.6. While extremely rare in biomineralization, it was detected as a minor component of only a few bio-mineralised structures, like in some ascidian spicules (Lowenstam and Abbott, 1975), in a variety of gravity receptors (Lowenstam and Weiner, 1989) and in the egg shells of some gastropods (Hall and Taylor, 1971). Vaterite is a common synthetic product of solution precipitations and high temperature preparations, being kinetically favored under certain conditions and subsequently transforming to a more stable polymorph (Sawada, 1999).

[2]Cleavage plane is the plane where a crack can propagate along a minimum-energy pathway (with minimum dispersion of energy).

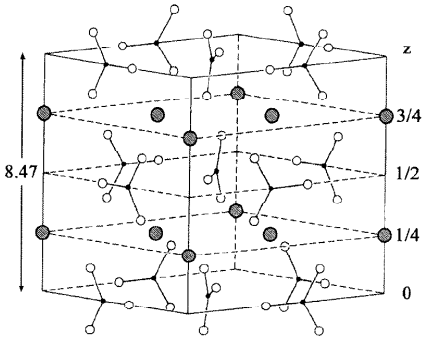

Fig. 3.6: Schematic diagrams of subcell of vaterite, where c'=c/2: reprinted from Ref. (Lippmann, 1973).

3.6 The Anhydrated Phases of Calcium Carbonate

Calcium carbonate monohydrate was identified first in the laboratory (Krauss and Schriever, 1930) as an intermediate in the degradation of $CaCO_3 \cdot 6H_2O$. In the natural environment, this compound seems to be preferably formed in magnesium-rich media. The appearance of $CaCO_3 \cdot H_2O$ has been related to the value of the ratio R = [Mg]/[Ca] of the mother solution. Water from Fellmongery lake, which has the largest ratio R ($16 < R < 34$) produces the purest calcium carbonate monohydrate (Taylor, 1975; Hull and Turnbull, 1973).

It was also reported that the monohydrate form was found in sea water (Duedal and Buckley, 1971), and in an old Gallery mine (Weil and Siat, 1975). Recently, it was characterized by micro-Raman spectroscopy (Tlili et al., 2002). It occurs also combined with another morphs of $CaCO_3$ in the otolith in the ear of sharks (Carlström, 1963). $CaCO_3 \cdot H_2O$ crystallizes in the hexagonal (trigonal) system P3112 with the lattice parameters a=10.55 Å and c=7.54 Å (Effenberg, 1981).

The hexahydrate phase (called also Ikaite), which forms in cold carbonate-rich marine environment, had been reported from laboratory studies made during the 19th century (Pelouze, 1865). It was first discovered as a mineral in 1963 by Pauly in unusual geological formations in sea water at Ikka Fjord, Greenland (Pauly, 1963).

It was also found in frozen shrimp shell, which rapidly transforms into a mixture of the anhydrous calcium carbonate forms, vaterite and calcite (Engelsen et al., 1999). Calcium carbonate hexahydrate, which crystallizes in the monoclinic system, consists of $CaCO_3 \cdot 6H_2O$ units linked by H bonding only, Each Ca^{2+} ion is coordinated by eight oxygens, two from the planar carbonate anion, and six from H_2O molecules, with lattice parameters a=8.87 Å, b=8.23 Å, c=11.02 Å, and β=110.2 (Dickens and Brown, 1970). However, another unit-cell parameters for Ikaite was reported: a = 8.8297(2), b= 8.3229(1), c= 11.0558(3) and β= 110.647(2) at 293 K (Lennie et al., 2004).

3.7 Amorphous Biominerals in Nature

The definition of an amorphous material is somewhat confusing. Not only is it technique dependent, but it is also characterized by the lack of certain properties rather than their presence. Amorphous materials are thus generally referred to as those that produce no X-ray and/or electron diffraction patterns. This implies that these materials have no long-range order. The local structure in amorphous calcium carbonate was studied by EXAFS (Extended X-ray Absorption Fine Structure) for the first time by Taylor *et al.* (Taylor et al., 1993) in cystoliths. It is likely that calcium carbonate materials that produce no diffraction pattern, but have different stoichiometries and different degrees of short-range order, have all been referred to as the same material, namely amorphous calcium carbonate (Levi-Kalisman et al., 2000).

In biology, amorphous silica (opal) is the most commonly formed biogenic amorphous mineral (Lowenstam and Weiner, 1989). Other widely distributed biogenic amorphous minerals are amorphous calcium phosphates and amorphous calcium carbonates.

3.7.1 The Use of Amorphous Biominerals in Biology

Amorphous biominerals can be used as temporary storage site or as a transient phase prior to their deposition into a denser crystalline phase. The amorphous metastable phase is either stabilized by the organism for its entire lifetime, or subsequently transforms into a more stable crystalline form to the formation of a particular crystalline phase (Lowenstam and Weiner, 1989). An important advantage of amorphous phases is their high solubility, allowing them to be deposited relatively easily and subsequently redissolved. Aizenberg *et al.* suggested that macromolecules are responsible for its inhibition of crystallization, its consequent precipitation, and its stabilization (Aizenberg et al., 1996). Other studies showed that magnesium and phosphate may also participate in the stabilization of amorphous phases (Becker et al., 1974; Dickens and Brown, 1970; Clarkson et al., 1992).

The cuticles of *Porcellio scaber* and *Armadillidium vulgare* contained crystalline calcium carbonate (magnesium calcite) in addition to

amorphous calcium carbonate (ACC) and amorphous calcium phosphate. These biominerals have considerable functional implications (Becker et al., 2005). The need for frequent recycling of cuticular calcium is the reason for the presence of large amounts of ACC in the cuticle. Most terrestrial isopods moult very frequently, *Porcellio scaber* for instance every six weeks. It seems likely that most of the amorphous fraction of $CaCO_3$ within the cuticle is resorbed and recycled during every moulting cycle, while most of the less soluble crystalline part is shed with the old cuticle (Fabritius and Ziegler, 2003).

ACC were reported to be found in marine arthropods, even though calcium concentration is very high in sea water. Some studies went to that the groups which live in freshwater or on land, where the availability of calcium at ecdysis (moment where the animal leaves its old cuticle) ranges from great to complete absence, have developed different strategies to solve the problem of calcification, notably by storing calcium during the pre-moult period as ACC (Greenaway, 1985).

Another use of the amorphous biominerals is might be as structural component. Its isotropic mechanical properties facilitate equal distribution of mechanical stress. It is also easier to mold isotropic materials into complex shapes as compared to crystalline materials. Isotropy in a material has obvious advantages. Macromolecules which forms the matrix in biological materials are always highly anisotropic as are the crystalline mineral components, so the substitution of a crystalline mineral for an amorphous mineral should contribute significantly toward improving the overall isotropic properties of a biological material (Weiner and Addadi, 1997).

3.7.2 Examples of Amorphous Biominerals

Silica (opal) is the most stable and the most abundant amorphous biomineral in nature. It occurs in the skeletons of many microscopic sized organisms, such as diatoms and radiolarians. These often have exquisite morphological features characterized by smooth surfaces. Silica is one of the three most abundant biogenic minerals (together with calcite and aragonite). Amorphous silica is indeed used by a wide range of organisms, from the complex beautifully sculpted diatoms to siliceous sponge spicules and plant phytoliths (Simpson

and Volcani, 1981). In addition to being isotropic, silica has the obvious advantage of being stable under ambient conditions, and therefore minimal energy is required for this aspect of its formation (Weiner and Addadi, 1997).

Another examples is the amorphous calcium phosphate ACP and the amorphous calcium carbonate ACC. They are the least stable amorphous form of biominerals, so that they tend to transform, in an uncontrolled environment, into a more stable crystalline phase. This transformation is both thermodynamically and kinetically favored under ambient conditions.

ACP is often used for temporary storage of ions, because its solubility is higher than that of the crystalline materials. It is also used, however, for skeletal strengthening purposes, for example in some ascidian spicules, the gizzard plates of some gastropods, and in the teeth of the chiton Acanthopleura (Lowenstam and Weiner, 1989). It also occurs in the internal skeleton of sea urchin embryo, which is composed of two spicules. Each specule is formed by the transformation of amorphous calcium carbonate into calcite single crystal (Beniash et al., 1997).

ACC is the least stable form the other five forms of calcium carbonate. This compound does not exhibit any crystalline shape; it occurs often in the form of spherulites with a diameter smaller than 1 μm (Clarkson et al., 1992; Aizenberg et al., 1996). It was reported that ACC can act as a temporary storage site in the terrestial isopod for the moult cycle, during which about 40% of the cuticular calcium is stored in the form of amorphous calcium deposits, as spherolites with dimater varying from 0.3 to 1.7 μm, to be incorporated rapidly into the new soft cuticle, due to its rapid mobilisation (Ziegler, 1994). However, ACC provide the cuticle with mechanical performance, since it is intrinsically isotropic. ACC could be moulded into more intricate structures than crystalline naterials, because they have no preferred morphology (Mann, 1986). It has been shown *in vitro* that specific proteins are responsible for the stabilization of ACC in ascidian and sponge specules (Aizenberg et al., 1996).

Amorphous phases in biology can be stabilized permanently, or for relatively long period of time, and then transform rapidly into the crystalline stable phase, which can therefore be advantageous when frequent replacement of the mineral in the cuticle is required, while the mineralized exoskeletons cyclically renewed with exogenous or

endogenous calcium carbonate. This requires a reservoir of calcium ions. Crustaceans obtain the calcium they need from their environment, and in addition certain species have developed calcium storage strategies. Even though, certain organisms from different groups of animals and plants are known to form stable ACC. It is widespread in plants as cystoliths (Taylor et al., 1993). Cystoliths are intracellular particles, made of amorphous calcium carbonate, that are found in great numbers in the leaves of higher plants. The Crustacea (Raabe et al., 2006) and a group called the ascidians (also known as the tunicates) also produce amorphous calcium carbonate minerals (Aizenberg et al., 1996). These deposit no less than six different minerals, including amorphous calcium phosphate and amorphous calcium carbonate (Lowenstam and Weiner, 1989).

Levi-Kalisman *et al* have characterized the amorphous calcium carbonate from the antler spicules of the ascidian *Pyura pachydermatina* (Levi-Kalisman et al., 2000). X-ray Absorption Spectroscopy studies (XAS) show however that ACC has characteristic short-range order (Taylor et al., 1993; Levi-Kalisman et al., 2000; Hasse et al., 2000).

The shell of the pink shrimp Pandalus borealis has a matrix of α-chitin associated with amorphous calcium carbonate. During continued frozen storage, the amorphous phase crystallizes in the form of the two polymorphs calcite and vaterite. The chitin is an integral part of the crystallized regions and therefore it is suggested to play an important role in calcium carbonate deposition (Miikkelsen et al., 1987).

Chapter 4

Biomineralization

4.1 Biomineralization Strategies

In biomineralization process, a biological control from the organism exerted over biomineralization process, which varies in its degree of contribution.

Upon that extent of biological regulation of biominerals formation, Lowenstam has devided the biomineralization processes into two fundamentally different groups (Lowenstam, 1981), namely, *biologically induced* and *biologically controlled*[1] mineralization.

The most common biomineralization strategy in nature is the extracellular biologically controlled process. Examples of tissues that use such kind of mineralization include bone, teeth, mollusc and arthropod shells. In this case, the cell produces a macromolecular matrix[2] outside the cell in an area that will become the site of mineralization, then transfer constituents to the matrix. cell works actively to supply cations to an external organic matrix for *on-site* nucleation and growth (Weiner and Dove, 2003).

Nature uses organic macromolecules to produce minerals of selected size, phase, morphology, crystallographic texture and assembly. At

[1] this term given by Mann (Mann, 1983) after it was before as *organic matrix-mediated* given by Lowenstam (Lowenstam, 1981).

[2] The term matrix refers to a group of macromolecules comprised of proteins, polysaccharides or glycoproteins that assemble to form a three-dimensional framework.

the most basic level, the isolated site at which mineralization occurs comprises a structured organic matrix such as the organised collagen fibrils in bone.

Organic Macromolecules are important in morphological and textural control (Addadi and Weiner, 1985, 1986). These macromolecules are usually highly negatively charged and contain carboxyl, sulphate and phosphate groups. Aspartic acid and glutamic acid are common examples, as are covalently bound polysaccharides, which are generally sulphated and carboxylated (Weiner and Hood, 1975).

Some common partial sequences of amino acids have also been identified, consisting of runs of poly-Asp and alternating sequences with poly-Asp at every other residue, commonly separated by either glycine or serine (Weiner and Hood, 1975). This sequence exhibits regular repeating negative charges which may bind Ca^{2+} ions and could be significant in controlling crystal growth. In addition, poly(aspartic acid) can adopt β-sheet structure on binding to Ca, which appears to be important in enabling structured interaction with crystal faces. Identification of common sequences enables synthetic analogues of macromolecules active in crystal growth control to be designed (Meldrum, 2003).

Macromolecules form an intimate mix or composite with the mineral phase at all different hierarchical levels, starting at the scale of nanometers, where they are found to be very diverse and heterogeneous. They function in the biological tissues in two ways: control Macromolecules and framework macromolecules. Control macromolecules which are usually the minor macromolecular components of a biological material, are difficult to extract or degrade without dissolving the mineral (Weiner and Addadi, 1997).

Many of these macromolecules are rich in carboxylate groups (Weiner et al., 1983b) in addition to phosphate and/or sulfate groups. The presence of all these charged groups makes these macromolecules excellent candidates for interacting with the mineral ions in solution or with the surfaces of the solid phase (Addadi and Weiner, 1992).

The control macromolecules of calcium carbonate-containing biological materials from several organisms can be somewhat arbitrarily subdivided into several groups (Weiner and Addadi, 1997):

1. Aspartic acid-rich proteins and glycoproteins, which tend to be associated with the crystalline mineral phases.

2. Glutamic acid (and/or glutamine)- and serine-rich glycoproteins, which are the major components of the several amorphous $CaCO_3$-containing mineralized tissues I have examined recently from two widely diverging taxa (Aizenberg et al., 1996).

3. Macromolecules rich in polysaccharides, with proteins. These macromolecules are the major components of echino-derm skeletons and are minor components of mollusc shells (Albeck et al., 1996).

The other type is the framework macromolecules which are the major components in the biological materials. These are more hydrophobic, often cross-linked and are hence relatively insoluble in mild acids or at neutral pH. Their function is to provide a three-dimensional matrix in which the mineral phase forms, and a substrate from which some of the control proteins interact with the mineral phase (Weiner et al., 1983b). Common examples of framework macromolecules are Gly- and Ala-rich proteins (structurally similar to silk-fibroin) in mollusc shells, type I collagen in bone and tooth dentin, amelogenin in tooth enamel, α-chitin in crustaceans and β-chitin in mollusc shells (Lowenstam and Weiner, 1989).

4.2 Nucleation and Crystal Growth

During the nucleation process of the mineral, selection of the number, orientation and structure of crystals produced within a given environment occurs. Oriented nucleation must be defined by an organized substrate, as simple concentration of positive ions at a negatively charged substrate (an ionotropic effect) should be non-specific with respect to crystal orientation and would be expected to yield the most stable polymorph (Weiner and Addadi, 1997). *In vitro* experiment has demonstrated that biological macromolecules are active in controlling crystal orientation (Addadi and Weiner, 1985, 1986). The aspartic acid rich proteins extracted from either the calcitic or the aragonitic layer of a bivalve were adsorbed on glass, producing a surface which nucleated calcite crystals from the (001) face.

The crystals then continued to grow into solution to develop regular, rhombohedral morphologies (Addadi and Weiner, 1985, 1986).

The ability of the proteins to induce oriented nucleation in mollusc nacre was attributed to their rigidity and adoption of a β-sheet conformation after binding to the substrate. In this conformation, the carboxylate groups of the aspartic acid moieties emerge in a planar array, which is available for binding to the crystal. Mollusc shell nacre has provided an excellent system in which to study biological control over nucleation, as there is a well defined relationship between nascent crystals and the underlying organic matrix (further details in section 5.2).

Following nucleation, the growth of crystal nuclei must be controlled to produce desired shapes, sizes and crystallographic textures. Every crystal has a characteristic morphology, which is governed by the crystal structure and symmetry, and the conditions in which the crystal grows. Some organisms override this basic growth form using a combination of mechanisms to produce crystals whose overall morphologies often bear no relation to the symmetry of the crystal lattice. An excellent example is provided by the skeletal elements of sea urchins. Despite their intricate sponge-like morphologies, the spines and skeletal plates of sea urchins are single crystals of calcite (Meldrum, 2003).

4.3 Biomineralization in Crustaceans

Crustacean *Orchestia cavimana* stores calcium originating mainly from its old cuticle (Graf and Meyran, 1983). The calcium stored in the concretions constitutes about 60% of the cuticle calcium content while the rest originates from the shed cuticle (also known as the exuviae) ingested by the animal just after ecdysis (molting), and from food (Luquet and Marin, 2004).

Since calcification of this new exoskeleton represents, among other things, a means of defense against environmental pressures, this process must occur as quickly as possible. The calcium is stored for about 15 days in the premolt period (Graf, 1986). After ecdysis, namely the moment when the animal leaves its old cuticle, the calcium is resorbed in less than 48 h to rapidly mineralize the new cuticle in a brief postmolt period (Graf, 1986; Graf and Meyran, 1985).

Calcium then passes through the epithelial cells by a paracellular pathway as calcified spherules. Other transitory mineralized struc-

tures are produced in a dilated intercellular membrane network by precipitation of calcium salts within an organic matrix synthesized by the storage organ cells (Luquet and Marin, 2004).

They are then resorbed at the basal part of the epithelium, and the Ca_2 released is discharged into the hemolymph through the basal lamina (Graf and Meyran, 1985; Meyran et al., 1986). After complete dissolution of the concretions, the organic matrix is probably removed via the midgut to which the storage organs are connected, as indicated by studies of orchestin, a well characterized component of the organic matrix (Luquet et al., 1996; Testeniere et al., 2002).

The calcified storage structures, called calcareous concretions, are composed of an organic matrix whose proteinaceous components have been analyzed (Luquet et al., 1996; Testeniere et al., 2002). The proteins are synthesized by the storage organ cells within which calcium salts are precipitated. Single spheruliths are firstly elaborated extracellularly in the lumen of the tubular storage organs. The integration of several single spheruliths forms compound spheruliths about 800 μm long and 400 μm in diameter in an adult individual. The concretions vary between single spheruliths and compound spheruliths in the 8-mm-long adult storage organs. This facilitates the flexibility required for these jumping animals. The concretions were initially considered to be excretion forms (Luquet and Marin, 2004).

Chapter 5

Exoskeleton Microstructure

5.1 Arthropod Cuticle

The phylum arthropoda exceeds all other groups of animals in number of species and diversity. In fact, arthropods, which include the crustaceans (e.g. crabs, lobsters, isopods), insects (e.g. wasps, bees, ants, beetles, etc.), arachnids (e.g. spiders, scorpions, ticks, mites), centipedes, millipedes and several lesser groups, account for approximately 80 percent of all known animal species. They have also radiated to occupy every conceivable type of ecological niche.

Arthropods are common with their hard exoskeleton, segmentation, and jointed appendages, which is related to their success. The appendages are used for feeding, sensory reception, defense, and locomotion. The muscle system is more or less assisted by hydraulics originated from the blood pressure created by the heart.

The cuticle in arthropods is a key factor in the eminence of the phylum, whose members possess a segmented body, jointed limbs and a strong external skeleton. It is composed mainly of chitin, which is periodically shed as the animal grows. They contain an inner zone (procuticle) which is made of protein and chitin and is responsible for the strength of the exoskeleton. The outer zone (epicuticle) lies on the surface of the procuticle. It is nonchitinous and is a complex of proteins and lipids. It provides the moisture proofing and protection to the procuticle.

The exoskeleton takes the form of plates called sclerites on the segments, plus rings on the appendages that divide them into segments

separated by joints. This is in fact what gives arthropods their name – jointed feet – and separates them from their relatives. The skeletons of arthropods strengthen them against attack by predators and are impermeable to water. In order to grow, an arthropod must shed its old exoskeleton and secrete a new one. This process, ecdysis, is expensive in terms of energy consumption, and during the moulting period, an arthropod is vulnerable.

5.1.1 Contents of Arthropod Cuticle

Arthropod cuticle contains mainly of eith α- or β-chitin as fibers embed with proteins. Crustaceans mineralize their exoskeleton with calcium carbonates. Since 1929, many studies have determined the contents of the cuticle for diverse organisms, in order to get informations about their biomineralization (Foster and Webber, 1960). However, modern studies employed more reliable techniques in element analysis, which are more attractive and plausible. Takai *et al* have determined the content percentage of chitin, ash and protein contents of some crustaceans obtained by element analysis (Takai et al., 1992), as well as other scientists.

Chitin source	Protein	Chitin	Ash	Lipids	Reference
Crab					
Blue Crab *Collinectes sapidus*	25.1	13.5	58.6	2.1	Muzzarelli, 1997
Queen Crab *Chinoecetes opilio*	29.2	26.6	40.6	1.3	Shahidi, 1991
King Crab *Paralithodes*	14.5	27.5	44.8	--	Takai, 1992
Shrimp					
Pink Shrimp *Pandalus borealis*	41.9	17.0	34.2	5.2	Shahidi, 1991
Brown Shrimp *Crangon crangon*	40.6	17.8	27.5	9.9	Synowiecki, 2000
Krill:					
Antarctic Krill *Euphausia superba*	41.0	24.0	23.0	11.6	Naczk, 1981
	48.4	7.9	33.6	--	Takai, 1992
Prawn:					
Dendrobranchiata	61.6	33.0	29.4	1.4	Muzzarelli, 1997
	35.5	23.5	33.6	--	Takai, 1992
Giant Tiger Prawn Penaeus monodon	47.4	40.4	23.0	1.3	Muzzarelli, 1997
	38.4	24.0	28.8	--	Takai, 1992
Argent. Pink Prawn Pleoticus muelleri	48.4	21.0	33.5	--	Takai, 1992
Lobster					
American Lobster *Homarus americanus*	30.6	10.0	40.0	--	Takai, 1992
Crawfish *Procamborus clarkia*	29.8	13.2	46.6	5.6	Muzzarelli, 1997

Fig. 5.1: Proximate composition on a percent (%) of arthropod cuticles based on recent references.

Fig. 5.1 shows proximate composition on a percent (%) of arthropod cuticles based on relatively modern references (Takai et al., 1992;

Muzzarelli et al., 1997; Naczk et al., 1981; Shahidi and Synowiecki, 1991; Synowiecki and Al-Khateeb, 2003). I have to point that the estimation of the degree of calcification can vary by the decalcification agent used, which was proved by Welinder (Welinder, 1974).

5.1.2 Cuticle Layers

The integument of the decapod Crustacea is, in general, comprised of a rigid exoskeleton or cuticle underlain by the cellular hypodermis (Richards, 1951).

Early studies done with light microscopes uncovered the two major structural divisions: a thin top layer known as the epicuticle and a thicker layer known as the procuticle. These layers rest above the epidermis, a single layer of cells that originally secrete the cuticle. Together the cuticle and epidermis form the integument, or outer covering, of the arthropod.

The cuticle contains four discrete layers. This observation was made more than a century ago (Williamson, 1860), and it has been the subject of numerous subsequent studies. The cuticle is formed by four superimposed layers, from the external to the most internal: the epicuticle, the exocuticle, the endocuticle, and the membranous layer (Travis, 1963), Fig. 5.2. Travis has created this terminology which has come to be widely accepted and will be used exclusively in this chapter. The nomenclature of the four layers of the cuticle varies from author to author, but I will use *procuticle* to represent the chitinous layers: exocuticle and endocuticle.

Travis, Hegdahl, and Roer have studies intensively the vertical composition of the crustacean cuticle since 1950s, their studies explored the layer structure of the cuticle and became widely accepted.

The three upper ayers are mineralised, essentially by precipitation of calcium carbonate into the twisted lamellar structure of the chitinŰprotein cholesteric matrix (Bouligand, 1972; Roer and Dillaman, 1984; Travis, 1963).

The epicuticle is the outermost and thinnest layer of the cuticle. It consists of tanned lipoprotein impregnated with calcium salts (Travis, 1955a). It is bilaminar, with the basal layer pervaded by mineral-filled canals normal to the surface (Hegdahl et al., 1977b).

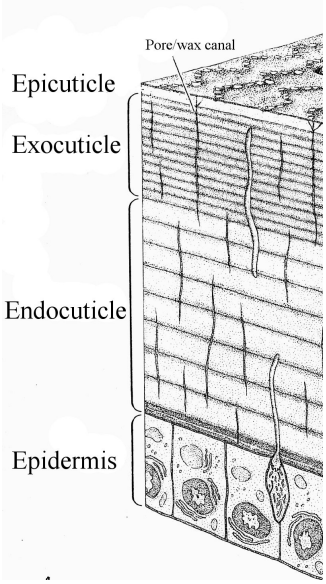

Fig. 5.2: The layers of the cutiticle (adapted from (Hadley, 1986)).

The epicuticle, which is important to the ability of most arthropods to retain water, contains at least two sublayers in spite of its being only from 0.1 micrometer to three micrometers thick. The colouring matter contains principally carotenoids, which do not appear to be complexed with either inorganic material or protein ((Montserrat, 2002), p.55). Carotenoids contribute to the yellow, orange, and red colors of the skin, shell, or exoskeleton of aquatic animals. Indeed, they are the most widespread pigments found in nature, as they occur in bacteria, yeasts, mold, all green plants, and many animals, and therefore various functions have been attributed to them. Carotenoids are a family of over 600 natural lipid-soluble pigments that areproduced within microalgae, phytoplankton, and higher plants.

The procuticle makes up the bulk of the integument and ranges in thickness from 10 up to several hundred microňmeters. The procuticle accounts for the shape and strength of the cuticle. It typically divides into a relatively thin exocuticle – a pigmented layer at the top – and a thicker endocuticle.

The exocuticle immediately underlies the epicuticle. It is composed of chitin-protein fibers stacked in layers of continuously changing orientation (Travis, 1955a; Green and Neff, 1972). The exocuticle is

hardened by quinone tanning and calcification (Travis, 1955a), with the mineral crystals situated between the fibers (Bouligand, 1972; Hegdahl et al., 1977a), and is pigmented layer (Giraud-Guille et al., 2004).

The endocuticle is the thickest and the most heavily calcified layer of the cuticle (Travis, 1955a, 1965). The endocuticle, like the exocuticle, is composed of horizontal lamellae of chitin-protein fibers with continuously changing orientation (Green and Neff, 1972; Hegdahl et al., 1977c). The endocuticle is apparently not tanned, but hardened solely by Ca salts (Travis, 1955a). The stacking of chitin fibers layers are more dense in the case of endocuticle.

The membranous layer is the innermost layer of the cuticle and is in contact with the hypodermis. It consists of chitin and protein, but contains no mineral (Travis, 1955a). The mineral in the outer three layers of the cuticle is calcite or amorphous calcium carbonate (Travis, 1963).

The hypodermis is heterogeneous, having numerous cell types arranged in three principal layers (Travis, 1955a,b, 1957, 1965). The layer in contact with the cuticle and apparently responsible for its formation is the outer epithelial layer or the cuticle secreting cells (Green and Neff, 1972). The cuticle is pervaded by vertically running pore canals first described by Valentin in 1837 (Richards, 1951). Further examination has revealed these to be cytoplasmic extensions of the outer epithelial cells which emanate from the apical cell borders, extend through the membranous layer, endocuticle and exocuticle, and terminate at the epicuticle (Travis, 1963; Green and Neff, 1972) or in it (Hegdahl et al., 1977b). Pore canals, which are thin cytoplasmic expansions of epidermal cells, play a role in the transport of calcium ions (Travis, 1963).

The pore canals may have a typical helical or twisted ribbon morphology (Drach, 1939; Neville et al., 1969) with the pitch of the helix being equal to the lamellar period (Drach, 1939). Thus, the cuticle is in close contact with the hypodermis at all levels and should be considered living tissue.

Calcification occurs at different sites within the cuticle: in the chitin–protein fibres, at the level of interprismatic septa and pore-canals (Cameron, 1989; Giraud-Guille, 1984; Roer, 1980; Roer and Dillaman, 1984; Travis, 1963).

5.1.3 Hierarchical Structure of arthropod cuticle

Arthropods are a very successful group of invertebrates, including insects, spiders, and crustaceans. The exoskeleton of arthropods is made of cuticle which may vary in its composition and properties within animals and between species, depending on the function the cuticle may have (Currey et al., 1982).

Arthropod cuticle is a fibrous materials, i.e. it composed of polysaccharides (α-chitin) arranged as fibers expanding through the cuticle plane. Most of biological materials which contains organic matrix, are fibrous materials from that organic matrix. Bone and dentin in human body for example contains fibers of collagen.

α-Chitin is the main polysaccharide component in arthropod cuticle. The chains of α-chitin are stiff and stable, as explained in section 2.2, the chains are arranged anti-parallel and combine into a highly crystalline structure within which its residues are heavily H-bonded. The stiffness of the cuticle depends on the amount of cross-linking, or tanning, that occurs, and also on the ratio of protein to chitin (Currey et al., 1982).

Hierarchical organisation is an essential characteristic of biological materials, at the nanometre-to millimetre scale, or more, allowing responses to solicitations at all these levels. arthropod cuticle is an example of the hierarchical structure design. The fibrillar networks often present similar three-dimensional arrangements, see Fig. 5.3.

The first level of the cuticle hierarchical organization is chitin chains. In the view of chitin crystal structure looking along the chain axis (c-axis), the hydrogen chains are laterally spaced by 0.475 nm, the same as the lateral distance between the adjacent protein chains of an antiparallel β-sheet such as silk, Fig. 5.4. However, in the view of the plane given by c- and b- axes, along the length of each chitin chain, the space between adjacent residues is 1.032 nm (which is the chitin monomer length, and c-lattice constant), while twice this repeat (2.064 nm) is almost exactly the same as three times the repeat of a protein β-sheet (0.69 nm) (Vincent, 2002). Atkins has suggested that in the chitin nanofibril, the lattice structure of α-chitin can be related to the spacings in a chain folded sheet of the associated protein β-sheet (Atkins, 1985) and the chitin is bonded to half the protein groups (Vincent, 2002).

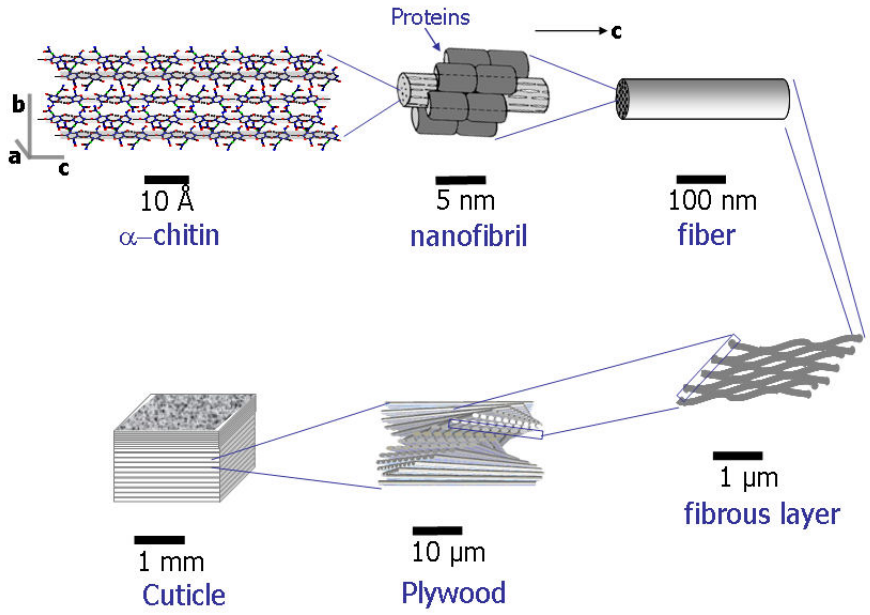

Fig. 5.3: Hierarchical structure of arthropod cuticle.

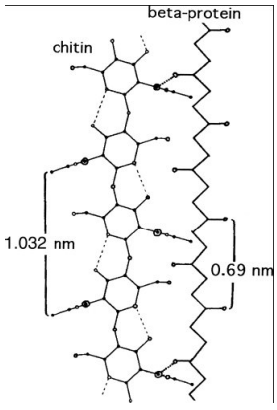

Fig. 5.4: Interaction between chitin and protein. The plane of the paper is given by the c- and b-axis. (adapted from (Vincent, 2002)).

The second level is nanofibrils. Within the body of the cuticle, the chitin chains surrounded by proteins are assembled into nanofibrils of about 2 to 3 nm in diameter, each containing 19 molecular chains and about 300 nm long. The number of chitin chains in the nanofibril is probably close to a minimum for stability; hence, the chitin nanofibrils present the maximum surface area for interfacial interactions within the cuticle (Vincent, 2002).

Chitin nanofibrils are covered with helical proteins. Protein is probably within and is certainly secreted from the epidermis. The protein produce a matrix of appropriate mechanical properties, and it interact with and stabilize the chitin. It interacts with the chitin in a narrow zone (the Schmidt layer) with relatively large amounts of water (about 90%), presumably to drive the hydrophobic interactions between chitin and protein (Vincent, 2002).

The third level is fibers. Dannell has suggested that in crustacean cuticle the fibrils may join up into quite thick fibres, and that some of these fibres may pass through the thickness of the cuticle (Dennell, 1973).

The fourth level is the planes of the fibers honeycomb structures. Chitin fibers are arranged in a honycomb fashion in one layer (Raabe et al., 2005a). But in ideal representation, the fibers directions are drawn as parallel and equidistant straight lines, because the fibers are almost in the same direction within the layer.

The fifth level is the blywood structure of the honeycomb layers. The fibers directions of neighbouring layers are displaced by a small amount typically 5 to 10 degrees, so the preferred orientation changes cyclically and vertically through the thickness of the cuticle (Currey et al., 1982; Bouligand, 1972), see Fig. 5.5.

This twisted fibrous arrangements in biological materials (plywood structure) was introduced for the first time by Bouligand in 1972. It was introduced originally from the liquid crystalline biological analogue (Bouligand, 1972). It is originated from the fact that some major biological macromolecules possess liquid crystalline self-assembly properties, which would appear, during morphogenesis, at different moments and in different compartments, when molecular concentrations reach critical levels. This applies on collagen and chitin in extracellular matrices as well as cellulose in plant cell walls and DNA in certain chromosomes. This liquid crystal hypothesis was refined and validated recently by many *in vitro* studies (Giraud-Guille, 1996).

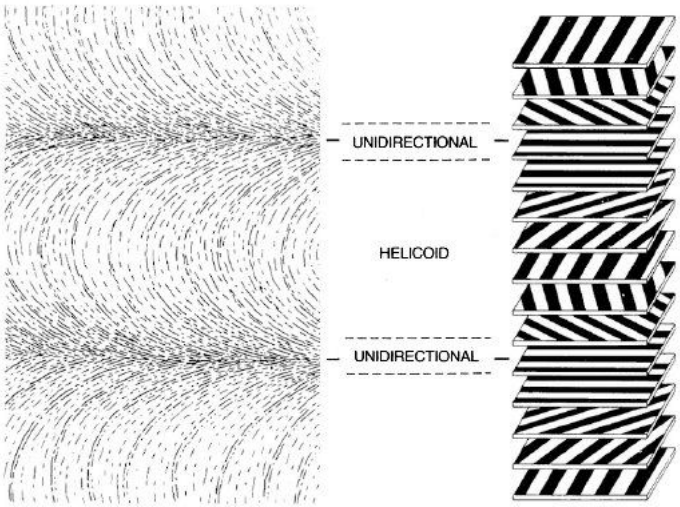

Fig. 5.5: The plywood structure of chitin layers (adapted from (Hadley, 1986)).

The band of layers corresponding to a 180° fiber rotation through the cuticle thickness, appear as lamina, and can be evidenced using optical microscopy. A cross section of the cuticle shows regular laminae in all the chitin-containing layers.

Such hierarchical structures of the organic matrix were evidenced in sections analyzed in optical microscopy or in transmission electron microscopy (TEM) (Giraud-Guille et al., 2004) (Raabe et al., 2005a).

5.2 Mollusc Shells

Molluscs (Sea Shells) are invertebrate animals like arthropods, but with an un-segmented, basically symmetrical body. The animal itself consists of head, foot, visceral hump and mantle. Above the body would be an external shell mounted on a visceral hump containing internal organs.

Molluscs are soft-bodied animals, protected by a hard external shell. Familiar mollusks (Sea Shells) include the clam, oyster, snail, slug, octopus, and squid. The mollusks are the second largest in the animal kingdom, after arthropods (prodiminated by insects).

The mollusks include a variety of familiar creatures well-known for their decorative shells or as seafood. These range from tiny snails, clams, and abalone to the octopus, cuttlefish and squid (which are considered the most intelligent invertebrates). Among them are some advanced animals, such as the octopus and squid.

Molluscs contains the following groups of animals :

1. Caudofoveata (deep-sea wormlike creatures; 70 known species)
2. Aplacophora (solenogasters, deep-sea wormlike creatures; 250 species)
3. Polyplacophora (chitons; 600 species, rocky marine shorelines)
4. Monoplacophora (deep-sea limpet-like creatures; 11 living species)
5. Bivalvia (also Pelecypoda) (clams, oysters, scallops, mussels; 8,000 species)
6. Scaphopoda (tusk shells; 350 species, all marine)
7. Gastropoda (Abalone, snails and slugs, limpets, sea hares; sea angel, sea butterfly, Sea Lemon; estimated 40,000 - 150,000 species)
8. Cephalopoda (squid, octopodes, nautilus, cuttlefish; 786 species, all marine)
9. Rostroconchia (fossils; probably more than 1,000 species; probable ancestors of bivalves)

The microstructure of mollusc shells, and especially abalone shells, are well studied, and got the attention of scientists and researchers from over the world. I want to point out that Abalone shells are different than bivalve shells, that the latter is composed of two parts, which are more or less symmetrical.

Mollusc nacre provides an example of a polycrystalline calcium carbonate biomineral with excellent mechanical properties. Despite having a very low organic content (1%), this material is superior to most other composite ceramics in stiffness, strength and toughness (Jackson et al., 1988, 1990); nacre is 3000 times more resistant to fracture

than a single crystal of pure aragonite (Currey, 1977). These properties can be attributed to the structural organisation of nacre, which comprises layers of interlocking aragonite platelets separated by a thin layer of organic material, which is explained hereafter. When a crack propagates through nacre it passes around the platelets by a tortuous path (Jackson et al., 1990; Wang et al., 1995), causing the plates to spring apart, and extending the organic sheets (Jackson et al., 1988; Wang et al., 1995). The organic *adhesive* between the plates appears to be key in the fracture resistance of this material (Wang et al., 1995; Currey et al., 2001), and elongates by pulling open folded domains and loops, or breaking interchain bonds (Smith et al., 1999).

Fig 5.6 (up) depicts a cross section near the growth front at the edge of the shell, illustrating the horizontal boundary plane which is adapted from Zaremba *et al.* (Zaremba et al., 1996). The outer layer is calcite and referred to as the prismatic layer due to the R3m (rhombohedral) symmetry of the calcite lattice. The prismatic layer, of thickness 0.5 - 3 mm, provides hardness to the exterior of the shell. The calcite crystals have dimensions of order 5×25 μm, and texture X-ray studies indicate the c-axis is preferentially oriented normal to the plane of the shell. Parallel to this prismatic layer is the mother-of pearl, or nacre. The nacreous layer of red abalone is assembled from flat platelets of aragonite (DiMasi and Sarikaya, 2004).

Aragonitic nacre comprises layers of tabular aragonite crystals which are separated by interlamellar organic sheets, and are further delineated laterally by vertical organic sheets, producing stacks of polygon shaped crystals (Weiner et al., 1983a; Weiner and Traub, 1980) as shown in fig 5.6 (down). In all mollusks the c axes of the aragonite tablets are oriented perpendicular to the shell surface, and the a and b axes of the crystals within a stack are co-aligned. The nacre is composed also of thin layers of β-chitin sandwiched between two thicker layers of silk-like proteins in a β-sheet conformation, onto which acidic macromolecules rich in aspartic acid are adsorbed (Nakahara et al., 1982; Weiner and Traub, 1984). The chitin polymers and the protein–polypeptide chains are orthogonally aligned, in a plywood-like construction. The fiber axis of the chitin and the silk proteins are perpendicular to each other and aligned with the a and b axes of the aragonite (Weiner and Traub, 1980; Weiner et al., 1983b). This well defined relationship between nascent crystals and the underlying organic matrix made mollusc shell nacre an excellent

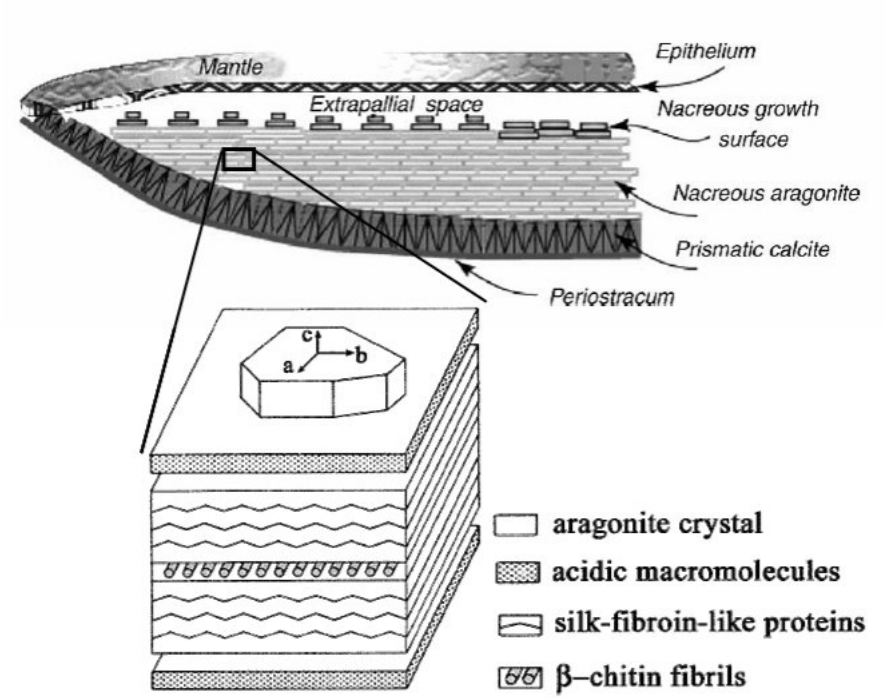

Fig. 5.6: Structure of typical mollusc shell :adapted from Zaremba et al. (Zaremba et al., 1996) (above). Schematic diagram of relationship between organic matrix and aragonite crystals in mollusc shell nacre: reprinted from Ref. (Lowenstam and Weiner, 1989) (down).

system in which to study biological control over nucleation. The interface region between the two layer has not been well characterized up to now.

The structure of the organic matrix appears to be the key in controlling the orientation of the aragonite crystals, due to the well defined spatial relationship between the matrix and inorganic crystal.

The biomineralized shells of mollusks mostly they mineralize with calcite or aragonite, but the third polymorph of CaCO3, vaterite, is found in the freshwater snail egg capsules of gastropods, which also precipitate goethite and opal in their radula. Further, weddellite $CaC_2O_4 \cdot 2H_2O$, fluorite CaF_2, and amorphous calcium phosphate are found in the gizzard plates of some species of gastropods.

Some mollusks possess an internal structure and not an outer shell. Cuttlefish (*Sepia officinalis*) has internal structure called cuttlebone, which is composed of calcium carbonate with elaborate macroporous architecture, to provide the cuttlefish with buoyancy. Buoyancy can be regulated – the cuttlefish can even decide to sink – by changing the gas-to-liquid ratio in the chambered cuttlebone. The structure consists of sheets of aragonitic calcium carbonate separated by pillars in a manner similar to an honeycomb (Birchall and Thomas, 1983; Seizen, 1986). The pillars are sigmoidal in crosssection. This provides maximum resistance to crushing with minimum mass of material. The complex inorganic structure is deposited on a preformed β-chitin template

Part II

Texture of Biological Materials

Chapter 6

Texture Measurements Using X-Ray Diffraction

6.1 Introduction

A considerable amounts of solid materials are crystalline, which means that their atoms or atom groups are arranged in periodic, three-dimensional crystal lattices. These crystalline solid materials can be of natural origin as, for example, geological and biological materials or they can be human-made as metals, ceramics or some polymers.

Generally saying, crystalline materials can be classified into two groups: polycrystalline or single crystal. The former is a material comprised of many crystals with different shape, size and orientation stacked to each other. The latter is a crystalline material that is made entirely of only one crystal of one phase and one orientation as well.

Polycrystalline materials can either be composed of a single phase or they may consist of different phases (such as composites like in our case) with different crystal structures and composition. Polycrystalline materials is basically built up of many grains with slight or big different crystal orientations. Most of naturally existing crystalline materials, but also those of technological significance, are polycrystalline polyphase materials. However, biological composites are different than fabricated and geological materials. They are composed

of at least two phases: organic fibrous phase, organic matrix filling the spaces between them, and can be associated with biominerals and/or mineral ions.

The physical properties of the polyphase polycrystalline materials depend on a large number of structural parameters. Information about the number and the volume fraction of constitutive phases, the size, shape and crystallographic orientation of the crystallites within each phase and boundary relations in neighbouring grains as well, are of fundamental importance to a comprehensive characteristic of the polycrystalline materials. Because of the statistical nature of the polycrystalline structure, appropriate structural parameters are also to be described by means of statistical distribution functions.

Microscopical methods, such as light microscopy and electron microscopy, are usually used to determine the grain size and the grain shape distributions, as well as the spatial arrangements of grains within a specimen. The same applies for structural fibers in biological nanocomposites to reveal the morphological texture of these materials. However, the orientation distribution of grains (how the atomic planes in a volume of grain are positioned) within a specimen is mainly determined in average by diffraction methods, especially by X-ray and neutron diffraction (high penetration), or in local using electron back-scattering diffraction.

Anisotropic properties are one of the characteristic of crystalline materials, as for example mechanical, electrical, magnetic, optic, acoustic or thermal properties. The resultant macroscopic property measured in a polycrystalline material is a mean value of the properties of the contained individual grains. It depends both on each grain property and on the orientation distribution of grains in the investigated material. In the case of random orientation distribution, partial anisotropies of individual crystallites are equalized and the material remains macroscopically quasi-isotropic, i.e. its physical properties are the same in any direction.

The anisotropic properties, especially the mechanical ones, of the polycrystalline materials are directly related to the crystallographic preferred orientation (texture) averaged over all its constituent grains. Therefore, the quantitative determination and interpretation of a preferred crystallite orientation in polycrystalline materials is very important in materials science and technology. By knowing and influencing the preferred orientation of crystallites (texture tai-

loring), materials with a particular type of anisotropy and required physical or technological properties can be designed and produced.

Furthermore, texture can reveal the history of the material, due to exhibiting a completely new texture after processes like deformation, recrystallization and phase transformation. This is of interest for geologists since it is fingerprinting history of the materials. Texture investigations performed on rocks and other minerals give informations about the origin, forming processes and evolution of the earth. However, this method can also reveal the biomineralization mechanism in explaining the control of the macromolecules on the orientation of the associated biominerals during biomineralization process as in the case of this study.

Texture studies are usually carried out by X-ray diffraction providing pole figures and being followed by the calculation of the orientation distribution function (ODF) of crystallites, if necessary. The next sections summerize the basics of texture analysis, which have been adapted to a large extent from the book "Introduction to Texture Analysis: Macrotexture, Microtexture and Orientation Mapping" (Randle and Engler, 2000) and "Texture Analysis in Materials Science" (Bunge, 1993).

6.2 Basic Concepts

The term "texture" is strongly related with a polycrystalline material consisting of individual grains (crystallites) with different spatial arrangements as well as different crystal orientations. The texture of a polycrystalline material is defined by the volume fraction of grains having the same orientation $\mathbf{g}$ with respect to a sample fixed reference system, Fig. 6.1.

The sample coordinate systems are usually chosen as right-handed Cartesian systems emphasizing the sample geometry which is related to its forming process or its natural shape. In rolled sheets of metals, for example, these are rolling, transverse and normal directions as appropriate coordinate axes. In biological materials, however, these are surface direction in case of flat shapes like the animal shells, added to axial and tangential direction like in the case of cylindrical shapes like femur bone.

The orientation of an individual crystallite within the investigated sample is then specified by the orientation g of its crystal axes with respect to the in advance chosen sample reference system, Fig. 6.1. The orientation distribution function (ODF) of the grains, however, can be defined either by the volume fraction $f^V(g)$ Eq.(6.1) or by the number fraction $f^N(g)$ Eq.6.2 of grains that have the orientation g within a certain orientation element dg.

$$\frac{dV(g)/V}{dg} = f^V(g) \tag{6.1}$$

$$\frac{dN(g)/N}{dg} = f^N(g) \tag{6.2}$$

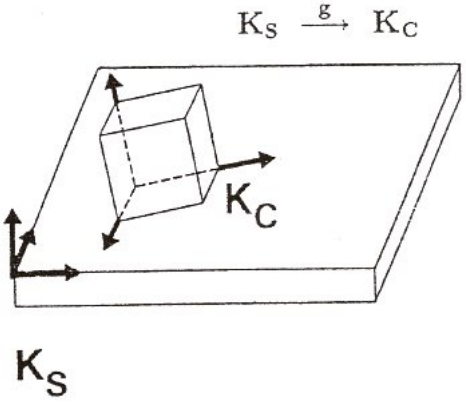

Fig. 6.1: The orientation g of the crystal coordinate system K_C with respect to the sample coordinate system K_S. Reprinted from (Bunge, 1993).

The texture function $f(g)$ is usually normalized in multiples of the random orientation density. In the case of the random distribution of orientations the normalization of the distribution function $f(g)$ can be expressed as follows:

$$f_{random}(g) \equiv 1 \tag{6.3}$$

This means that the integral over the complete orientation space is unity

$$\oint f(g)dg = 1 \tag{6.4}$$

The crystallographic orientation g and dg as well of an individual crystallite is defined by the orientation of its crystal coordinate system K_C with respect to the sample fixed coordinate system K_S as shown in Fig. 6.1.

Any sample orientation in space is defined by the sample direction $\vec{y}$ described in the sample coordinate system K_S. The sample direction is usually given by its Cartesian or spherical coordinates $y = [y_1, y_2, y_3] = \{\alpha, \beta\}$. A crystallite orientation in the sample is defined by the crystal direction $\vec{h}$ given in the crystal coordinate system K_C. The crystal direction is also described by Cartesian or spherical coordinates $h = [h_1, h_2, h_3] = \{\theta, \gamma\}$, Fig. 6.2. The orientation g of an individual crystallite is thus understood as a rotation bringing the movable sample coordinate system into coincidence with the crystal coordinate system.

$$K_C = g * K_S \qquad , \qquad K_S \xrightarrow{g} K_C \tag{6.5}$$

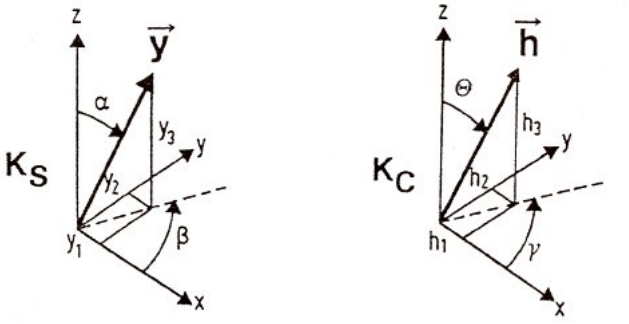

Fig. 6.2: Sample direction $\vec{y}$ specified in the sample coordinate system K_S, and crystal direction $\vec{h}$ specified in the crystal coordinate system K_C. Reprinted from (Bunge, 1993).

There are several ways how to specify the orientation g and hence of representing the orientation distribution function *f(g)*. For instance, by an orientation matrix $[g_{ij}]$, by crystallographic (Miller) indices

(hkl)[uvw], by spherical polar coordinates (Θ,Ψ,Ω), and by Eulerian angles $g\{\varphi_1, \Phi, \varphi_2\}$ which are described in Fig. 6.3.

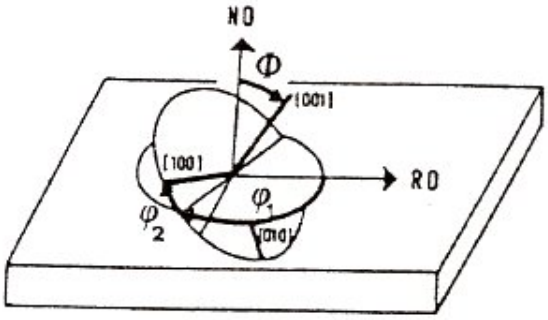

Fig. 6.3: Euler angles to describe the orientation g and hence of representing the orientation distribution function *f(g)*. Reprinted from (Bunge, 1993).

The orientation element dg is expressed in terms of the Eulerian angles (φ_1, Φ and φ_2) as follows

$$dg = \frac{1}{8\pi^2} sin\Phi \cdot d\varphi_1 d\Phi d\varphi_2 \tag{6.6}$$

Fig. 6.3 represents the Euler angles with respect to sample and crystal geometry. However, it is more convenient to plot the orientation parameters as three Cartesian coordinates in a three-dimensional space, which is then termed the orientation space (or Euler space), so that each orientation of the crystal coordinate system K_C is then represented uniquely by a point in this space, and vice versa. The totality of all individual orientations of several crystallites forms a "cloud" of orientation points, from which a continuous orientation distribution function may be obtained.

6.3 Texture Determination

In practice, the most frequently used method of texture determination is that of pole figure measurement followed by pole figure inversion resulting in the orientation distribution function (ODF) f(g).

Pole figures are being measured by X-ray diffraction both in the reflection and the transmission mode using flat compact samples with an appropriate thickness.

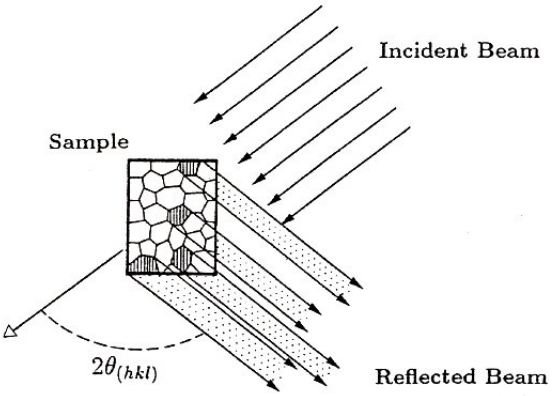

Fig. 6.4: X-ray diffraction in a polycrystalline sample. Reprinted from (Bunge, 1993).

X-ray can be diffracted at a certain lattice plane if Bragg's law is fulfilled (the diffracted beam is measured at an angle $2\theta_{(hkl)}$ corresponding to the lattice plane (hkl), Fig. 6.4), so that the normal direction to the plane (hkl) is the bisectrix between the incident and diffracted beam (the diffraction vector $\vec{s}$).

Pole figures are measures of preferred orientations of crystallites expressed as continuous density distributions of certain (hkl)-poles represented either on the pole sphere or in some projection to the equatorial plane, e.g. the stereographic projection as shown in Fig. 6.5.

The pole density in the sample direction $\vec{y}$ is parallel to the bisectrix $\vec{s}$, which may be represented, for example, by the polar coordinates α and β referred to the sample coordinate system K_S

$$\frac{dV}{V} = P_{hkl}(y)dy; \qquad \begin{cases} y = \{\alpha, \beta\} \\ \mathrm{d}y = sin\alpha \, \mathrm{d}\alpha \, \mathrm{d}\beta \end{cases}$$

here dy is the solid angular element on the pole sphere surrounding the sample direction. This function is called the (hkl)-pole density

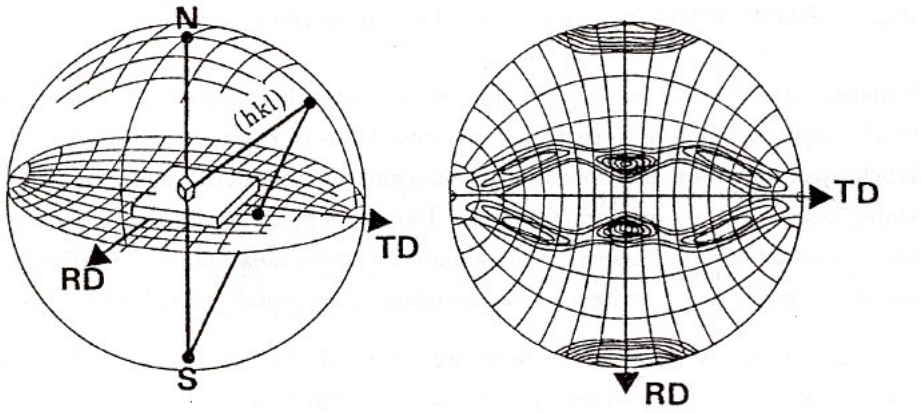

Fig. 6.5: The direction $\vec{h} \perp (hkl)$ on the pole sphere and its stereographic projection (left), and pole density distribution in the stereographic projection (right). Reprinted from (Bunge, 1993).

function. Pole figures are two-dimensional functions, only, but there is one such function for each crystallographic plane (hkl).

The pole density distribution $P_{(hkl)}(\alpha, \beta)$ is obtained in the measurement as the ratios of the reflected intensity to the constant intensity of the incident beam in dependence on the sample orientation. The reflected intensity is then directly proportional to the volume fraction of crystallites being in reflection position.

A pole figure is an integral (two-dimensional projection) of the three-dimensional texture function $f(g)$ taken over all orientations for which the crystal direction $\vec{h}$ is parallel to the sample direction $\vec{y}$

$$P_{(hkl)}(\alpha, \beta) = \frac{1}{2\pi} \int\limits_{\vec{h} \parallel \vec{y}} f(g) d\psi = \frac{1}{2\pi} \int\limits_{(\vec{hkl}) \parallel (\vec{\alpha}, \vec{\beta})} f(\varphi_1, \Phi, \varphi_2) d\psi \quad (6.7)$$

where ψ is a rotation about the diffraction direction $\vec{s} \parallel \vec{h} \parallel \vec{y}$. The above equation is fundamental equation of texture analysis, from which the orientation distribution function (ODF) f(g) can be calculated.

In case of using area detector in the transmission method, it measures a diffracted intensity $I_{(hkl)}(\alpha, \beta)$ over the whole cone (Debye-Scherrer ring) which is proportional to the volume fraction of crystals fulfilling this reflection condition

$$I_{(hkl)}(\alpha, \beta) = N_{(hkl)} \cdot P(hkl)(\alpha, \beta) \tag{6.8}$$

where $N_{(hkl)}$ is a normalization factor depending on the intensity of the incident beam $I_\circ$, on the irradiated sample volume and the beam divergence, as well as on the reflectivity of the given lattice plane (hkl). The above equation is the basis of experimental texture analysis in case of X-ray diffraction.

With the normalization condition Eq.(6.3), the normalization factor $N_{(hkl)}$ can be determined from the whole pole figure according to Eq.(6.2).

$$N_{(hkl)} = \frac{1}{2\pi} \oint I_{(hkl)}(\alpha, \beta) \cdot sin\alpha \, d\alpha \, d\beta \tag{6.9}$$

The orientation distribution function $f(g)$ can then be calculated by measuring the intensity $I_{(hkl)}(\alpha, \beta)$ for several (hkl) according to Eq.(6.8) and solving Eq.(6.9).

6.4 Texture Measurements by X-ray Diffraction

X-ray texture measurements can be carried out either in the reflection or in the transmission mode which are both illustrated in Fig. 6.6.

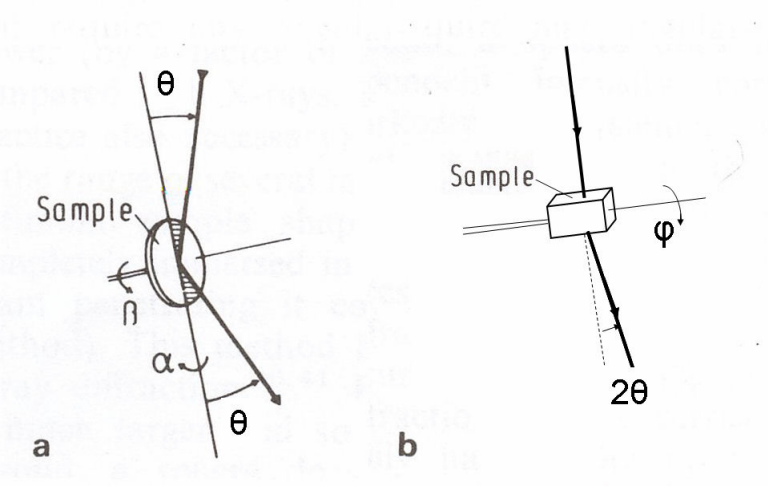

Fig. 6.6: *a* X-ray reflection (Reprinted from (Bunge, 1993)) and *b* transmission geometry.

Before performing texture measurement, it is necessary to know the crystal structure (lattice constants and symmetry) of the phases contained in the specimen, in order to achieve a correct identification, indexing, and separating (if necessary) of the X-ray peaks occurs in the diffraction profiles. X-ray attenuation length for the material of the specimen also should be calculated for absorption correction in case of reflection technique, and in order to choose the right sample size in case of transmission.

In order to measure pole figures in reflection mode using area detector, it is necessary to adjust it at the angle with respect to the incident beam and then to rotate the sample through at least two angles in order to make all sample directions $\vec{y}$ successively parallel to the bisectrix direction $\vec{s}$. Hence, at least a three-circle diffractometer is needed for pole figure measurements. Modern texture goniometers mostly use the geometry of the so-called "Eulerian cra-

dle", Fig. 6.7, which allows a sample rotation through three angles ω, χ, Φ. These texture goniometers are thus four-circle diffractometers (four angles θ, ω, χ, Φ) which are identical, in principle, with the four-circle diffractometers used in single-crystal structure analysis.

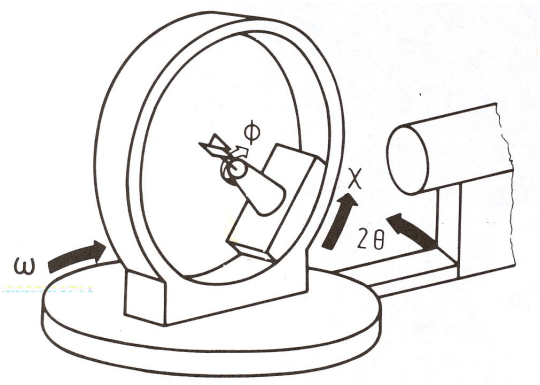

Fig. 6.7: Geometry of Eulerian cradle and the angles $\theta, \omega, \chi, and \Phi$. Reprinted from (Bunge, 1993).

The measured intensity values are in general not yet pole density values. They have to be corrected for background scattering, absorption, defocusing, and peak separation if needed. This can be carried out in the controlling computer immediately after measurement, and finally, the data can be plotted in the form of pole density charts in any desired projection (e.g. the stereographic projection mostly used in metallurgy or the equal area projection frequently used in mineralogical applications.)

In reflection technique only part of the whole pole figure can be obtained, the ranges being limited by either incident or reflected beam (or both) becoming nearly parallel to the sample surface, see Fig. 6.8

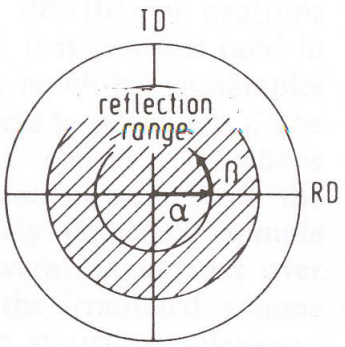

Fig. 6.8: Incomplete pole figures measured using reflection technique. Reprented from (Bunge, 1993).

Chapter 7

Texture of Biological Materials

7.1 Introduction

Texture research up to now has focused on engineering and earth materials such as metals, ceramics, polymers and rocks more than on natural (biological) materials. However, there is increasing awareness that texture is significant in organisms' hard tissues, where texturing has a direct mechanical support function and organisms optimize texture patterns for particular environments. Crystallographic texture in biological materials are a new field of endeavour, with a few quantitative investigations (Lowenstam, 1989; Raabe et al., 2005a).

Recently, many studies concentrated on the highly mineralized skeletons like bone and mollusc shells. These studies lead to more advancement of functional biomaterials with demanded mechanical properties. Texturing is important in bone implants of titanium alloy, for example, as was documented by Benmarouane using a neutron diffraction to inspect the reorganisation of the apatite (Ap) crystallite distribution after implantation (Benmarouane et al., 2005). His study suggests that the orientation of apatite crystallites at the interface with an implant depends on the coating of the surface of the implant. Surface coating can reduce significantly the rejection rate of implants, therefore the apatite coating on titanium alloy should possess a very good combination of biocompability and mechanical

properties, which reveals that it is necessary to cover implants with apatites.

Here we will briefly summarize the orientation of the biominerals and their associated organic matrix in bone and molusc inspired by successful studies and outstanding literature.

7.2 Orientation of Apatites in Bone

The apatite exists mainly as long needle-shaped crystallites which are approximately 300-1000 Å in length and 25-75 Å in diameter, but also exists in the amorphous state $\sim$ 35 to 45% of the mineral is amorphous in adult bone (Matsushima et al., 1982). The bone mineral is basically apatite with variable amounts of OH (hydroxyapatite) and CO_3 (carbonated apatite or dahllite). We refer to it as apatite in what follows.

Because the function of the bone is primarily mechanical, it is very important to determine the orientation of the mineral in macroscopic bone samples. Indeed, it provides an index to the distribution of stress in the bones.

Quantitative texture and microstructure characterization is needed to gain a meaningful understanding of the relationship between bone structure and strength, because both crystallographic texture (the c-axis representing the weak elastic direction) and grain morphology (elongated platelets) influence mechanical properties (Wenk and Van-Houtte, 2004), for example, the angular dependence of mechanical properties of plexiform bone is explained by the distribution of bone mineral orientation and its morphology (Sasaki et al., 1991).

A quantitative texture characterization is feasible if presently available methods are adapted for the special features of bone like synchrotron radiation. Since the structure of bone and teeth is locally very heterogeneous and crystallite size is very small, only with the advent of microfocus X-ray beams at synchrotron sources these materials become accessible to quantitative analysis usinf wide angle and small angle X-ray scattering (Wenk and Van-Houtte, 2004; Fratzl et al., 1997).

The preferred arrangement of the c-axis of biological apatite crystallites in some calcified tissues was evaluated using the wide-angle

X-ray diffraction technique, which includes three dimensional pole figure analysis (Chen and Gundjian, 1974; Nightingale and Lewis, 1971; Sasaki et al., 1989; Sasaki and Sudoh, 1997) and the neutron diffraction technique (Bacon et al., 1979, 1980; Bacon and Griffiths, 1985).

The qualitative results indicate a strong alignment of apatite c-axes parallel to the long axis of bones. Earlier studies have even documented a secondary maximum of c-axes perpendicular to the longitudinal direction and parallel to the bone surface (Sasaki et al., 1991, 1989) but only one study of a bovine ankle bone has so far documented complete rotational freedom of c-axes about the normal surface (Wenk and Heidelbach, 1999).

I will present here an overview on the orientation of apatites in bone supported by some pole figures inspired by recent studies using μ-beam X-ray diffraction.

Lonardelli *et al.* 2005 (Lonardelli et al., 2005) Figure 7.1 shows a c-axis pole figure of apatite in a well-preserved dinosaur tendon, with a very strong crystallite alignment.

Lonardelli used Rietveld method to extract information on crystal structure, texture and microstructure directly from two-dimensional synchrotron diffraction images. This is advantageous over conventional texture analysis that relies on individual diffraction peaks, particularly for low-symmetry materials with many overlapping peaks and images with a poor peak-to-background ratio.

In Lonardelli's study, Rietveld method was applied to two mineralized biological samples with hydroxylapatite fabrics: an ossified pachycephalosaurid dinosaur tendon and an Atlantic salmon scale. Both are measured using monochromatic synchrotron X-rays. The dinosaur tendon has very strongly oriented crystals with c-axes parallel to the tendon direction. The salmon scale displays a weak texture.

Nakano *et al.* 2002 (Nakano et al., 2002) Preferential orientation of biological apatite crystallites in typical calcified tissues of rabbit ulna, rabbit skull, and monkey dentulous mandible was investigated using a microbeam X-ray diffractometer, with a beam spot

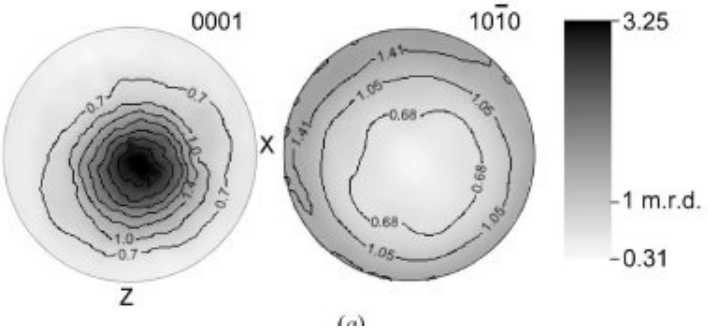

Fig. 7.1: Pole figures of hexagonal apatite in tissue of a dinosaur tendon. The texture was measured by synchrotron radiation and analysed with the Rietveld method (Lonardelli et al., 2005). The tendon axis is in the centre of the pole figure. Contour levels logarithmic; some are indicated (maximum 3.2 m.r.d.). Equal area projection (Lonardelli et al., 2005).

of 100 *mu*m in diameter, to clarify relationship between the apatite orientation and mechanical function.

Preferential alignment of apatites varied depending on the shape and stress condition in vivo. The *c*-axes of biological apatite in the rabbit ulna and the rabbit skull bone were preferentially observed as a one-dimensional orientation along the longitudinal axis and a two-dimensional orientation along the surface, respectively.

Precise analysis of the preferential alignment along the skull surface showed an elliptical distribution of the *c*-axis aligned along the suture inside the skull surface of both lamina exterior and interior. The *c*-axis of biological apatite in a monkey dentulous mandible basically aligned along the mesiodistal direction in the flat bone, but this alignment changed along the normal direction to the flat bone surface parallel to the biting direction near the tooth, due to the force of mastication.

Wenk and Heidelbach 1999 (Wenk and Heidelbach, 1999) While in turkey tendon c-axes of pseudohexagonal needleshaped apatite crystals are aligned parallel to the tendon axis, a bovine ankle bone displays a strong alignment of *c*-axes parallel to the surface of the bone (Wenk and Heidelbach, 1999).

In the study of Wenk and Heidelbach, methods of quantitative X-ray texture analysis were used to determine the orientation distribution and texture strength of apatite in a calcified turkey tendon and in trabecular and cortical regions of osteonal bovine ankle bone (metacarpus) using a 2 or 10 μm synchrotron microfocus X-ray beam (λ= 0.78 Å), to resolve local heterogeneity.

Both samples revealed a strong texture. In the case of turkey tendon, 12 times more c-axes of hexagonal apatite were parallel to the fibril axis than perpendicular to it, and a-axes had rotational freedom about the c-axis, Fig. 7.2a. In bovine bone, the orientation density of the c-axes was three times higher parallel to the bone surface (that is, parallel to the collagen fibril directiono) than perpendicular to it, and there was no preferential alignment with respect to the long axis of the bone (fiber texture), Fig. 7.2b. Whereas half of the apatite crystallites were strongly oriented, the remaining half had a random orientation distribution. This conclusion was observed consistently when referred to microscopic internal surfaces, even though the 2 and 10 μm beam documented much heterogeneity.

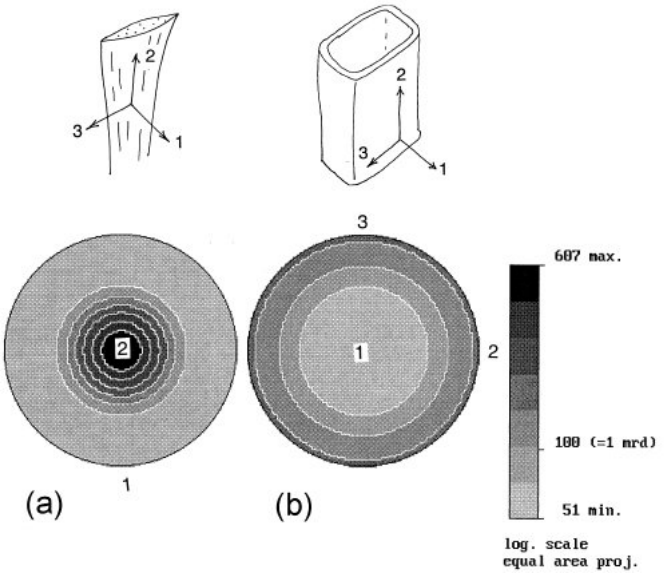

Fig. 7.2: The (001) pole figures (c-axis) of apatite in turkey tendon (a) and cow bone (b). Compare the direction numbers with the corresponding illustration of the sample defining the directions (Wenk and Heidelbach, 1999).

Sasaki *et al.* (Sasaki and Sudoh, 1997) X-ray pole figure analysis was performed on apatite crystals in bone mineral and collagen molecules in the bone matrix. The c-axis of apatite and the helical axis of the collagen molecule have strongly preferred orientations in a direction parallel to the bone axis. However, the c-axis of apatite has an appreciable pole density peak also in the radial and tangential direction of the bone, whereas collagen molecules were almost uniaxially oriented in the bone axis direction though having an appreciable distribution, see Fig 7.3.

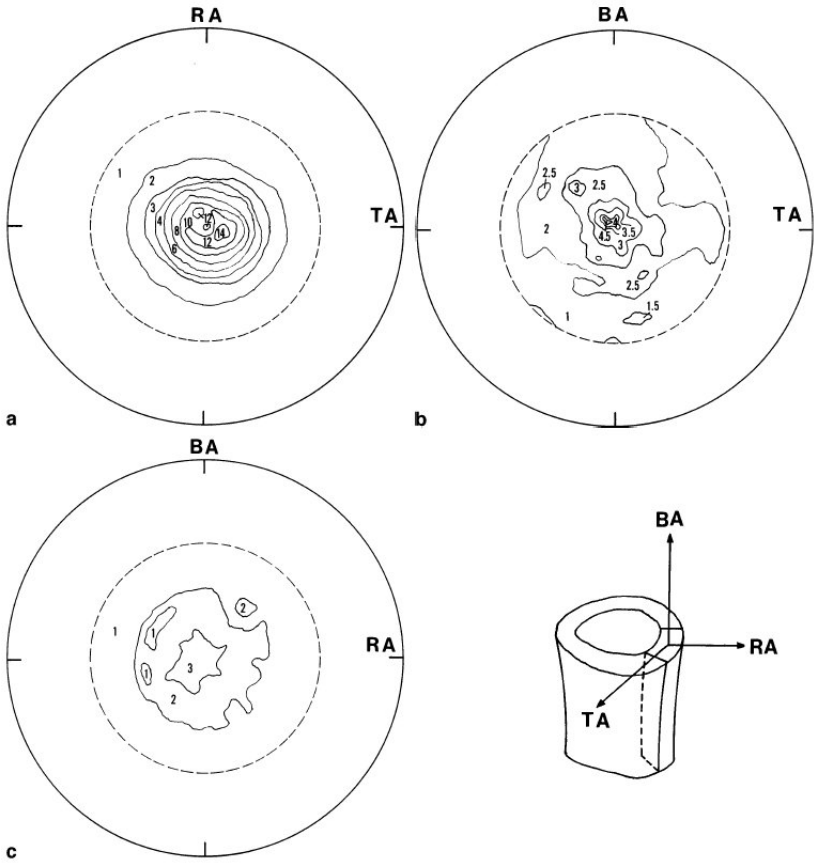

Fig. 7.3: (0002) pole figure of apatite crystal in bovine bone mineral measured for (a) BA, (b) RA, and (c) TA surfaces based on the Cartesian coordinate system chosen for cortical bone specimens (right down) (Sasaki and Sudoh, 1997).

7.3 Orientation of Calcite, Aragonite, and β-Chitin in Abalone Shell

In section 5.2 we explained in details the microstructure of abalone shells. One of the recent texture studies on the orientation of calcite and aragonite in mollusk shells was done by DiMasi and Sarikaya (DiMasi and Sarikaya, 2004) on Red abalone using synchrotron microbeam X-ray diffraction and electron microscopy observations near the nacre/prismatic interface of red abalone shell.

Long calcite grains impinge the nacre-prismatic boundary at 45° angles, suggestive of nucleation on (104) planes followed by growth along the c-axis of both, see Fig. 7.4. In the region within 100 μm of the boundary, calcite and aragonite crystals lose their bulk orientational order, but no evidence for qualitative changes in long range order such as ideal powder texture or an amorphous structure factor.

In Red abalone, the c-axes of the calcite prisms and aragonite tablets are oriented perpendicular to the shell surface, and the a and b-axes of the crystals within a stack are co-aligned. The chitin polymers and the proteinÚ-polypeptide chains are orthogonally aligned, in a plywood-like construction. The aragonite crystals nucleate at specific sites on the predeposited matrix such that the a and b-axes of the aragonite lattice are aligned with the directions of the chitin fibres and the protein fibres respectively.

Chateigner *et al.* used X-ray diffraction to characterise textures of the aragonite layers of shells from different species in mollusk group: monoplacophoras, bivalves, cephalopods and gastropods. He found that textures vary in strength, pattern and through the thickness of the shells (Chateigner et al., 2000). He also compared the texture patterns exhibited in the studied taxa, which can be quantitatively described by a limited number of parameters, with the microstructure types observed with scanning electron microscopy. There are a wide variety of texture patterns and some systematic trends for the araganoitic layers from different species. Fig. 7.5 shows {001} and {100} pole figures of the inner radial crossed lamellar layer of Cyclophorus woodianus. c-axis is found to be perpindicular to the shell surface as explained above, but in these species of molluscs, a-axis is not co-aligned as in Red Abalone, but has a single crystal pattern.

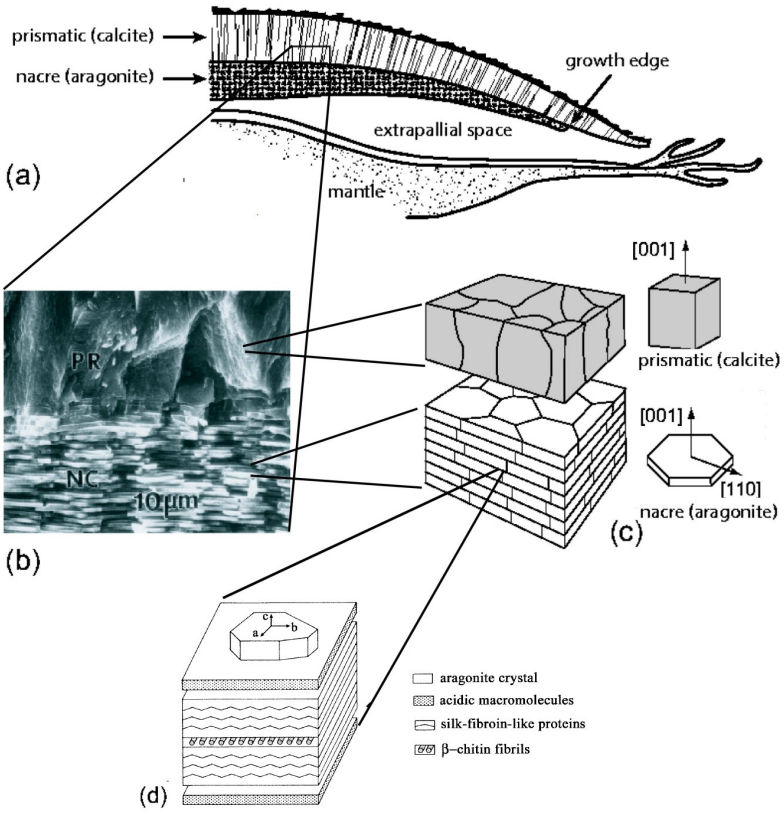

Fig. 7.4: (a) Red abalone shell cross section, showing the relationships between the mineralized layers and soft tissue in the vicinity of the growth edge, where new layers of nacre are deposited onto the prismatic layer making up the exterior of the shell. The vertical scale is exaggerated in the drawing. (b) SEM micrograph (secondary electron image) from fractured shell sample, showing prismatic (PR) and nacreous (NC) regions near the nacre-prismatic boundary. From Ref. (Jackson et al., 1988). (c) Idealized depiction of the crystal alignment and morphology in the prismatic and nacre regions: calcite crystals with dimensions ≥ 20 μm, aligned with c-axis normal to the interface; and aragonite platelets 10 μm across and 0.4 μm thick, also with c-axis normal to the interface. (d) Schematic diagram of relationship between organic matrix and aragonite crystals in mollusk shell nacre: adapted from Ref. (Lowenstam, 1989).

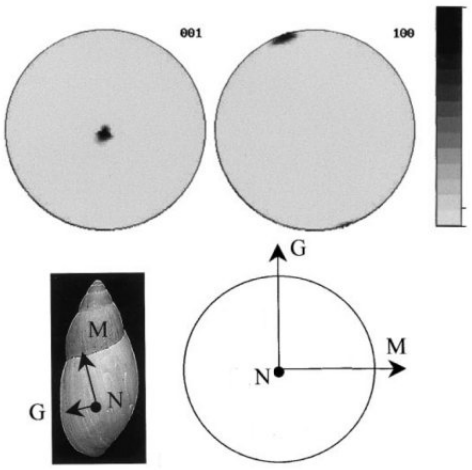

Fig. 7.5: (above) {001} and {100} pole figures of the inner radial crossed lamellar layer of *Cyclophorus woodianus* (max . 100 m.r.d., min . 0). Logarithmic density scale, equal area projection. (down) Sample reference.

7.4 Orientation of Apatite and β-chitin in Lingula shell

Unlike other invertebrates such arthropods and molluscs which mineralize calcium carbonates in their skeletal materials, Lingula (*Brachiopoda*) has shells composed of calcium phosphates (apatites). It is a unique case of apatite mineralization as exoskeleton.

Lingula is often considered a *living-fossil* based on its supposed lengthy morphological conservatism owing to its absence of evolution, and its remarkable survival for more than 550 million years (Chapman, 1914). Nevertheless, it was reported recently that Lingula is not a living-fossil (Eming, 2003).

The shell of Lingula unguis is composed of apatite and an organic matrix. The apatite crystals precipitate in the organic scaffold, forming consecutive mineralized and organic layers to produce a laminated structure with improved mechanical properties. The organic matrix is constituted mainly of β-chitin. The degree of orientation of apatite showed correlation to that of β-chitin, the fiber axis of β-chitin being parallel to the c axis of apatite. Furthermore, close relation-

ship of unit cell dimensions of chitin and apatite indicates that the fibrous structure of the organic matrix may play a role in assisting the orientation of the apatite crystals (Iijima and Moriwaki, 1990).

Part III

Experimental Setup and Procedure

Chapter 8

Materials and Methods

8.1 Sample Preparation

Specimens of cuticle were dissected from different parts of the crab *Cancer pagurus*, lobster *Homarus americanus*, and horseshoe crab *Limulus polyphemus* which are shown in Fig. 8.1. For pole figure measurements, samples were prepared immediately after sacrificing the animal by cutting rectangular pieces of the following dimensions (1x1x10 mm) with a jewelers saw. The further procedure consisted in washing in distilled water for 5 seconds, rinsing in 100% methanol for 5 seconds and placing them in Eppendorf caps to be stored at a temperature of -70°C.

The low temperature storage before the actual measurements is required for suppressing any non-biological crystallization effects of a possible amorphous calcium carbonate (ACC). This will avoid also any natural decaying effects of the polymer-protein matrix. So that, all specimens were kept at that temperature except for the time of the actual synchrotron measurement which required about 40 - 120 minutes.

Microstructural analysis was conducted on dry specimens which were dissected mainly from different locations in the american lobster and edible crab cuticle. We used an adult american lobster (Homarus americanus) in intermolt stage acquired from a local seafood supplier. The samples for scanning electron microscopy (SEM) were air-dried and cleaved either perpendicular to the cuticle surface in order to

Fig. 8.1: Lobster *Homarus americanus*) (top), crab (*Cancer pagurus*) (middle) and horseshoe crab *Limulus polyphemus* (bottom) which were used for samples source for X-ray crystallographic texture measurements and scanning electron microscopy.

expose the cross section or parallel to the surface in areas exposing either exo- or endocuticle. The obtained samples were sputter-coated with 5 nm of gold. Contrast and brightness of the digital images were adjusted where necessary using Adobe Photoshop CS2 (Adobe Inc.)

8.2 Experimental Setup and Procedure

Preferred orientation of crystals (crystallographic texture) in polycrystalline materials can be measured by X-ray diffraction using specific Bragg reflections, as explained in details in section 6.4. The experiments for this study were performed employing synchrotron X-ray beam of a wavelength of λ= 0.8 Å in the transmission mode (illustrated schematically in Fig. 8.2) at the BL9-beamline of the DELTA synchrotron facility (Dortmund, Germany), Figs. 8.6 and 8.7, and the SCD-beamline (former PX) of the ANKA synchrotron facility (Karlsruhe, Germany), Figs. 8.4 and 8.5. The basic idea of the trasmission method technique was introduced a long time ago with photographic film as the only available area detector at that time (Wenk, 1965).

Fig. 8.2 shows some of the experimental details and the sample coordinates which were used as reference system for the specimen selected from the exoskeleton, to be used later as a pole figure coordinate system. The initial position of the sample should be identical for all measured samples in order to retain the same pole figure dimensions for all samples.

Basically, diffracted monochromatic X-rays from a polycrystalline material describe a cone for each lattice plane *(hkl)*, Fig. 8.3, and these cones of variable intensity according to the texture. These cones are recorded by an area detector as circles (Debye-Scherrer rings). For a given sample orientation, a ring contains diffractions from those crystallites that had lattice planes inclined by θ to the primary beam (θ is the Bragg angle). The radii depend on θ and, therefore, on the interplanar spacing d. If crystallites are randomly oriented relative to the axis of the primary beam, the rings showes uniform intensity. If a preferred orientation distribution occurs, then there is a change of intensity along the Debye-Scherrer ring.

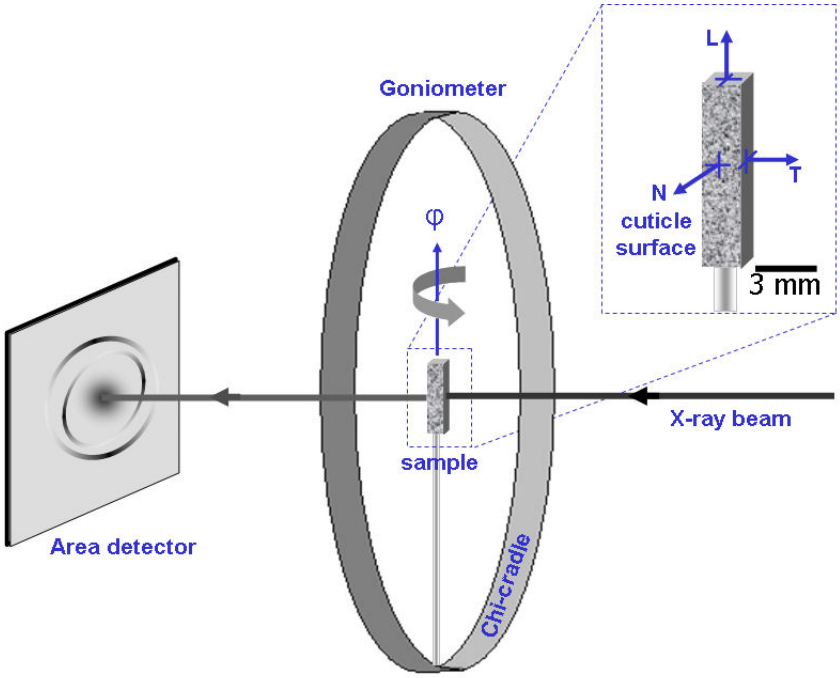

Fig. 8.2: Geometry of the X-ray setup used for pole figure measurements. The detailed sample part indicates the sample local coordinates, L: longitudinal direction, T: transverse direction, and N: cuticle surface direction.

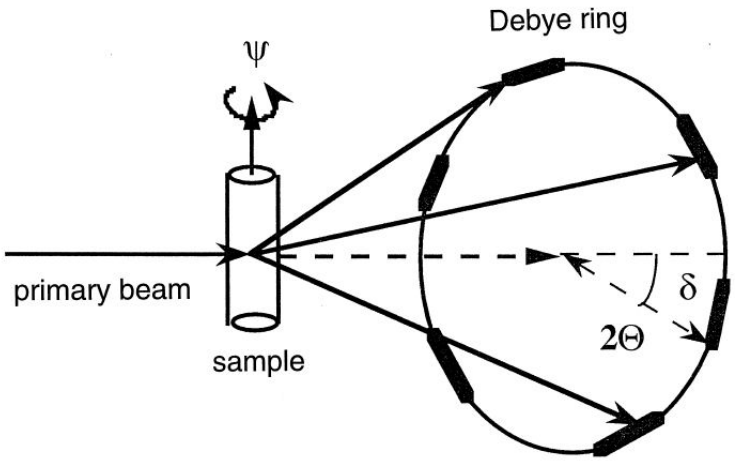

Fig. 8.3: Schematic illustration of the diffraction experiment with primary monochromatic beam, sample, and diffraction ring. Adapted from (Wenk and Heidelbach, 1999).

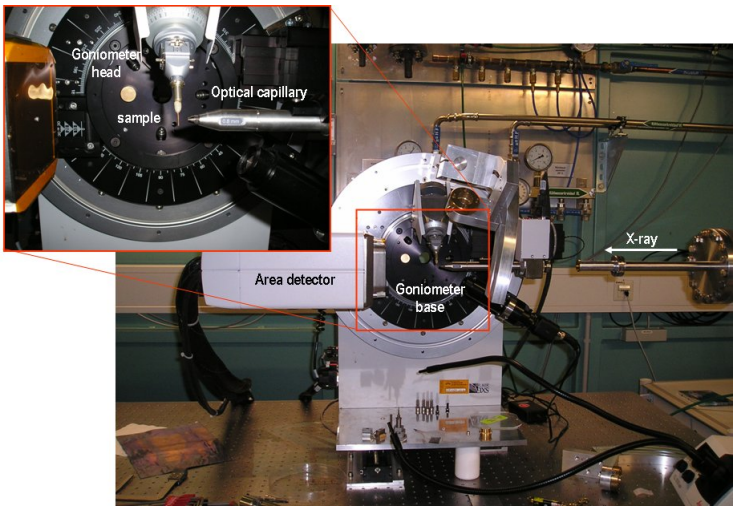

Fig. 8.4: Experimental end-station of the SCD-beamline at ANKA synchrotron/Karlsruhe.

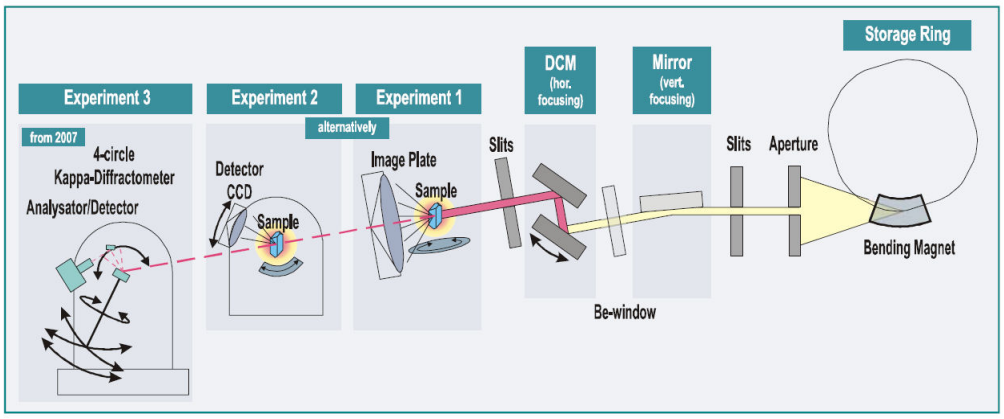

Fig. 8.5: Schematic layout of the SCD beamline (former PX) at ANKA synchrotron/Karlsruhe. Adapted from (Baumbach et al., 2006).

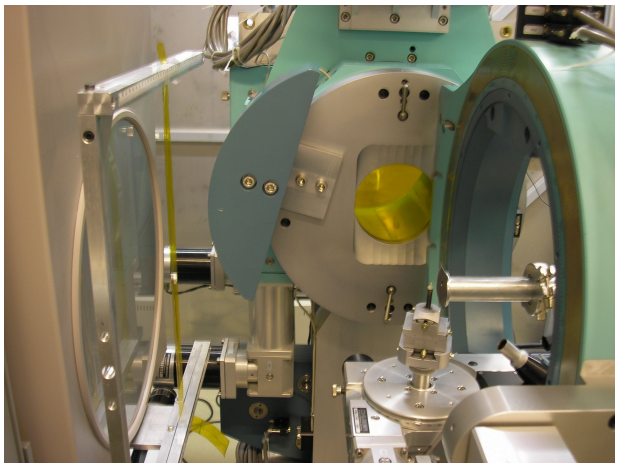

Fig. 8.6: Experimental end-station of the BL9-beamline at DELTA synchrotron facility in Dortmund.

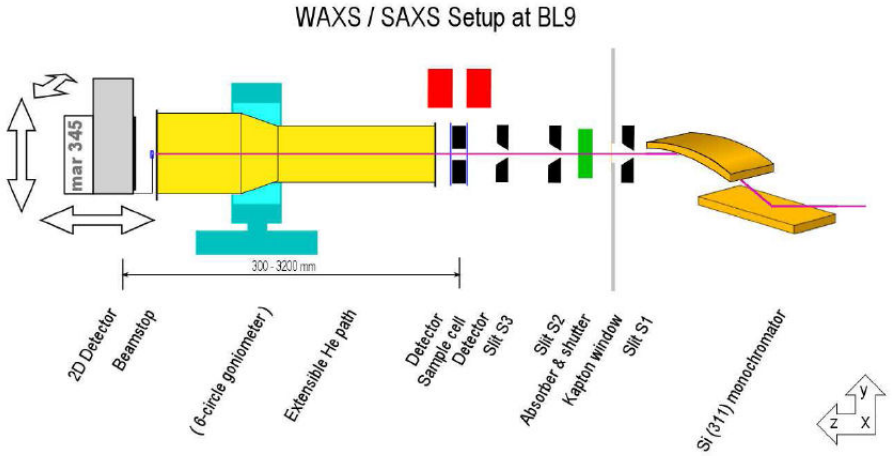

Fig. 8.7: Outline of the experimental setup on the BL9-beamline at DELTA synchrotron facility in Dortmund with the sample mounted at maximum sample-to-detector distance. For wide angle X-ray scattering, the detector can be placed closer to the sample and the helium path can be reduced in length. Adapted from (Krywka et al., 2006).

For pole figure measurements on edible crab and horseshoe crab cuticle samples, we used the BL9-beamline (DELTA synchrotron facility), while for the lobster cuticle samples, we used the SCD-beamline (ANKA synchrotron facility).

At the BL-9 beamline (DELTA) (Krywka et al., 2006), amples were mounted vertically on the goniometer head in a six-circle Euler cradle equipped with a MAR-345 area detector perpendicular to the primary beam, while at the SCD beamline (ANKA), samples were mounted in a three-circle diffractometer with a fixed chi (54.7°) equipped with a CCD area detector mounted also perpendicular to the primary beam, Fig. 8.2. The data set recorded for each sample consisted of a series of frames recorded with a MAR-345 (or CCD) detector for a sequence of rotations, from 0° to 180° in 60 steps, around the φ axis (sample L-axis), as defined in Fig. 8.2. Exposure time for each frame ranged from 60 to 180 seconds.

8.3 Data Analysis

The center position of the detector image and the positions of Debye-Scherrer rings (hkl) were determined using MarView or Fit2d (Hammersley AP, 1994), developed by MAR-Rreaserch and ESRF (European Synchrotron Radiation Facility), respectively . Then Debye-Scherrer rings were read-out from detector images (see Fig. 9.1) collected during sample rotation. The detector images are converted to ASCII format using *marcvt* developed by MARreaserch for MAR-images, and using *xconv* developed by CCP13.

The data reduction procedure for obtaining intensities was performed only on the interesting Debye-Scherrer rings using a program written by Sangbong Yi (Yi, 2005). After background correction, a reduced file for each different types of lattice planes is written separately. Then, the intensities in the reduced files are corrected according to the decay of incident beams' intensity, called logfile correction, since the intensity of the incident beam decreases continually with decay of the accelerating particles in the storage ring.

The data achieved from the above steps are expressed by laboratory coordinate in terms of the angles describing the sample position and diffraction geometry, $\{\chi, \varphi, \omega\}$ and $\{\gamma, \theta\}$, respectively. The description on the Euler cradle angles, $\{\chi, \varphi\}$, is found in Chapter 6. The laboratory coordinate should be converted into the pole figure angles $\{\alpha, \beta\}$ for representing pole figure, pole distance α and azimuth angle β. The final step is the determination of the ODF from a set of (hkl) pole figures. The pole figure should be expressed in one of the standard regular distributions in α, β, e.g. 5° x 5° or even finer grids.

Fig. 8.8 shows an example of the data points represented on a pole figure. The measured data points are distributed according to regular $\{\omega, \gamma\}$ angles, while the interpolated one has a regular distribution on $\{\alpha, \beta\}$ grid. Usually intensity along γ is collected in every 1°, however, 3° of γ-step is applied in Fig. 8.8(a) for the graphical representation.

The following reflections were chosen for the pole figure analysis: (020) (b-axis), (021) and (013) for α-chitin reflections and (00.6)(c-axis) and (10.4) for calcite in crab and lobster, respectively (Fig. 9.2 and Fig. 9.1).

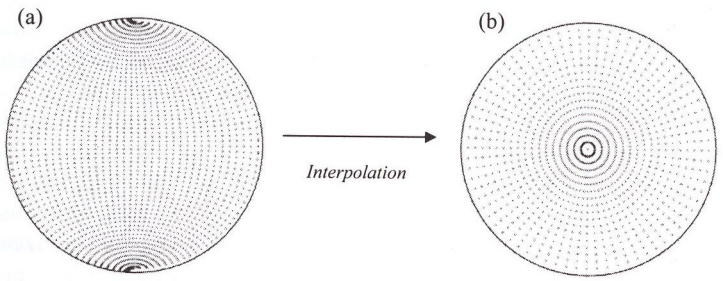

Fig. 8.8: The data points represented on a pole figure; (a) measured one presented on regular $\{\omega, \gamma\}$ with 5° x 3° steps and (b) after interpolation on regular $\{\alpha, \beta\}$ with 5° x 5° steps. Adapted from (Yi, 2005).

Pole figures are stereographic projections showing the density of crystallographic pole of certain planes as a function of the sample geometry, and so provide a good method of representing orientation. The scattering intensity is measured as a function of two angular coordinates, α and β, which is corresponding to radial (declinational) and circumferential (azimuthal) coordinates, respectively, in a polar net (Fig. 8.8(b)).

If the crystallite orientation is completely random, the poles will be scattered all over the polar net. If the orientation is present, on the other hand, the poles will tend to be concentrated in certain areas within the polar net and the remaining areas will be completely unpopulated.

Part IV

Results and Discussion

Chapter 9

Experimental Results and Discussion

9.1 X-ray Diffraction From Calcite and α-Chitin

Since α-chitin is an organic biopolymer and has a large unit cell, it diffracts poorly and only at relatively low 2θ angles, whereas calcite, with its highly ordered three-dimensional lattice structure and small unit cell (at least in two dimensions), diffracts very strongly at higher 2θ angles, as observed in the diffractogram of lobster and crab shells (see Fig. 9.2).

Furthermore, the crystallographic interplanar spacings d of α-chitin are in close proximity, causing overlapping diffraction peaks. This made the analysis of diffraction patterns rather difficult. The synchrotron diffractogram given in Fig. 9.1 indicates the challenge of separating a sufficiently large number of corresponding diffraction peaks at an accuracy which suffices for pole figures reproduction. The main diffraction peaks for α-chitin observed in the diffraction patterns are (020), (021), (002), (110) and (013).

According to the present X-ray diffractograms of crab and lobster, Fig. 9.2, one can deduce that the mineral part in crab cuticle is composed mainly of calcite and minute chitin. However, the lobster cuticle contains only small portion of calcite but large amounts of

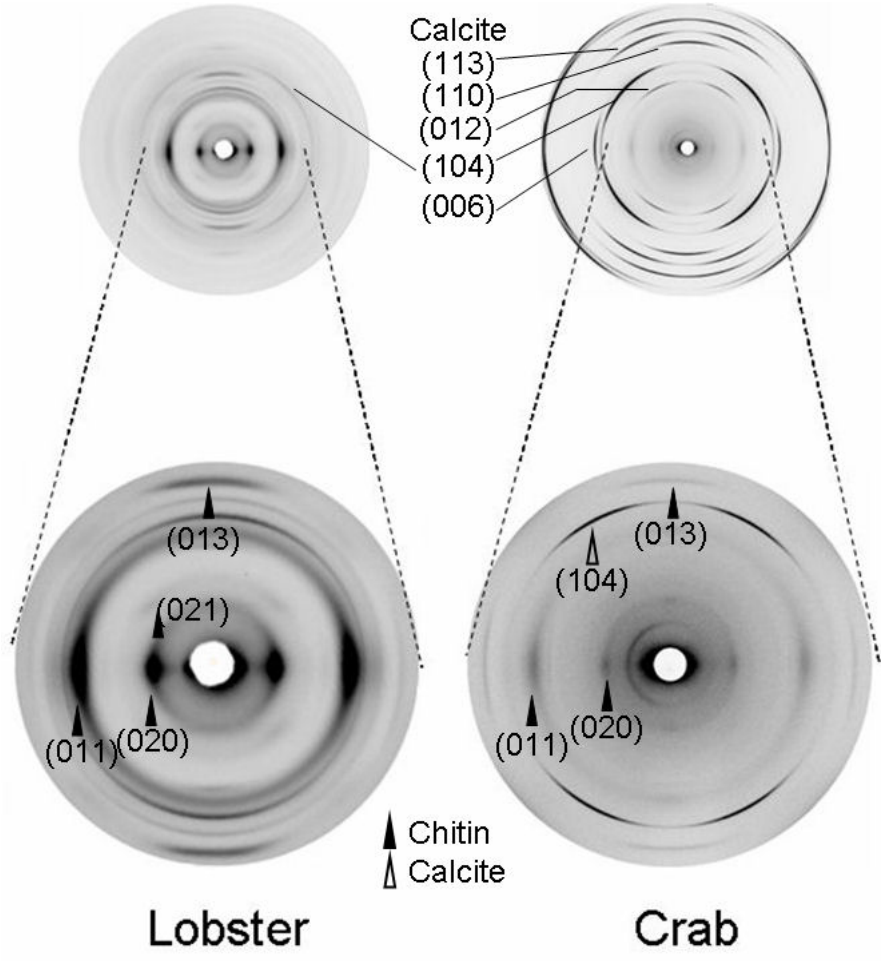

Fig. 9.1: X-ray diffraction patterns of lobster (a) and crab shell (b) showing the X-ray Debye-Scherrer rings of α-chitin and calcite. These patterns were obtained when the X-ray beam is normal to the cuticle surface normal. The detailed patterns show the inner Debye-Scherrer rings whih belongs mostly to α-chitin.

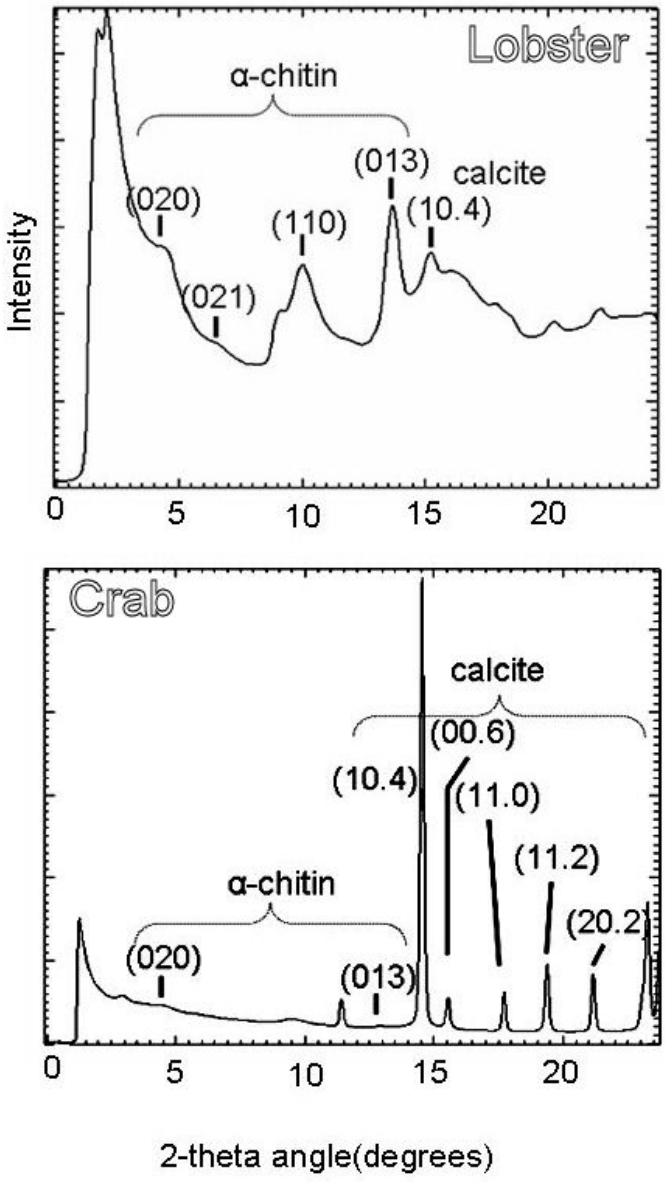

Fig. 9.2: X-ray diffraction diffractogram of the lobster (a) and the crab cuicle (b) showing the X-ray reflections of α-chitin and calcite (only in crab). The baseline rise in the X-ray profile from lobster shell is attributed to an amorphous phase (mostly ACC).

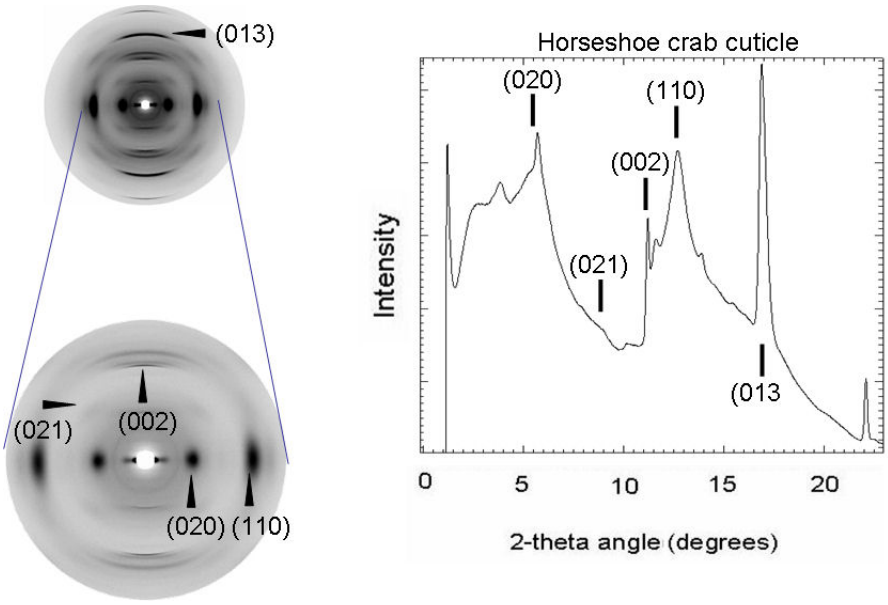

Fig. 9.3: X-ray diffraction diffractogram of the horseshoe crab cuticle showing the X-ray reflections of α-chitin.

amorphous calcium carbonate (ACC). ACC appeared as a large intensity halo in the diffraction pattern and as a base-line rise in the diffractogram for the lobster cuticle, matching earlier observations on the crustacean *Orchestia cavimana* (Raz et al., 2002), Fig. 9.4. The halo of the ACC created difficulties in the identification of reliable peak position for calcite in the lobster cuticle, so that, only {10.4}-calcite pole figures in lobster were reproduced. From those samples where a sufficiently large amount of crystalline calcite was found, such as in the tail and in the carapace parts of the lobster, the orientation relationship between the α-chitin and the calcite was studied (see section 9.5. Fig. 9.3 shows the diffraction pattern from the horseshoe crab cuticle and its corresponding diffractogram. It reveals that the horseshoe crab cuticle contains only a α-chitin fibers but no crystalline minerals.

One reflection of the α-chitin was sometimes mis-interpreted as (110) in earlier X-ray studies on α-chitin (Cardenas et al., 2004; Zhang et al., 2000; Takai et al., 1992), Fig. 9.5. It has similar corresponding interplaner spacing d as (040) and occurs together with (020) on the same equatorial X-ray diffraction intensities. Morover, our current crystallographic texture measurements show that the distribution of

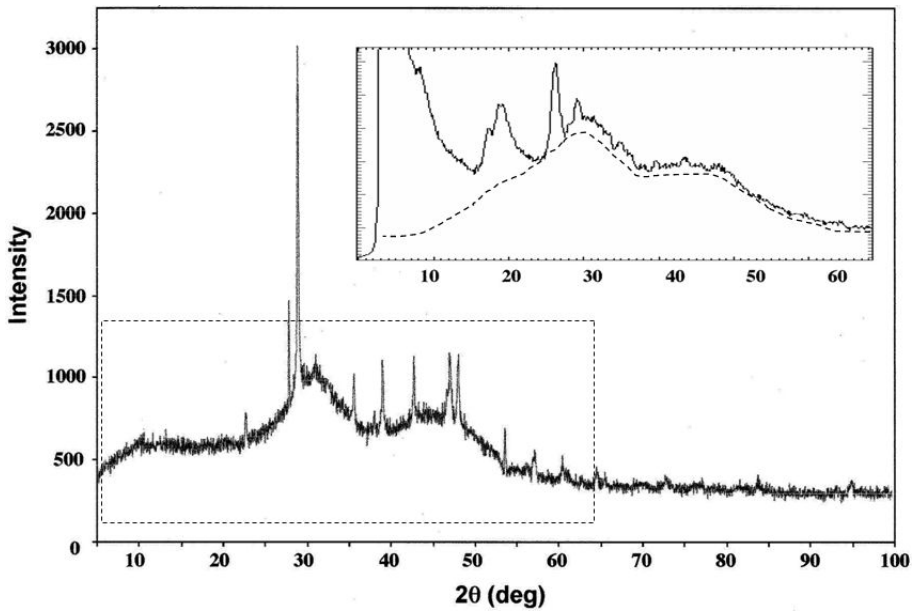

Fig. 9.4: X-ray diffractogram of the *Orchestia* calcareous concretions (Raz et al., 2002). The detailed diffractogram belongs to X-ray diffractogram of the lobster cuticle. The lobster cuticle and the *Orchestia* calcareous concretions contain big amounts of ACC which appeared as a large intensity halo in the diffraction pattern and as a base-line rise in the diffractogram for the lobster cuticle.

the poles in the (110) projection matches that of the poles in the (020) projection confirming the assumption that the peak may indeed be assigned to the (040) lattice plane. On the contrary, and according to the calculated diffraction pattern of α-chitin, the (040) reflection should be weak and cannot be stronger than the (020) one. We, hence, avoided using this reflection in our data processing.

9.2 Microstructure and Crystallographic Texture of the Arthropod Cuticle

The tissue of the exo- and the endocuticle of the lobster *Homarus americanus* and crab *Cancer pagurus* consists at the mesoscale level (μm-regime) of a three dimensional complex woven α-chitin-protein fiber network (Bouligand, 1972; Giraud-Guille, 1998). Fig. 9.6 show

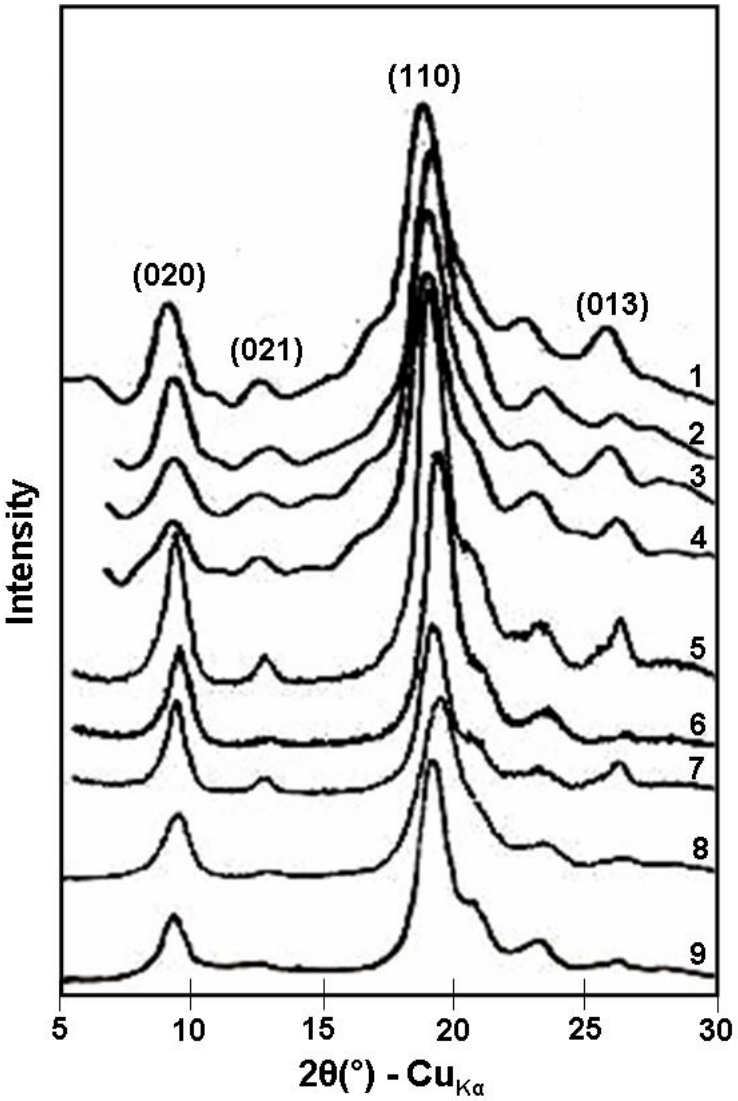

Fig. 9.5: X-ray diffraction patterns of α-chitin isolated from six references and from different arthropod's. 1) shrimp, 2) prawn, 3) lobster, 4) king crab (Cardenas et al., 2004), 5) beetle larva cuticles, 6) silkworm pupa exuvia, 7) shrimp (Zhang et al., 2000), 8) shrimp (Andrade et al., 2002), 9) crab (Takai et al., 1992).

an SEM micrograph of the structure network where the samples is cross section cuts from the crusher claw of lobster (Raabe et al., 2006).

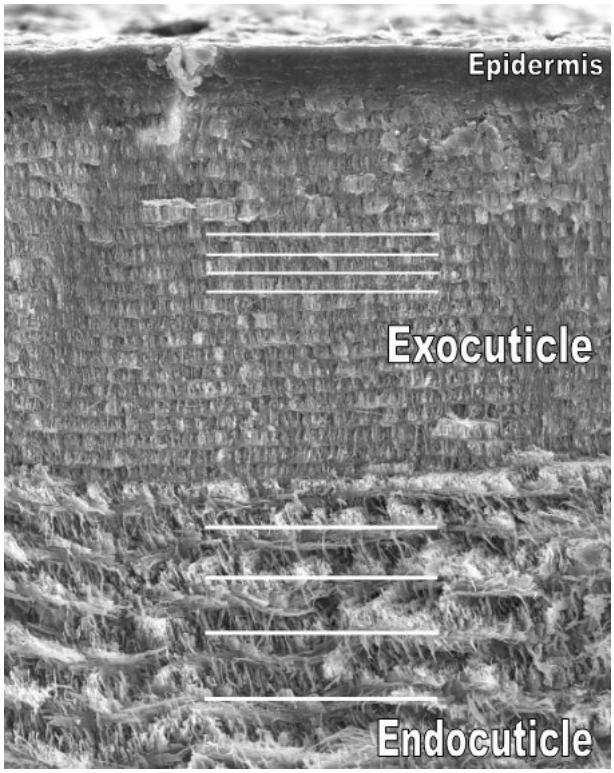

Fig. 9.6: Scanning electron micrograph of a cross section through the cuticle showing the epicuticle, the exocuticle and the endocuticle of the exoskeleton of the lobster Homarus americanus (Raabe et al., 2006).

The micrograph show that both endo- and exocuticle comprise from lamellae parallel to each other firstly and to the surface secondly. These lamellae show twisted plywood-type pattern of the α-chitin-protein fiber planes, which is a characteristic of the cuticle of arthropods (Bouligand, 1972; Giraud-Guille, 1998). According to Bouligand (Bouligand, 1972), such lamella consist of helicoidal stacks of α-chitin-protein planes that are gradually rotated about their normal axis, Fig. 9.6.

Figs. 9.9 and 9.10 show the twisted-plywood arrangement of the honeycomb α-chitin-protein fibers in lobster and crab cuticle, re-

spectively. The fiber orientation is parallel to the cuticle surface, and gradually rotates along the normal direction. The thick lamellae visible particularly in Fig. 9.6 are referred to as twisted plywood lamellae. According to the work of Giraud-Guille and Bouligand, the flat building units of one lamella through the thickness of the cuticle are planar α-chitin-protein fibers (Figs. 9.7 and 9.8).

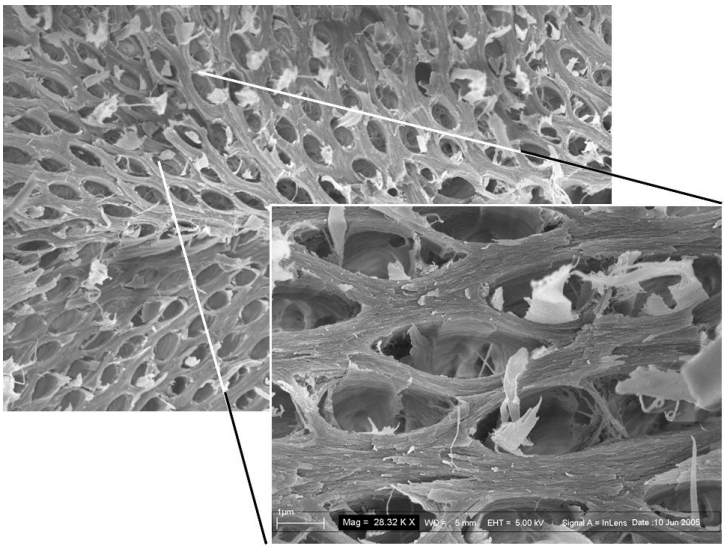

Fig. 9.7: High resolution SEM micrographs of the lobster cuticle showing the architecture of the chitin-protein fibers forming the honeycomb structure. It also shows the residues of the soft hose like structures in the pore canals of the honeycomb layers (Raabe et al., 2006).

The thickness of the plywood lamellae corresponds to the stacking height of the α-chitin-protein planes that is required for an accumulated total rotation of 180° about their normal direction, Figs. 9.9, 9.10 and 9.6 (Raabe et al., 2006).

Besides these basic features of the inner structure of the twisted plywood pattern, Fig. 9.6 also reveals structural difference between the exo- and the endocuticle; the density of the α-chitin-protein stacks is different in the two regions. This observation was confirmed for different cutting directions. Fig. 9.6 shows that the exocuticle has much finer twisted plywood-type mesostructure than the endocuticle. The stacks density in lobster is $\sim$ 15-20 μm for the exocuticle and $\sim$ 30-40 for the endocuticle.

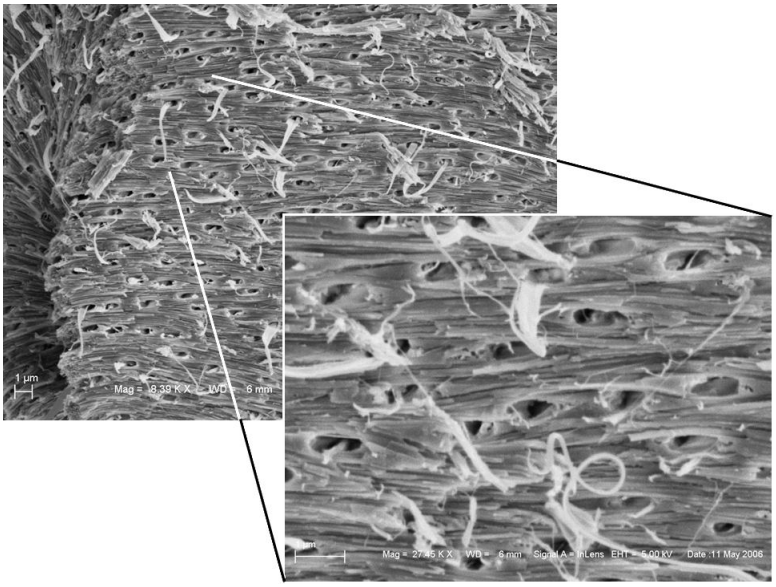

Fig. 9.8: SEM micrographs showing of the crab cuticle the architecture of the chitin-protein fibers forming the honeycomb structure. It also shows the residues of the soft hose like structures in the pore canals of the honeycomb layers (Raabe et al., 2006).

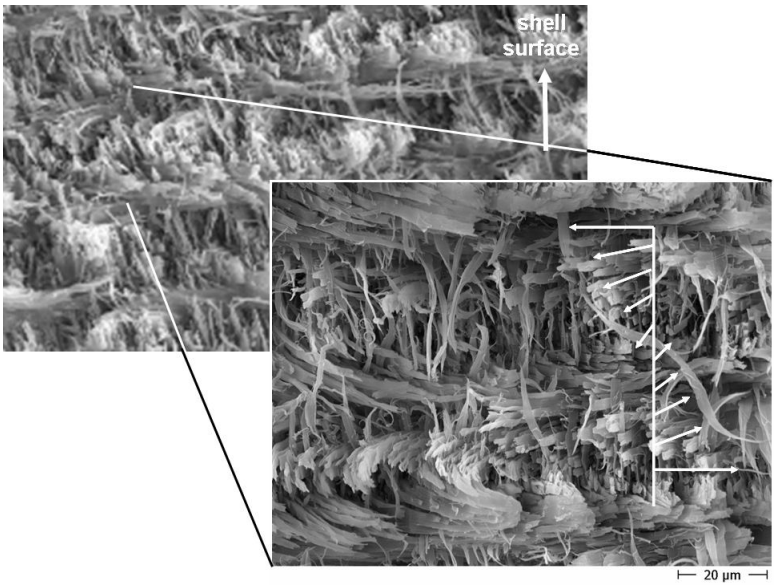

Fig. 9.9: Cross section SEM image showing the plywood structure in lobster cuticle (Raabe et al., 2006).

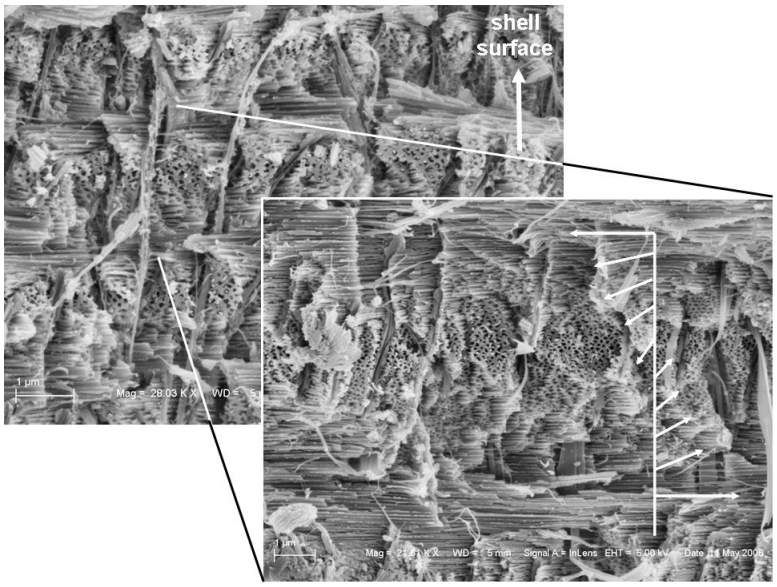

Fig. 9.10: Cross section SEM image showing the plywood structure in crab cuticle (Raabe et al., 2006).

Another interesting feature is the presence of long hose-like structures in the holes of the honeycomb structure (Figs. 9.7 and 9.8). Judging from the poor preservation and shrinkage of these structures especially in the samples prepared for SEM, they seem to be of rather soft consistence and thus not mineralized.

It is conceivable that the role of these hose-like structures could be the transport of calcium and carbonate through the cuticle for hardening it after the molt of the animals. Similar pore canal systems have been described for other species of decapod crustaceans before (Travis, 1963). They play a role in the transport of calcium ions during the mineralization of the exoskeleton after the molt. Such ion transport systems would be advantageous for large arthropods with thick cuticles where large amounts of mineral have to be deposited in order to harden the cuticle in a relatively short period of time.

Applying synchrotron wide angle x-ray diffraction on arthropod cuticle is necessary for a more detailed study of the arrangement of the nanofibrils within the mesostructure. The advantage of this approach is that the nanofibrils are crystalline, i.e. the polysaccharide molecules arranged in the form of the α-chitin phase. Furthermore, the elongated crystalline arrangement of the molecules within the

nanofibrils means that their crystallographic orientation distribution reflects also the topological orientation distribution of their longitudinal axis. Only when discussing rotations of the crystalline nanofibrils about their common longitudinal axis one has to carefully distinguish between the crystallographic and the topological orientation.

Fig. 9.11 shows the crystallographic texture of the α-chitin. The data are presented as four pole figures, {020} and {013} for lobster and crab cuticle. These pole figure were processed after background correction, normalization, and volume correction. The reference system of coordinates for the projection of the three pole figures is the normal direction of the cuticle surface (vertical direction in pole figure) the longitudinal direction which is parallel to the axis of the cheliped, and the transverse direction within the cuticle cross section.

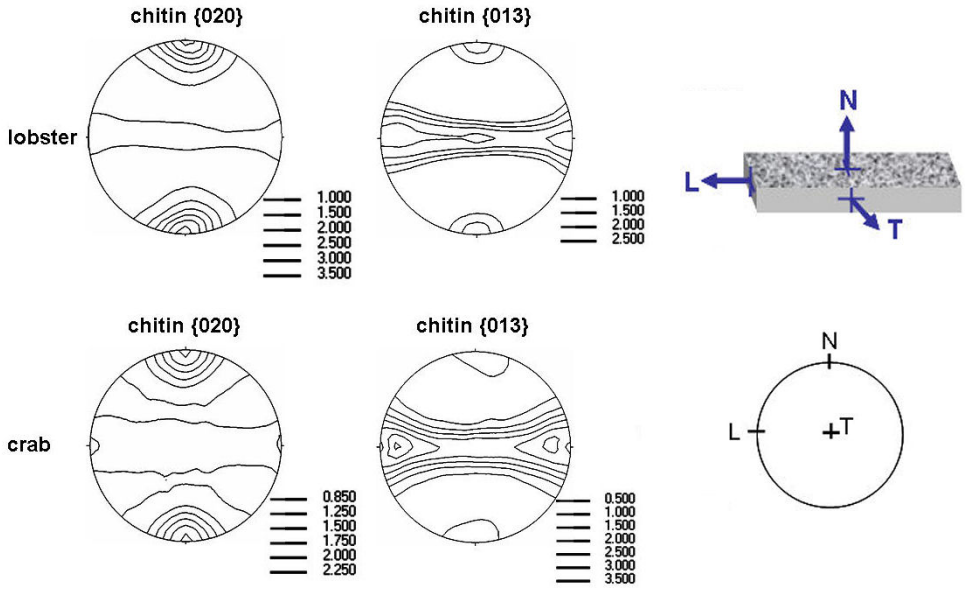

Fig. 9.11: Pole figures of the α-chitin of a sample taken from the left cheliped of the american lobster *Homarus americanus* and the carapace of the edible crab *Cancer pagurus*. The reference system of coordinates for the projection of the two pole figures is the normal direction of the claw surface (upper direction in pole figure) the longitudinal direction which is parallel to the axis of the cheliped, and the transverse direction within the cuticle cross section.

The crystallographic orientation distribution of the α-chitin-protein network in lobster and crab cuticle, Fig. 9.11, is characterized by various distinct features. First, it reveals a pronounced fiber texture with a very strong crystallographic <020>fiber axis parallel to the surface normal axis of the cuticle (see {020} pole figure in 9.11). This means that a large volume fraction of the α-chitin crystals is oriented in such a way that the long b-axis of their unit cell points towards the surface of the exoskeleton as shown in Fig. 9.12. This observation corresponds to the {013} pole figure which reveals a strong center fiber in the equatorial plane of the projection matching the 90° orientation relationship between the b-axis and the c-axis of the orthorhombic unit cell. This part of the texture analysis supports the observation of a very strong alignment of the α-chitin fibers parallel to the surface of the cuticle in a twisted plywood pattern, as mentioned in the beginning of this section, which is drawn from the fact that the crystallographic orientation of the c-axis is in the case of the α-chitin crystals strictly equivalent to the topographical orientation of the longitudinal axis of the α-chitin-fibers.

Second, another less pronounced crystallographic fiber is visible both, in the {020} and {013} pole figures. It reveals that a second weaker fiber texture exists, which is characterized by the alignment of fibers not only parallel (as in the case of the first strong fiber texture) but also perpendicular to the surface, Fig. 9.12. This observation suggests that the α-chitin-protein network reveals not only a main fiber orientation parallel to the surface but contains also some interpenetrating fibers perpendicular to the surface. The coincidence with the presence of hose-like structures in the pore canals of the honeycomb shaped α-chitin-protein planes indicates that the walls of these structures are at least partially composed of α-chitin fibers oriented longitudinally to the long axis of the canals. Another possibility could be that parts of the fibrous network filling the spaces of the canals consist of α-chitin.

9.3 Orientation of α-Chitin in Lobster

Fig. 9.14 gives a survey of the complete sets of the {020} and {013} synchrotron pole figures for the orthorhombic α-chitin which were determined for different parts of the lobster exoskeleton. Specimens were taken from the mineralized part of the cuticle (L_1, L_2, L_3, R_1,

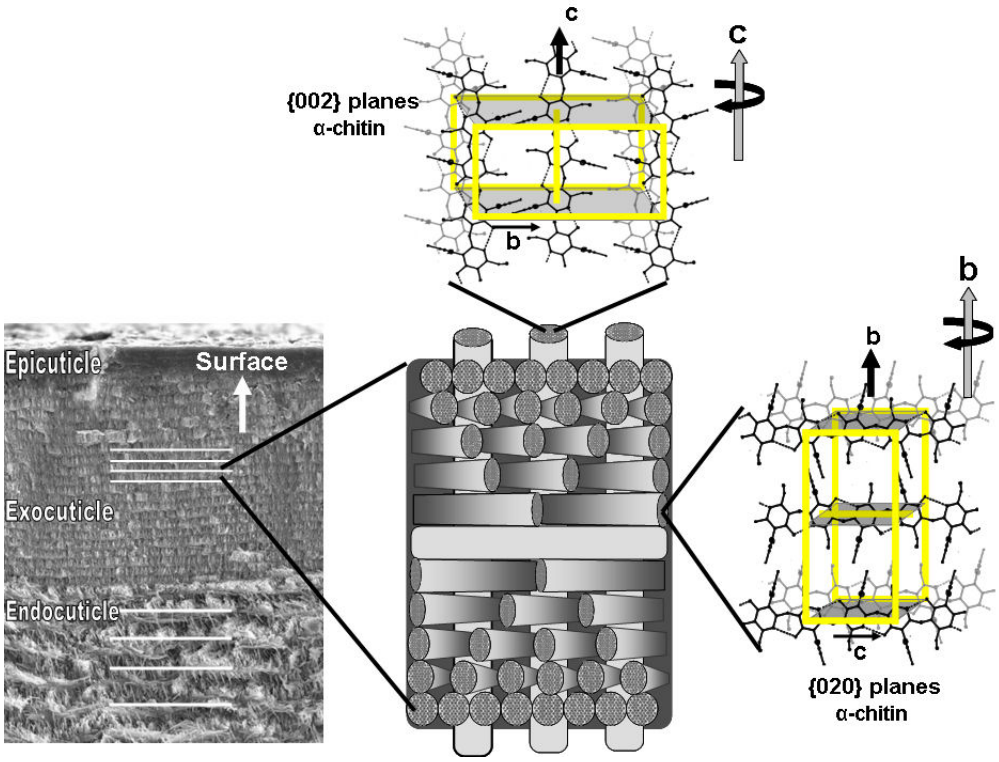

Fig. 9.12: The crystallographic texture of α-chitin in lobster and crab cuticle is characterized by two fiber texture components.

R_2, R_3, R_4, C_1, C_2, C_3, A_1, T_1, T_2). The annex m indicates that the sample was extracted from a soft membranous or respectively telson area (A_m, R_m).

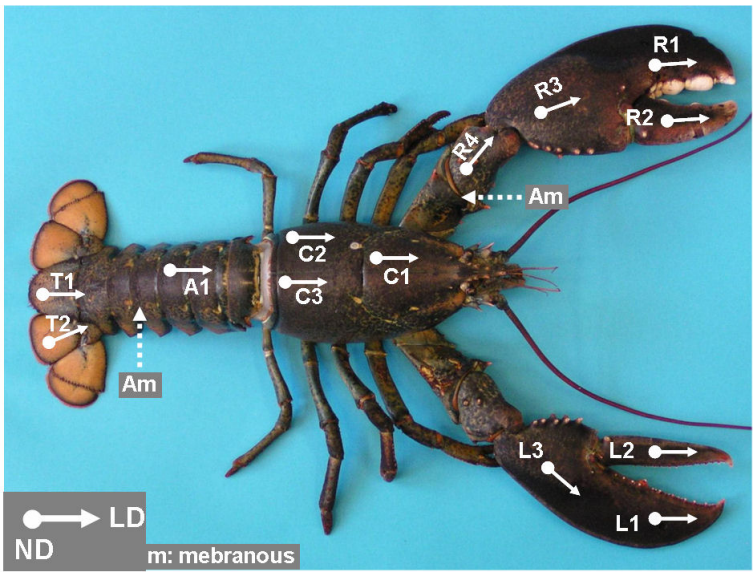

Fig. 9.13: Sample positions and the local reference systems defined for each specimen that was selected from the lobster cuticle for texture measurements. LD: longitudinal reference direction; ND: reference direction normal to the local sample surface; TD: transverse direction.

The {020} projection indicates the distribution of the longest crystallographic axis of the lattice cell (b=18.86 Å), while the {013} projection indicates the approximate distribution of the α-chitin chain axis (c=10.32 Å). The local reference system used for each pole figure is given in each figure. The projection plane is set up be the normal and the longitudinal directions. This projection was chosen to better elucidate the presence of the two most relevant fiber texture components, namely, of the strong <020>fiber texture component parallel to the normal direction (<020>// ND) and of the weaker <002>fiber texture component parallel to the normal direction (<002>// ND), explained in the last section.

The texture of the α-chitin in the lobster cuticle is characterized by the fact that all pole figures taken from the different regions of the cuticle reveal a pronounced fiber texture which is characterized by

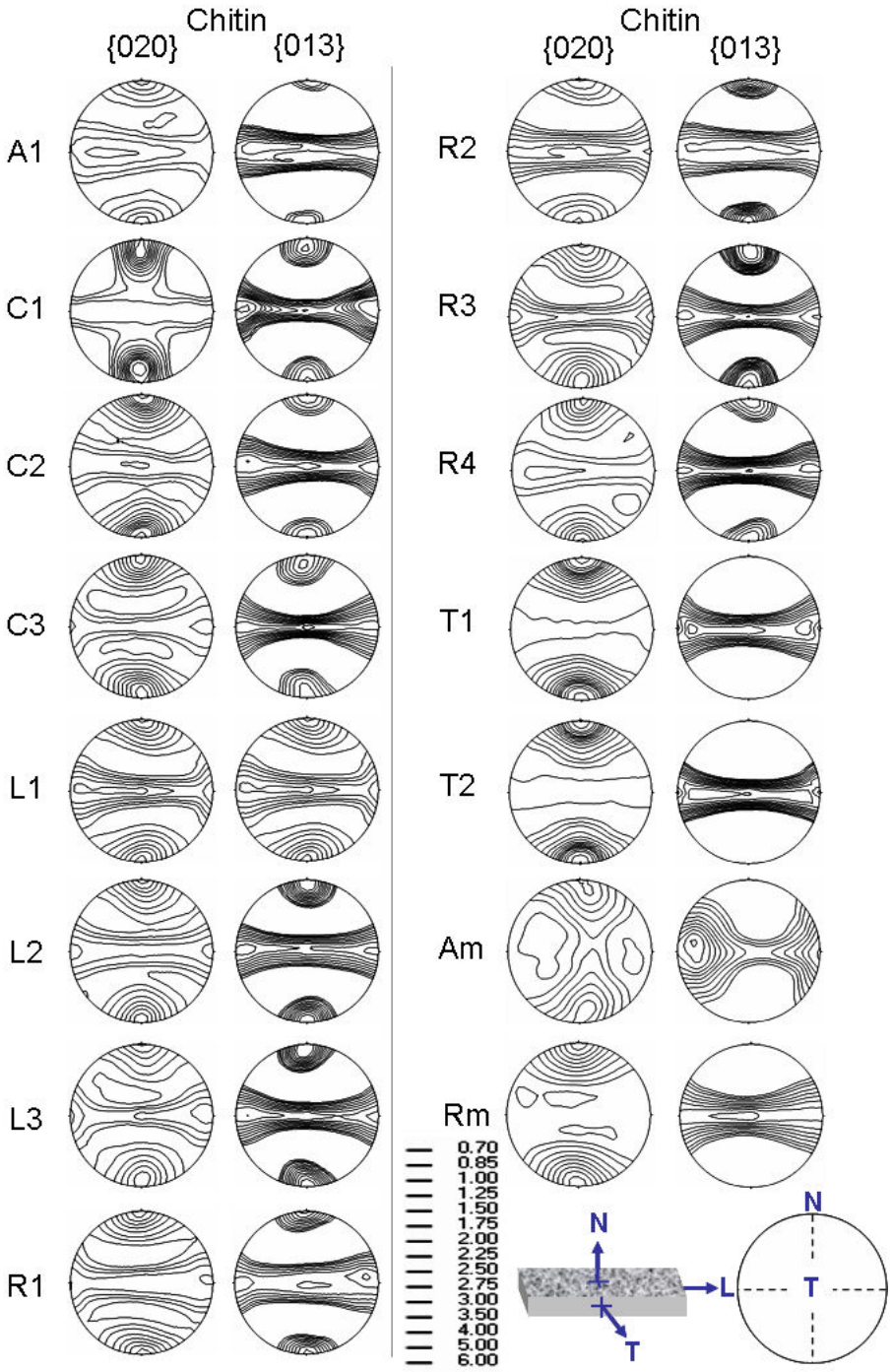

Fig. 9.14: Overview of the pole figures obtained by the synchrotron measurements for the orthorhombic α-chitin in different regions of the lobster cuticle shown in Fig. 9.13. The coordinate system and sample positions are indicated.

a very strong crystallographic <020>fiber axis preferentially aligned parallel to the surface normal axis of the lobster cuticle (<020>// ND), Fig. 9.12, in addition to a weaker <002>fiber texture component preferentially aligned parallel to the surface normal.

In particular the four samples probed from the membranous (weakly mineralized) portions of the lobster cuticle (A_m, R_m) and from the telson part of the lobster (T_1, T_2) reveal a strong <020>// ND fiber texture component, but the other texture component occur in a weak form. Fig. 9.14 shows that this texture component is not a completely homogeneous fiber in the membranous and telson samples but it reveals pronounced maximum zones as visible in the {020} and in {013} pole figures. Such fiber-type texture components with a preference of some main orientations are referred to as incomplete fibers.

The α-chitin texture of the membranous lobster sample referred to A_m even resembles more that of a single crystal than that of an incomplete fiber. The {020} pole figure of sample A_m in Fig. 9.14 shows - like the {020} pole figures of the other samples - strong {020} peaks along ND but the {013} projections clearly reveal the single crystal character of this texture. This main orientation has a strong preference of the <020>crystal axis (b-axis parallel to ND, Fig. 9.12), and of the <002>crystal axis (b-axis, longitudinal axis of the polymer chain and of the fibrils parallel to LD). In Miller notation such an orientation is referred to as {010}<001>texture where the first triple indicates the crystallographic axis parallel to ND and the second one that parallel to LD. This observation suggests that a large volume fraction of the α-chitin crystals is in this membranous sample oriented in such a way that the long b-axis of the unit cell (see Fig. 9.14) points strictly towards the surface of the exoskeleton and the b-axis which corresponds to the longitudinal axis both, of the polymer chains and at the same time of the α-chitin nanofibrils (c-axis) points towards the longitudinal reference direction of the local coordinate system. The two large pole spots in the {020} pole figure of sample A_m in reveal a small deviation from the exact 90° symmetry of the orthorhombic lattice of α-chitin. This effect is due to the strong natural curvature of the sample surface at this position of the exoskeleton.

In some samples, for instance those taken from the left and the right claw (L2, L3, R1, R3), there is a slight maximum within the

<002>//ND fiber distribution with weak maxima along LD (Fig. 9.14). The other specimens (L1, R1, R3, R4, C1, C2, C3, A1) reveal a more continuous distribution of the 020 poles perpendicular to the <002>//ND fiber axis.

This slightly anisotropic distribution of the orientations along the <002>fiber axis can be attributed to the planer network of the woven chitin-protein fibers. This feature can be seen in Fig. 9.15 where some of the [002] vectors (c-axis) are exemplary indicated by arrows to show the variation in the topographic arrangement of the fibers which may explain the spread in the corresponding texture fiber. This observation matches in part the topological analysis (top-view micrographs) made for the fiber alignment mentioned in the last section.

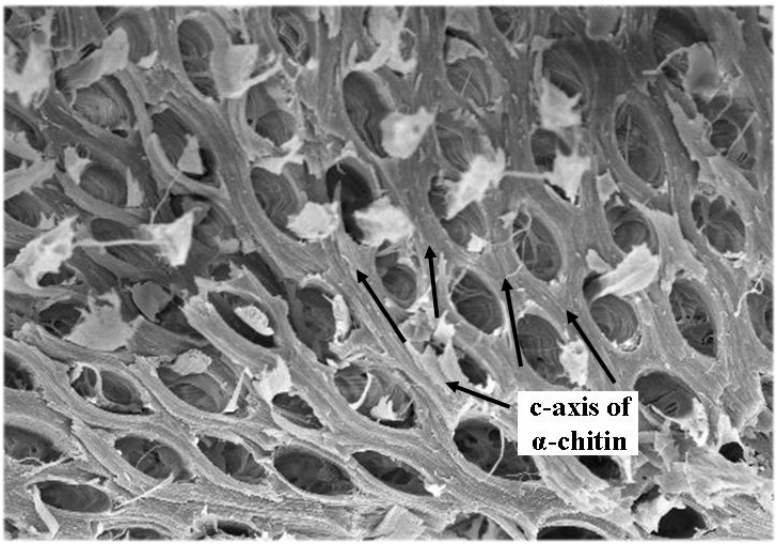

Fig. 9.15: Experimental images of one twisted plywood layer as in-plane view. The SEM micrographs were taken from the endocuticle which was fractured parallel to the surface. The crystallographic [002] vectors (c-axis) of the chitin long crystals are exemplary indicated by arrows to show the topographic arrangement of the fibers which may explain the spread in the corresponding {002} pole figures. The long b-axis ([020]-vectors) are normal to the images pointing to the surface of the cuticle.

For a first glance, the crystallographic arrangement of the α-chitin-matrix relative to the local sample coordinates can be assumed as

they turned out during biological evolution to be mechanically most favorable, providing maximum protection against external loads imposed by predators. In this case, the existence of a general mechanically motivated construction principle for the cuticle is related directly to the crystallographic mechanical anisotropy of the α-chitin lattice. Nevertheless, this speculation is not completely convincing because the directionality and magnitude of the stiffness of the composite can be accomplished by a number of different structural means such as the amount, size, and dispersion of the calcite minerals or by the density and structure of the woven chitin-protein matrix and not only by the crystallographic orientation of the lattice of the chitin-matrixand. That is even not consistent with mechanical tests data which has clearly shown that these different parameters may strongly affect the overall mechanical properties (including anisotropy) of the composite which are an integral response consisting of different structural, morphological, topographical, and crystallographic aspects (Raabe et al., 2005b). Another study of indentation (Sachs et al., 2006) have also revealed that even for samples with similar crystallographic texture, pronounced differences in the structural mechanical response can be found for different microstructures along different directions.

9.4 Orientation of α-Chitin in Horseshoe Crab

Fig. 9.16 shows an SEM micrograph of a cross section through the cuticle of the horseshoe crab. It reveals that the exocuticle is composed of a helicoidal sequence of the chitin-protein fibers planes corresponds to the plywood structure discussed in the last section. This plywood structure is commonly assumed model for arthropod cuticles. The stack of the 180° rotated chitin fibers planes around the normal axis is creating lamella which is shown by a white parallel lines. On the other hand, the endocuticle does not display simple plywood structure as in the exocuticle and as one would expect from this study and earlier literature . The endocuticle is characterized by a one-directional orientation of the chitin fibers viewed parallel to each other and to the surface as well.

Fig. 9.17 gives a survey of the complete sets of the {020} and {031}

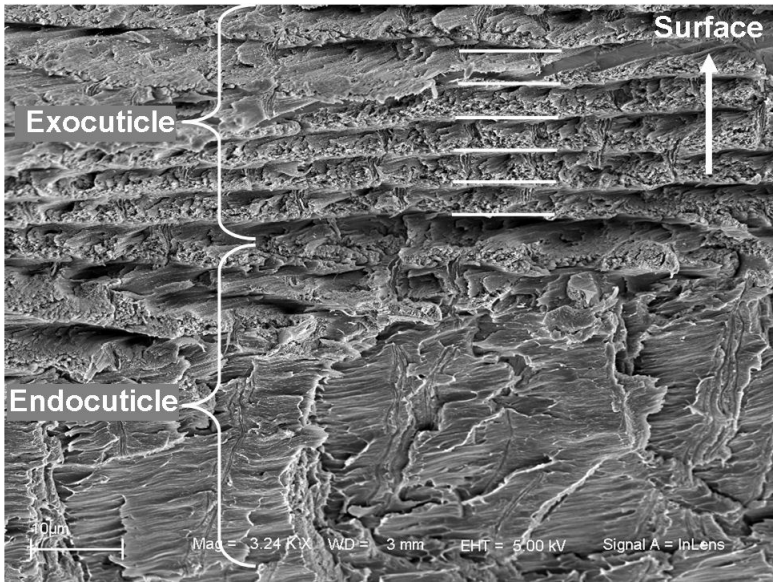

Fig. 9.16: SEM micrograph of a cross section through the cuticle of the horseshoe crab showing the exocuticle and the endocuticle. The exocuticle is composed the plywood structure of the chitin fibers. The parallel white lines is separating the lamella created by a 180° rotated chitin fibers planes around the normal axis. The endocuticle is characterized by a one-directional orientation of the chitin fibers viewed parallel to each other and to the surface as well.

synchrotron pole figures for the orthorhombic α-chitin, which were determined for different parts of the horseshoe crab exoskeleton.

The texture of the horseshoe crab samples is characterized by two strong texture components perpendicular to each other, which are summarized as two texture patterns, Fig. 9.18. The first one is characterized by a very strong crystallographic <020>fiber axis (b-axis) parallel to the surface normal axis ND, as shown in {020} pole figure, while the c-axis is co-aligned and freely rotated parallel to the surface plane as described in the horizontal continuous intensity in {013} pole figures between TD and LD in the sample coordinate system. This fiber texture corresponds to the plywood structure (the 180° rotated chitin fibers planes) of the exocuticle as shown in the SEM micrograph, Fig. 9.16, which is drawn from the fact that the crystallographic orientation of the c-axis is in the case of the α-chitin crystals strictly equivalent to the topographical orientation of the longitudinal axis of the α-chitin-fibers. is its corresponding freely rotating α-chitin fibers (c-axis) through the cuticle plane. This part of the texture analysis supports the observation of a very strong alignment of the α-chitin fibers parallel to the surface of the cuticle in a twisted plywood pattern, as noted in the beginning of this section.

The second fiber texture component is characterized by a strong crystallographic <002>fiber axis (c-axis) with a preferred alignment pointing to a direction between LD and TD in the cuticle plane varies between part to another as shown in {020} pole figure. However, the b-axis is co-aligned and freely distributed between the surface and the bottom of the cuticle, perpendicular to the c-axis, which appears as an arc in the {020} pole figure between the upper and the lower strong poles in the ND. As the direction of the c-axis is parallel the chitin fiber longitudinal axis, this fiber texture component is represented in the SEM micrograph by the parallel fibers in the endocuticle which do not feature the plywood structure. Fig. 9.19 shows the α-chitin fibers direction in the second fiber texture component with respect to the exoskeleton geometry.

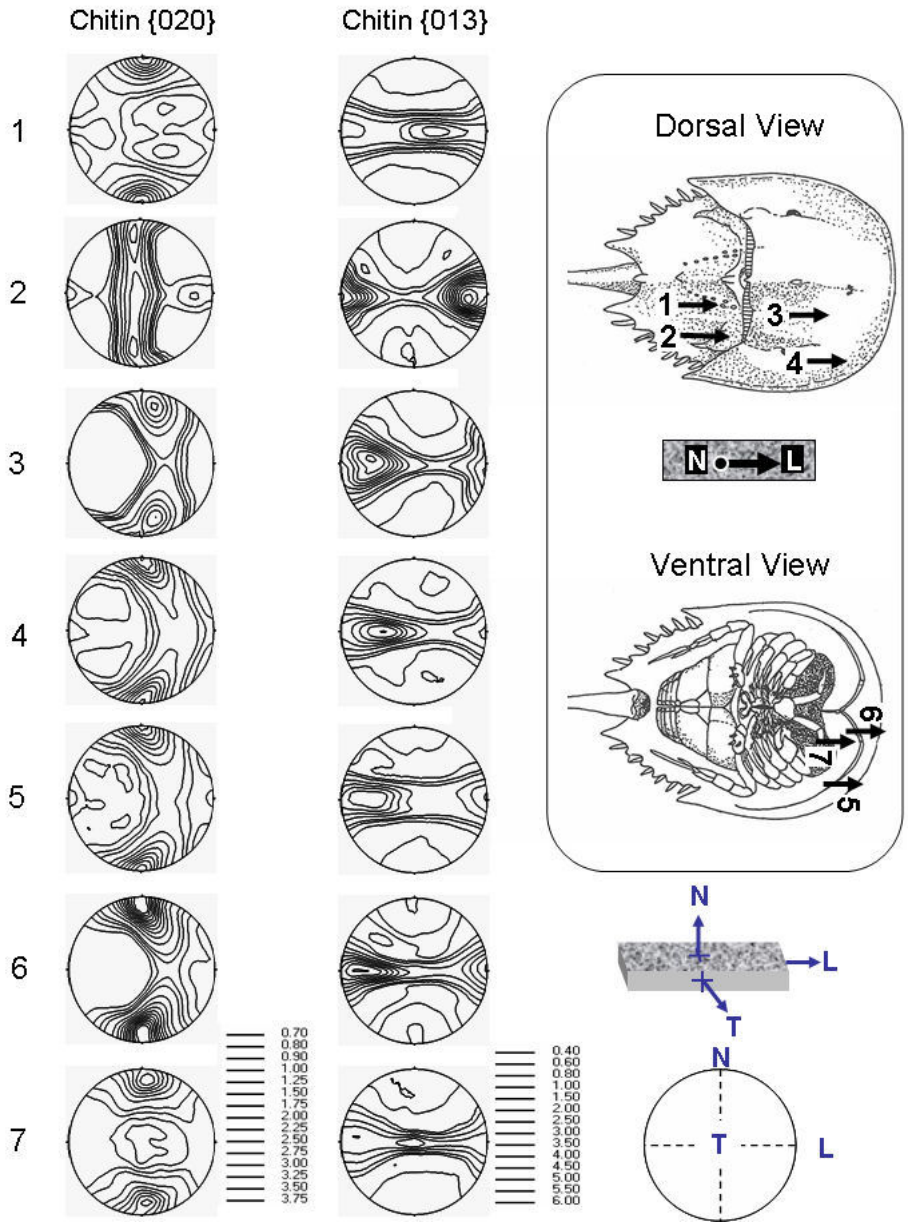

Fig. 9.17: Overview of the pole figures obtained by the synchrotron measurements for the α-chitin for different Samples that was selected from the horseshoe crab cuticle for texture measurements. LD: longitudinal reference direction; ND: reference direction normal to the local sample surface; TD: transverse direction.

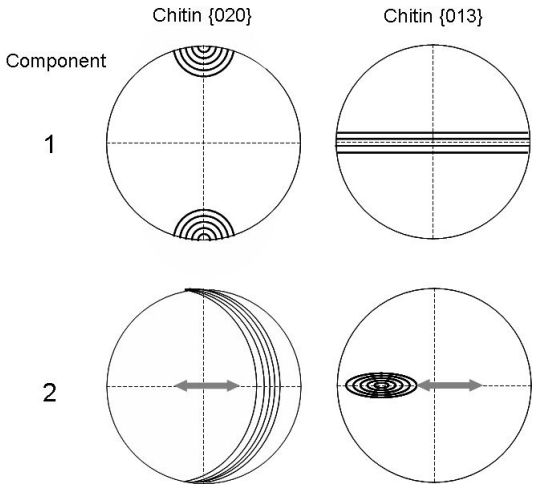

Fig. 9.18: Texture patterns of the horseshoe crab cuticle showing the two main fiber components. The direction of the second fiber component axis is different from sample to another, which is corresponding to the α-chitin fibers direction.

9.5 Orientation Relationship Between α-Chitin and Calcite

The complete sets of the pole figures of α-chitin ($\{020\}$, $\{021\}$ and $\{013\}$) and calcite ($\{00.6\}$ and $\{10.4\}$) are shown in Fig. 9.21. These planes are presented with respect to the calcite and α-chitin unit cells in lobster and crab cuticle, in Fig.s 9.22 and 9.23 respectively. The $\{020\}$ pole figure of α-chitin indicates the orientation distribution of the longest crystallographic axis of the lattice cell b=18.86 Å (Fig. 9.20), while the $\{00.6\}$ pole figure of calcite represents the orientation of the c-axis (Fig. 9.20). The local reference system used for each pole figure is included. From this, two possible orientation relationships between chitin and calcite and corresponding association with one of the two chitin texture fiber components are suggested: i) the calcite c-axis is parallel to the chitin c-axis with the calcite being associated with the out-of-plane fibers or ii) the calcite c-axis is perpendicular to the chitin c-axis with the calcite being associated with the in-plane fibers, as presented in Fig. 9.24.

In Fig. 9.24 a geometrical interpretation of one possibility for the orientation relationship between calcite and α-chitin. α-Chitin has a

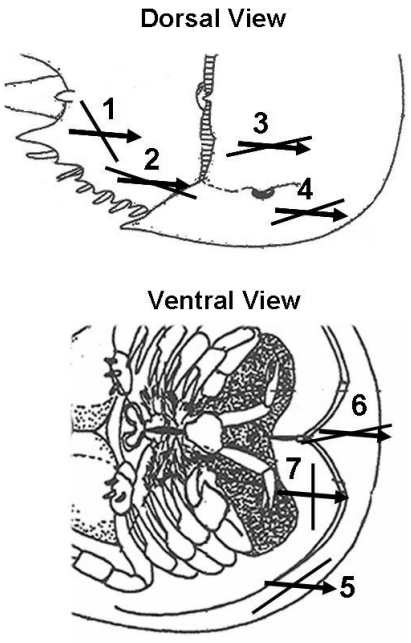

Fig. 9.19: Schematic representation of the α-chitin fibers direction in the second fiber texture component with respect to the exoskeleton geometry. This fiber texture component is represented in the SEM micrograph by the parallel fibers in the endocuticle which do not feature the plywood structure, Fig.

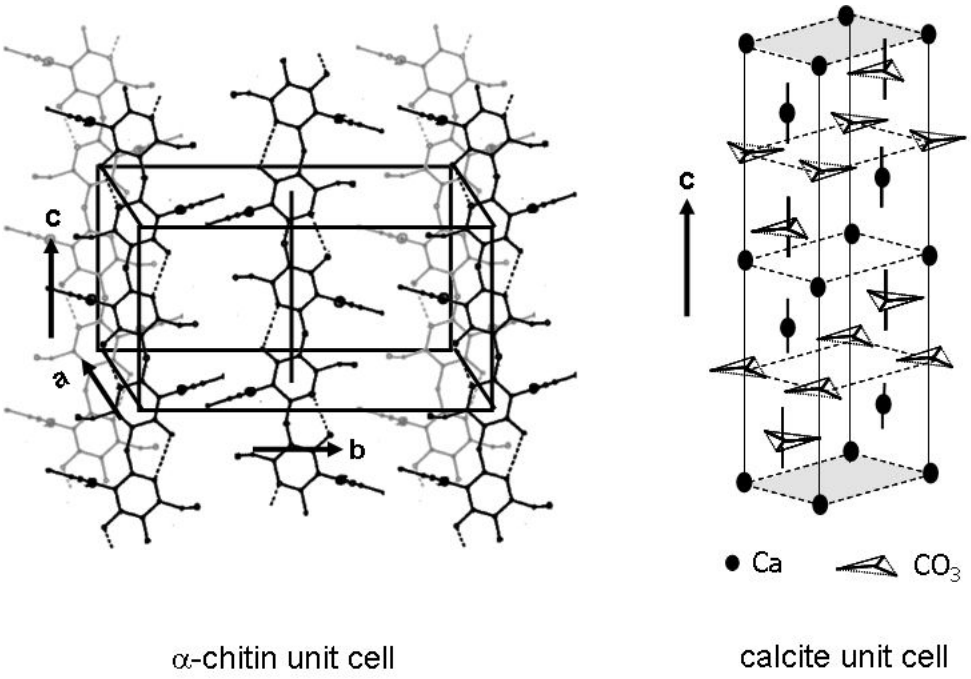

Fig. 9.20: The orthorhombic unit cell of chitin and the hexagonal unit cell of calcite.

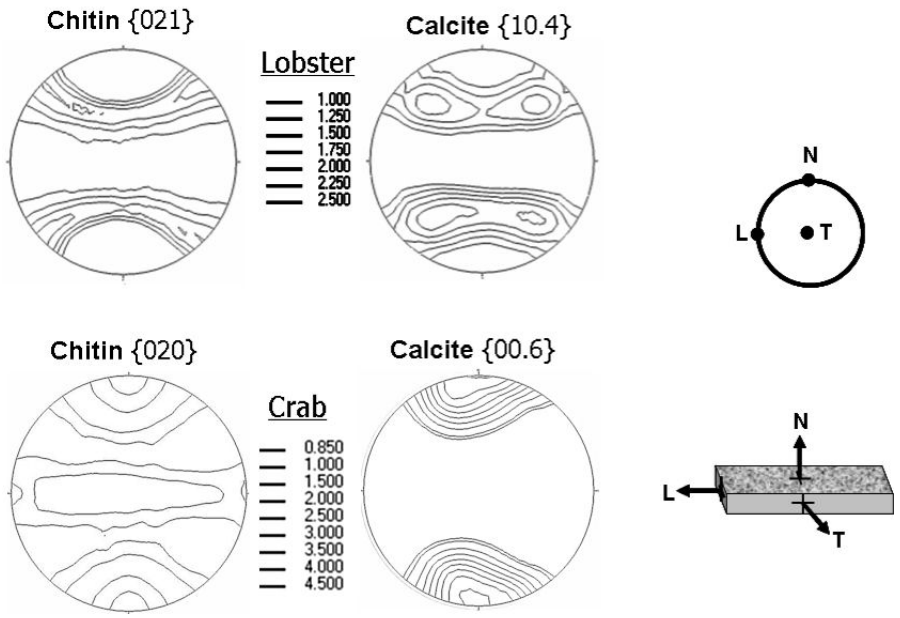

Fig. 9.21: Pole figures of reflection from α-chitin and calcite used to identify the orientation relation between the two phases with respect to the cuticle geometry. The sample reference system is included.

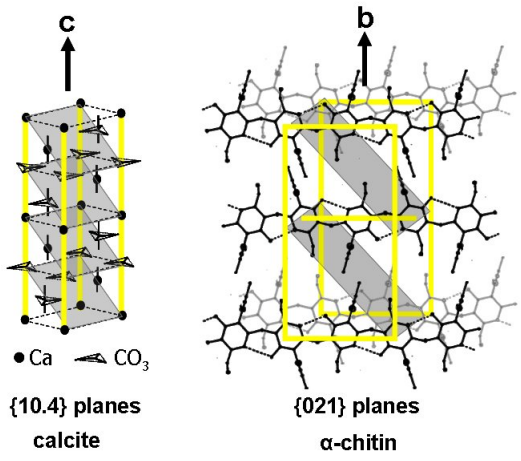

Fig. 9.22: {10.4} planes of calcite and {021} planes of chitin. Both have the same pole figure and the same geometrical inclination fulfilling that c and b axis of calcite and α-chitin respectively are parallel.

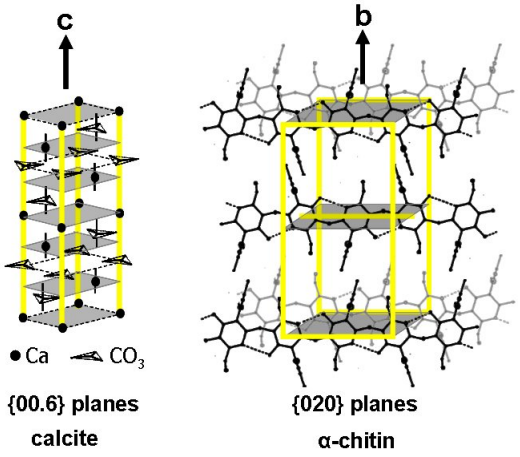

Fig. 9.23: {00.6} planes of calcite and {020} planes of chitin. Both have the same pole figure and the same geometrical inclination fulfilling that c and b axis of calcite and α-chitin respectively are parallel.

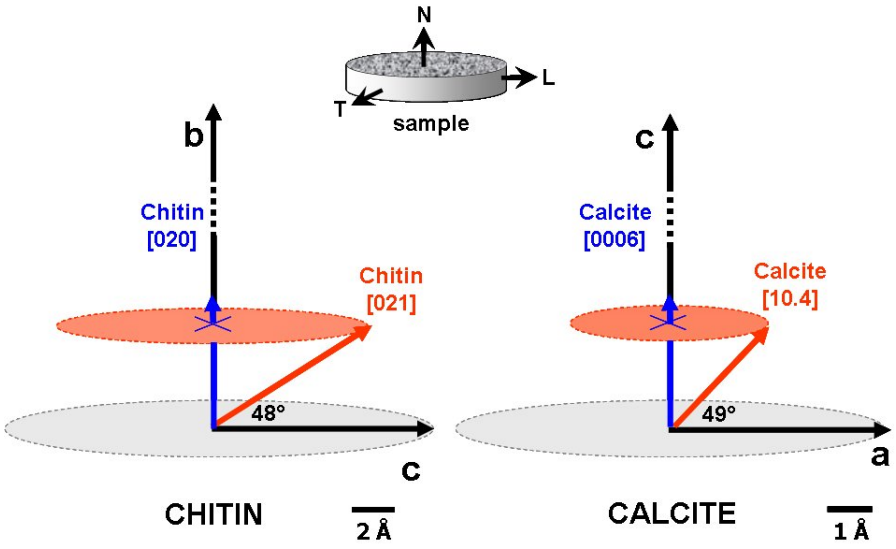

Fig. 9.24: Schematic shows the orientation of α-chitin and calcite in lobster and crab cuticl, with respect to the sample geometry.

strong <020>texture parallel to N-direction so that the result shown in the pole figures (Fig. 9.21) translates into the orientation relationship: c-axis$_{calcite}$ // b-axis$_{chitin}$ // exoskeleton surface direction N.

The alignment of calcite the c-axis in crustaceans toward the shell surface (or growth direction) is obvious because the nucleation of calcite and aragonite from the {001} plane is common in biomineralization Hunter (1996). Well studied examples are, in addition to crustacean cuticle, mollusk shells DiMasi and Sarikaya (2004); Chateigner et al. (2000) and sea urchin larval spicules Okazaki and Inoue (1976).

The orientation relationship between the organic chitin unit cell and the inorganic hexagonal calcite can explan the way by which organisms like crustaceans control the nucleation and growth of calcite during the molt cycle. Furthermore, as the crustacean cuticle reveals remarkable mechanical properties Raabe et al. (2005b), this material can be an ideal candidate for materials science studies on the relationship between its hierarchical microstructure and the resulting mechanical properties.

Chapter 10

Summary

X-ray wide angle Bragg diffraction was employed for the investigation of the crystallographic texture of the exoskeleton of the american lobster *Homarus americanus*, edible crab *Cancer pagurus* and horseshoe crab *Limulus polyphemus*.

The study reveals a pronounced hierarchical structure of the material and a strong crystallographic texture of the α-chitin-protein network in crab and lobster cuticle. Our experiments show that the organization of the lobster and crab cuticle is more complex than the commonly assumed model, especially on the level of the twisted plywood structure where it displays a complex honeycombed structure instead of simple planar fibrous layers. The orientation distribution is characterized by a very strong fiber texture with the <020>fiber axis pointing toward the surface of the cuticle and a less pronounced fiber texture with the <002>fiber axis pointing perpendicular to the surface of the cuticle. The strong <020>fiber texture correlates with the arrangement of the chitin on all hierarchical levels observed in the cuticle. The weak <002>fiber texture results probably from the presence of chitin in the structures that fill the pore canals of the honeycomb, which penetrate the cuticle perpendicularly to its surface.

This slightly anisotropic distribution of the orientations along the <002>fiber axis can be attributed to the honeycomb structure of the woven α-chitin-protein network. This detail can be seen in Figs. 9.7 and 9.8 where some of the [002] vectors are exemplary indicated by arrows to show the variation in the topographic arrangement of

the fibers which may explain the spread in the corresponding texture fiber. This observation matches in part the topological analysis made for the fiber alignment reported in earlier investigations.

The texture of the horseshoe crab is characterized by two strong texture components perpendicular to each other. The first one is characterized by a very strong crystallographic <020>fiber axis (b-axis) parallel to the surface normal axis ND, as shown in {020} pole figure. The second fiber texture component is characterized by a strong crystallographic <002>fiber axis (c-axis) with a preferred alignment pointing between LD and TD in the cuticle plane with a tilt angle from the longitudinal direction LD as shown in {020} pole figure.

A relationship between the orientations of α-chitin and calcite was also observed, namely, the b-axis of α-chitin was almost parallel to the c-axis of calcite, and both are oriented toward the cuticle surface normal. The other axes were randomly co-aligned through the cuticle plane. This unique property can be combined with the biochemical explanations about the mechanism of the oriented nucleation, as well as crystal growth and shap-sellection in crustaceans cuticle, which are poorly understood compared to mollusc shells which are among the best studied $CaCO_3$-containing biological materials in these respects.

The degree of matching of the d-spaces between calcite and α-chitin is a convenient scale to estimate the possibility that epitaxial growth takes place. When the c-axis of calcite is parallel to the b-axis of chitin, a close relationship is found between the ab-planes of calcite and α-chitin.

One conceivable strategy for calcite orientation correlation with α-chitin revealed in this study could be the involvement of α-chitin fibers in “physical” assistance of calcite orientation, functioning directly or indirectly as a template for nucleation of calcite and its epitaxial growth, in addition to the “biochemical” control of its associated macromolecules The high degree of mineral crystal alignment appears to reflect the high degree of orientation of the organic fibers, like the case in mollusks.

Bibliography

L. Addadi and S. Weiner. Interaction between acidic proteins and crystals: stereochemical requirements in biomineralization. *Proc. Natl. Acad. Sci. USA*, 82:4110, 1985.

L. Addadi and S. Weiner. Interactions between acidic macromolecules and structured crystal surfaces: stereochemistry and biomineralization. *Mol. Cryst. Liq. Cryst.*, 134:305, 1986.

L. Addadi and S. Weiner. Control and design principles in biological mineralization. *Angew. Chem. (English)*, 31(2):153, 1992.

J. Aizenberg, G. Lambert, L. Addadi, and S. Weiner. Stabilization of amorphous calcium carbonate by specialized macromolecules in biological and synthetic precipitates. *Adv. Mat.*, 8 (3):222, 1996.

N. Akhtar and MA. Haleem. Studies on the structure of beta-chitin. *Z. Natorfor. B*, 45 (1):87, 1990.

S. Albeck, S. Weiner, and L. Addadi. Polysaccharides of intracrystalline glycoproteins modulate calcite crystal growth in vitro. *Eur. J. Chem. A*, 2(3):278, 1996.

CT. Andrade, KMP. Silva, MI. Tavares, RA. Simao, C. Achete, and CA. Perez. Comparative study on structural features of alpha chitin from xiphopenaeus kroyeri and its precipitated product from phosphoric acid solution. *J. App. Poly. Sci.*, 83:151, 2002.

MF. Ashby, LJ. Gibson, U. Wegst, and R. Olive. Themechanical roperties of natural materials i: material property charts. *Proc. R. Soc. Lond. A*, 450:123, 1995.

EDT. Atkins. Conformations in polysaccharides and complex carbohydrates. proceedings of the international symposium on biomolecular structure interactions. *Suppl. J. Biosci.*, 8:375, 1985.

GE. Bacon and RK. Griffiths. Texture, stress and age in the human femur. *J Anat*, 143:97, 1985.

GE. Bacon, PJ. Bacon, and RK. Griffiths. The orientation of apatite crystals in bone. *J Appl Crystallogr*, 12:99, 1979.

GE. Bacon, PJ. Bacon, and RK. Griffiths. Orientation of apatite crystals in relation to muscle attachment in the mandible. *J Biomech*, 13:725, 1980.

T. Baumbach, J. Göttlicher, and M. Hagelstein. *ANKA Instrumentation Book*. ANKA Angstroemquelle Karlsruhe, ISS Institute for Synchrotron Radiation, Forschungszentrum Karlsruhe GmbH, 2006.

A. Becker, A. Ziegler, and M. Epple. The mineral phase in the cuticles of two species of crustacea consists of magnesium calcite, amorphous calcium carbonate, and amorphous calcium phosphate. *Dalt. Trans.*, 10:1814, 2005.

GL. Becker, CH. Chen, JW. Greenaway, and AL. Lehninge. Calcium-phosphate granules in hepatopancreas of blue-crab callinectes-sapidus. *J. Cell. Biol.*, 61(2):316, 1974.

E. Beniash, J. Aizenberg, L. Addad, and S. Weiner. Amorphous calcium carbonate transforms into calcite during sea urchin larval spicule growth. *Proc. Roy. Soc. Lond. B*, 264:461, 1997.

A. Benmarouane, T. Hansen, , P. Millet, and A. Lodini. Texture measurements of hydroxyapatite crystallites at bone-implant interfaces in sheep tibia. *Text. Anisot. Polycrys II*, 105:427, 2005.

JD. Birchall and NL. Thomas. On the architecture and function of cuttlefish bone. *J. Mater. Sci.*, 18:2081, 1983.

J. Blackwell. Structure of beta-chitin or parallel chain systems of poly-beta-(1-4)-n-acetyl-d-glucosamine. *Biopol.*, 7:281, 1969.

Y. Bouligand. Twisted fibrous arrangements in biological-materials and cholesteric mesophases. *Tiss. Cell*, 4 (2):189, 1972.

H. Braconnot. Sur la nature des champignons. *Ann. chim. Paris*, 79:265, 1811.

HJ. Bunge. *Texture analysis in materials science.* Cuvillier-Verlag, 1993.

JN. Cameron. Post-moult calcification in the blue crab, callinectes sapidus: timing and mechanism. *J. Exp. Biol.*, 143:285, 1989.

G. Cardenas, Cabrera G., E.Taboada, and SP. Mia. Chitin characterization by sem, ftir, xrd, and c-13 cross polarization/massangle spinning nmr. *J. App. Polym. Sci.*, 93 (4):1876, 2004.

D. Carlström. The crystal structure of alpha-chitin (poly-n-acetyl-d-glucosamine). *J. Biophy. Bioch.*, 3 (5):669, 1957.

D. Carlström. The polysaccharide chain of chitin. *Biochim. Biophys. Acta*, 59:361, 1962.

D. Carlström. A crystallographic study ofvertebrate otoliths. *Biol. Bull.*, 125(3):441, 1963.

EN. Caspi, B. Pokroy, PL. Lee, JP. Quintana, and E. Zolotoyabko. On the structure of aragonite. *Acta Cryst. B*, 61:129, 2005.

F. Chapman. Notes on shell-structure in the genus lingula, recent and fossil. *J. R. Micro. Soc.*, 5:28, 1914.

D. Chateigner, C. Hedegaard, and HR. Wenke. Mollusc shell microstructures and crystallographic textures. *J. Struct. Geol.*, 22 (11-12):1723, 2000.

HL. Chen and AA. Gundjian. Determination of the bone-crystallites distribution function by x ray diffraction. *Med Biol Eng*, page 531, 1974.

JR. Clarkson, TJ. Price, and CJ. Adams. Role of metastable phases in the spontaneous precipitation of calcium-carbonate. *J. Chem. Soc. Far. Trans.*, 88(2):243, 1992.

JD. Currey. Mechanical properties of mother of pearl in tension. *Proc. R. Soc. Lond. B*, 196:443, 1977.

JD. Currey, A. Nash, and W. Bonfield. Calcified cuticle in the stomatopod smashing limb. *J. Mater. Sci.*, 17:1939, 1982.

JD. Currey, P. Zioupos, P. Davies, and A. Casinos. Mechanical properties of nacre and highly mineralised bone. *Proc. R. Soc. Lond. B*, 268:107, 2001.

R. Dennell. Structure of cuticle of shore-crab carcinus-maenas. *Zool. J. Linnean Soci.*, 52 (2):159, 1973.

B. Dickens and WE. Brown. The crystal structure of calcium carbonate hexahydrate at 120c. *Inorg. Chem.*, 9:480, 1970.

E. DiMasi and M. Sarikaya. Synchrotron x-ray microbeam diffraction from abalone shell. *J. Mat. Res.*, 19(5):1471, May 2004.

P. Drach. Mue et cycle d'intermue chez les crustacees decapodes. *Ann. Inst. Oceanogr., Monaco*, 19:103, 1939.

IW. Duedal and DE. Buckley. Calcium carbonate monohydrate in seawater. *Nature*, 234 (45):39, 1971.

NE. Dweltz. Structure of beta-chitin. *Biochim. Biophys. Acta*, 51: 283, 1961.

NE. Dweltz and JR. Colvin. Structure of diatom thalassiosira fluviatilis. *Can. J. Microb.*, 14(10):1049, 1968.

H. Effenberg. Kristallstruktur und infrarot-absorptionsspektrum von synthetischem monohydrocalcit, caco3ůh2o. *Monatsh. Chem.*, 112:899, 1981.

C. Eming. Proof that lingula (brachiopoda) is not a living-fossil, and emended diagnoses of the family lingulidae. *Carnets de Géologie*, CG2003:1, 2003.

SB. Engelsen, A. Mikkelsen, AB. Andersen, HCB. Hansen, O. Larsen, and LH.Skibsted. Presence and dehydration of ikaite, calcium carbonate hexahydrate, in frozen shrimp shell. *J. Agric. Food Chem.*, 47(3):911, 1999.

H. Fabritius and A. Ziegler. Nano-architecture and structural changes in the sternal caco3 deposits of the terrestrial isopod porcellio scaber during the molt cycle. *Microscopy and Microanalysis*, 9:376, 2003.

AB. Foster and JM. Webber. Chitin. *Adv. Carboh. chem.*, 15:371, 1960.

P. Fratzl, HF. Jakob, S. Rinnerthaler, P. Roschger, and K. Klaushofer. Position-resolved small-angle x-ray scattering of complex biological materials. *J Appl Cryst*, 30:765, 1997.

RV. Gaines, HCW. Skinner, EE. Foord, B. Mason, and A.Rosensweig. *DanaŠs New Mineralogy.* Wiley, 1997.

KH. Gardner and J. Blackwell. Refinement of structure of beta-chitin. *Biopol.*, 14:1581, 1975.

RW. Gauldie. Continuous and discontinuous growth in the otolith of macuronus novaezelandiae (merlucciidae: Teleostei). :-294. *J. Morph.*, 216:271, 1993.

RW. Gauldie and DGA. Nelson. Otolith growth in fishes. *Comp. Biochem. Physiol.*, 97A:119, 1990.

MM. Giraud-Guille. Calcification initiation sites in the crab cuticle: the interprismatic septa. an ultrastructural cytochemical study. *Cell Tiss. Res.*, 236:413, 1984.

MM. Giraud-Guille. Twisted liquid crystalline supramolecular arrangements in morphogenesis. *Int. Rev. Cytol.*, 166:59, 1996.

MM. Giraud-Guille. Plywood structures in nature. *Curr. Opin. Sol. St. Mat. Sci.*, 3(3):221, 1998.

MM. Giraud-Guille, E. Belamie, and G. Mosser. Organic and mineral networks in carapaces, bones and. biomimetic materials. *CR Palevol*, 3:503, 2004.

F. Graf. Fine determination of the molt cycle stages in orchestia cavimana heller (crustacea: Amphipoda). *J. Crustac. Biol.*, 6:666, 1986.

F. Graf and JC. Meyran. Premolt calcium secretion in the midgut posterior cæca of the crustacean orchestia: ultrastructure of the epithelium. *J. Morphol.*, 177:1, 1983.

F. Graf and JC. Meyran. Calcium reabsorption in the posterior caca of the midgut in a terrestrial crustacean, orchestia cavimana. *Cell Tiss. Res.*, 242:83, 1985.

JP. Green and MR. Neff. A survey of the fine structure of the integument of the fiddler crab. *Tiss. Cell*, 4:137, 1972.

P. Greenaway. Calcium balance and moulting in the crustacea. *Biol. Rev.*, 60:425, 1985.

NF. Hadley. The arthropod cuticle. *Sci.c Am.*, 255(1):104, 1986.

MA. Haleem and KD. Parker. X-ray diffraction studies on the structure of alpha-chitin. *Z . Naturtforsch.*, 31c:383, 1976.

A. Hall and JD. Taylor. The occurrence of vaterite in gastropod egg-shells. *Min. Mag.*, 38:521, 1971.

Thompson A. Hammersley AP, Svensson SO. Calibration and correction of spatial distortions in 2d detector systems. *Nuclear Inst Meth Phys Res*, A346:312, 1994.

YH. Han, H. Li, TY. Wong, and RC. Brad. Knoop microhardness anisotropy of single-crystal aragonite. *J. Am. Ceram. Soc*, 74:3129, 1991.

B. Hasse, H. Ehrenberg, JC. Marxen, W. Becker, and M. Epple. Calcium carbonate modifications in the mineralized shell of the freshwater snail biomphalaria glabrata. *Eur. J. Chem. A*, 6:3679, 2000.

T. Hegdahl, F. Gustavsen, and J. Silness. The structure and mineralization of the carapace of the crab (cancer pagurus l.) ii. the exocuticle. *Zool. Scripta*, 6:101, 1977a.

T. Hegdahl, F. Gustavsen, and J. Silness. The structure and mineralization of the carapace of the crab (cancer pagurus l.) iii. the epicuticle. *Zool. Scripta*, 6:215, 1977b.

T. Hegdahl, J. Silness, and F. Gustavsen. The structure and mineralization of the carapace of the crab (cancer pagurus l.) i. the endocuticle. *Zool. Scripta*, 6:89, 1977c.

A. Heredia, M. Aguilar-Franco, C. Magana, C. Flores, C. Pina, R. Velazquez, TE. Schäffer, L. Bucio, and VA. Basiuk. Structure and interactions of calcite spherulites with alpha-chitin in the brown shrimp (penaeus aztecus) shell. *Mat. Sci. Engi. C*, 11:11, 2006.

W. Herth and W. Barthlott. The site of beta-chitin fibril formation in centric diatoms. *J. Ultrastruct. Res.*, 68:6, 1979.

MN. Horst and JA. Freeman. *The Crustacean Integument: Morphology and Biochemistry*. CRC Press, 1993.

H. Hull and AG. Turnbull. A thermochemical study of monohydrocalcite. *Geochim. Cosmochim. Acta*, 37:685, 1973.

GK. Hunter. Interfacial aspects of biomineralization. *Curr. Opin. Solid State Mat. Sci.*, 1(3):430, June 1996.

M. Iijima and Y. Moriwaki. Orientation of apatite and organic matrix lingula unguis shell. *Calcif. Tissue Int.*, 47:237, 1990.

AP. Jackson, JFV. Vincent, and RM. Turner. The mechanical design of nacre. *Proc. R. Soc. Lond. B*, 234:415, 1988.

AP. Jackson, JFV. Vincent, and RM. Turner. Comparison of nacre with other ceramic composites. *J. Mater. Sci.*, 25:3137, 1990.

MK. Jang, BG. Kong, YI. Jeong, CH. Lee, and JW. Nah. Physicochemical characterization of alpha-chitin, beta-chitin, and gamma-chitin separated from natural resources. *J. Polym. Sci. A*, 42 (14): 3423, 2004.

P. Jolles and RAA. Muzzarelli. *Chitin and Chitinases*. Birkhauser: Basel, Switzerland, 1999.

F. Krauss and W. Schriever. The hydrates of calciumcarbonate. *Z. Anorg. Allg. Chem.*, 188:259, 1930.

C. Krywka, M. Paulus, C. Sternemann, M. Volmer, A. Remhof, G. Nowak, A. Nefedov, B. Poter, M. Spiegel, and M. Tolan. The new diffractometer for surface x-ray diffraction at beamline bl9 of delta. *J. Synchr. Rad.*, 13:8, January 2006.

B. Lawn. *Fracture of brittle solids*, chapter 6, page 143. Cambridge University Press, 1993.

AR. Lennie, CC. Tang, and SP. Thompson. The structure and thermal expansion behaviour of ikaite, $caco_{3.6}h_2o$, from t = 114 to t = 295 k. *Min. Mag.*, 68:135, 2004.

Y. Levi-Kalisman, S. Raz, S. Weiner, L. Addadi, and I. Sagi. X-ray absorption spectroscopy studies on the structure of a biogenic amorphous calcium carbonate phase. *J. Chem. Soci. -Dalton Trans.*, 2000(21):3977, 2000.

F. Lippmann. *Sedimentary carbonate minerals*. Springer Verlag, 1973.

I. Lonardelli, HR. Wenk, L. Lutterotti, and M. Goodwin. Texture analysis from synchrotron diffraction images with the rietveld method: dinosaur tendon and salmon scale. *J. Synhr. Rad.*, 12: 354, May 2005.

W. Lotmar and LER. Picken. A new crystallographic modification of chitin and. its distribution. *Experientia*, 6:58, 1950.

HA. Lowenstam. Minerals formed by organisms. *Science*, 211:1126, 1981.

HA. Lowenstam. Spicular morphology and mineralogy in some pyuridae (ascidiacea). *Bull. Mar. Sci.*, 45(2):243, 1989.

HA. Lowenstam and DP. Abbott. Vaterite: a mineralization product of the hard tissues of a marine organism (ascidiacea). *Science*, 188(4186):363, 1975.

HA. Lowenstam and S. Weiner. *On biomineralization.* Oxford University Press, New York, 1989.

G. Luquet and F. Marin. Biomineralisations in crustaceans: storage strategies. *Comptes Rendus Palevol*, 3:515, 2004.

GO. Luquet, Testeniere, and F. Graf. Characterization and n-terminal sequencing of a calcium binding protein from the calcareous concretion organic matrix of the terrestrial crustacean orchestia cavimana. *Biochim. Biophys. Acta*, 1293:272, 1996.

S. Mann. Mineralization in biological systems. *Struct Bonding*, 54: 125, 1983.

S. Mann. On the nature of boundary-organized biomineralization (bob). *J. Inorg. Biochem.*, 28:363, 1986.

S. Mann. *Biomineralization: Principles and concepts in bioinorganic material chemistry.* Oxford universiry Press, 2001.

RH. Marchessault and A. Sarko. X-ray structure of polysaccharides. *Adv Carbohydr Chem Biochem.*, 22:421, 1967.

SA. Markgraf and RJ. Reeder. High-temperature structure refinements of calcite and magnesite. *Am. Miner.*, 70:590, 1985.

EN. Maslen, VA. Streltsov, and NR. Streltsova. X-ray study of the electron density in calcite, caco3. *Acta Cryst.*, B49:636, 1993.

M. Matsushima, M. Akiyama, and Y. Terayama. Quantitative analysis of the orientation of mineral in bone from small-angle x-ray scattering patterns. *Jpn J Appl Phys*, 21:186, 1982.

FA. Mattheus. *Applications of Chitin and Chitosan.* Technomic Publication Company, Pennsylvania, 1997.

FC. Meldrum. Calcium carbonate in biomineralization and biomimetic chemistry. *Intl. Mat. rev.*, 48:187, 2003.

JC. Meyran, F. Graf, and G. Nicaise. Pulse discharge of calcium through a demineralizing epithelium in the crustacean orchestia: ultrastructural cytochemistry and x-ray microanalysis. *Tissue Cell*, 18:267, 1986.

A. Miikkelsen, SB. Engelsen, HCB. Hansen, O. Larsen, and LH. Skisted. Calcium carbonate crystallization in the a-chitin matrix of the shell of pink shrimp, pandulus borealis, during frozen storage. *J. Crystal Growth*, 117:125, 1987.

R. Minke and J. Blackwell. The structure of alpha-chitin. *J Mol Biol*, 120:167, 1978.

RP. Montserrat. *Development of Techniques Based on Natural Polymers for the Recovery of Precious Metals.* PhD thesis, Technical University of Catalonia, 2002.

RAA. Muzzarelli, M. Mattioli-Belmonte, B. Muzzarelli, G. Mattei, M. Fini, and M. Biagini. *Advances in Chitin Science*, chapter Medical and veterinary applications of chitin and chitosan, page 580. Lyon: Jacques Andre Publishers, 1997.

M. Naczk, J. Synowiecki, and ZE. Sikorski. The gross chemical composition of antarctic krill shell waste. *Food Chem.*, 7:175, 1981.

H. Nakahara, G. Bevelander, and M. Kakei. Electron microscopy and amino acid studies on the outer and inner shells of haliotis rufescens. *Venus*, 41:34, 1982.

T. Nakano, K. Kaibaral, Y. Tabata, N. Nagata, S. Enomoto, E. Marukawa, and Y. Umakoshi1>2. *Tissue Engineering for Therapeutic Use 6* -, chapter Analysis of hydroxyapatite (HAp) texture

in regenerated hard tissues using micro-beam X-ray diffractometer technique, page 95. Elsevier, 2002.

JD. Neilson, GH. Green, and B. Chan. Variability in dimensions of salmonid otolith nuclei: implications for stock identification and microstructure interpretation. :. *Fish. Bull.*, 83:81, 1985.

AC. Neville, MG. Thomas, and B. Zelazny. Pore canal shape related to molecular architecture of arthropod cuticle. *Tissue Cell*, 1:183, 1969.

JP. Nightingale and D. Lewis. Pole figures of the orientation of apatites in bones. *Nature*, 232:334, 1971.

A. Odier. Memoire sur la composition chimique des parties cornees des insects. *soc. histoire nat. Paris*, 1:29, 1823.

K. Okazaki and S. Inoue. Crystal property of the. larval sea urchin spicule. *Dev. Growth Differ.*, 18:413, 1976.

KM. Paralikar and RH. Balasubramanya. Electron diffraction study of alpha-chitin. *J. Polym. Sci. C*, 22(10):543, 1984.

H. Pauly. "ikaite", a new mineral from greenland. *Artic*, 16:263, 1963.

M.J. Pelouze. Sur une combinaison nouvelle d'eau et de carbonate de chaux. *Chem. Rev.*, 60:429, 1865.

SM. Pervaiz and MA. Haleem. Studies on the structure of alpha-chitin. *Z. Naturforsch.*, 30 c:571, 1975.

LER. Picken. *Phil. Trans. Roy. Soc. London*, B234:1, 1949.

B. Pokroy, JP. Quintana, EN. Caspi, A. Berner, and E. Zolotoyabko. Anisotropic lattice distortions in biogenic aragonite. *Nature*, 3:900, 2004.

B. Pokroy, AN. Fitch, P. L. Lee, JP. Quintana, EN. Caspi, and E. Zolotoyabko. Anisotropic lattice distortions in the mollusk-made aragonite: A widespread phenomenon. *J. Struc. Biol.*, 153: 145, 2006a.

B. Pokroy, AN. Fitch, F. Marin, M. Kapon, N. Adir, and E. Zolotoyabko. Anisotropic lattice distortions in biogenic calcite induced by intra-crystalline organic molecules. *J. of Str. Biol.*, 155:???, 2006b.

D. Raabe, P. Romano, C. Sachs, A. Al-Sawalmih, HG. Brokmeier, SB. Yi, G. Servos, and H.G. Hartwig. Discovery of a honeycomb structure in the twisted plywood patterns of fibrous biological nanocomposite tissue. *J. Cryst. Growth*, 283:1, 2005a.

D. Raabe, C. Sachs, and P. Romano. The crustacean exoskeleton as an example of a structurally and mechanically graded biological nanocomposite material. *Acta Materialia*, 53:4281, 2005b.

D. Raabe, P. Romano, C. Sachs, H. Fabritius, A. Al-Sawalmih, SB.. Yi, G. Servos, and H.G. Hartwig. Microstructure and crystallographic texture of the chitinŰprotein network in the biological composite material of the exoskeleton of the lobster homarus americanus. *Mat. Sci. Eng. A*, 421:143, 2006.

G. N. Ramachandran and C. Ramakrishnan. The structure of chitin. *Biochim. Biophys. Acta*, 63:307, 1962.

V. Randle and O. Engler. *Introduction to Texture Analysis: Macrotexture, Microtexture and Orientation Mapping.* Gordon and Breach Science Publishers, 2000.

S. Raz, O. Testeniere, A. Hecker, S. Weiner, and G. Luquet. Stable amorphous calcium carbonate is the main component of the calcium storage structures of the crustacean orchestia cavimana. *Biol. Bull.*, 203:269, 2002.

RJ. Reeder. *Carbonates: Mineralogy and Chemistry*, chapter 11, page 1. Mineralogical Society of America, 1983.

AG. Richards. *The Integument of Arthropods.* University of Minnesota Press, New York, 1951.

R. Roer. Mechanisms of resorption and deposition of calcium in the carapace of the crab carcinus maenas. *J. Exp. Biol.*, 88:205, 1980.

R. Roer and R. Dillaman. The structure and calcification of the crustacean cuticle. *Am. Zool.*, 24:893, 1984.

KM. Rudall. The distribution of collagen and chitin. *Symp. Soc. Exp. Biol.*, 9:49, 1955.

KM. Rudall and W. Kenchington. The chitin system. *Biol Rev*, 49: 597, 1973.

C. Sachs, H. Fabritius, and D. Raabe. Hardness and elastic properties of dehydrated cuticle from the lobster homarus americanus obtained by nanoindentation. *J. Mat. Res.*, 21(8):1987, August 2006.

Y. Saito, T. Okano, JL. Putaux, F. Gaill, and H. Chanzy. *Advances in Chitin Science 7th ICCC*, chapter II, page 507. Jacques Andre Publisher-France, 1998.

Y. Saito, T. Okano, F. Gail, H. Chanzy, and JL. Putaux. Structural data on the intra-crystalline swelling of beta-chitin. *Int'l J. Biol. Macromol.*, 28:81, 2000.

N. Sasaki and Y. Sudoh. X-ray pole figure analysis of apatite crystals and collagen molecules in bone. *Calcif Tissue Int*, 60:361, 1997.

N. Sasaki, N. Matsushima, T. Ikawa, H. Yamamura, and A. Fukuda. Orientation of bone mineral and its role in the anisotropic mechanical properties of bone-transverse anisotropy. *J Biomech*, 22:157, 1989.

N. Sasaki, T. Ikawa, and A. Fukuda. Orientation of mineral in bovine bone and the anisotropic mechanical properties of plexiform bone. *J Biomechanics*, 24(1):57, 1991.

K. Sawada. *Crystallization Processes*, chapter 3, pages 39–68. John Wiley and Sons, 1999.

R. Seizen. Cuttlebone: The buoyant skeleton. *Sea Front.*, 32:115, 1986.

F. Shahidi and J. Synowiecki. Isolation and characterization of nutrients and value-added products from snow crab (cinoecetes opilio) and shrimp (pandalus borealis) processing discards. *J. Agric. Food Chem.*, 39:1527, 1991.

TL. Simpson and BE. Volcani. *Biological Systems*, chapter Silicon and Silicous Structures. Springer Verlag, 1981.

BL. Smith, TE. Schaefer, M. Viani, JB. Thompson, NA. Frederick, J. Kindt, A. Belcher, GD. Stucky, DE. Morse, and PK. Hansma. Molecular mechanistic origin of the toughness of natural adhesives, fibers and composites. *Nature*, 399:761, 1999.

JR. Smyth. The crystal structure of calcite iii. *Geoph. Res. Lett.*, 24(13):1595, 1997.

JA. Speer. *Carbonates: Mineralogy and Chemistry*, chapter 11, page 145. Mineralogical Society of America, 1983.

J. Synowiecki and NA. Al-Khateeb. Production, properties, and some new applications of chitin and its derivatives. *Crit Rev Food Sci Nutr.*, 43(2):145, 2003.

M. Takai, Y. Shimizu, J. Hayashi, S. Tokura, M., M. Ogawa, T. Kohriyama, M. Satake, and T. Fujita. Structure-property relationship of alpha- and beta-chitin. *ACS Symposium Series*, 489: 38, 1992.

GF. Taylor. The occurrence of monohydrocalcite in two small lakes in the south-east of south australia. *Am. Mineral.*, 60:690, 1975.

MG. Taylor, K. Simkiss, GN. Greaves, M. Okazaki, and S. Mann. An x-ray-absorption spectroscopy study of the structure and transformation of amorphous calcium-carbonate from plant cystoliths. *Proc. R. Soc. London, Ser. B*, 252 (1333):75, 1993.

O. Testeniere, A. Hecker, S. Le Gurun, B. Quennedey, F. Graf, and G. Luquet. Characterization and spatiotemporal expression of orchestin, a gene encoding an ecdysone-inducible protein from a crustacean organic matrix. *Biochem. J.*, 361:327, 2002.

MM. Tlili, M. Ben-Amor, and C. Gabrielli. Characterization of caco3 hydrates by micro-raman spectroscopy. *J. Raman Spect.*, 33 (1):10, 2002.

DF. Travis. The molting cycle of the spiny lobster, panulirus argus latreille. ii. pre-ecdysial histological and histochemical changes in the hepatopancreas and integumental tissues. 108:88-112. *Biol. Bull.*, 108:88, 1955a.

DF. Travis. The molting cycle of the spiny lobster, panulirus argus latreille. iii. physiological changes which occur in the blood and urine during the normal molting cycle. *Biol. Bull.*, 109:484, 1955b.

DF. Travis. The molting cycle of the spiny lobster, panulirus argus latreille. iv. post-ecdysial histological and histochemical changes in the hepatopancreas and integumental tissues. *Biol. Bull.*, 113: 451, 1957.

DF. Travis. Structural features of mineralization from tissue to macromolecular levels of organization in the decapod crustacea. *Ann. N.Y. Acad. Sci.*, 109:177, 1963.

DF. Travis. The deposition of skeletal structures in the crustacea. v. the histomorphological and histochemical changes associated with the development and calcification of the branchial exoskeleton in the crayfish, orconectes virilis hagen. *Acta Histochem.*, 20:193, 1965.

FJ. Vernberg and WB. Vernberg. *The biology of crustacea.* Academic Press, New York, 1983.

JVC. Vincent. Arthropod cuticle: a natural composite shell system. *Composites A*, 33(10):1311, 2002.

AG. Walton and J. Blackwell. *Biopolymers.* Academic Press, England, 1973.

RZ. Wang, HB. Wen, FZ. Cui, HB. Zhang, and HD. Li. Observations of damage morphologies in nacre during deformation and fracture. *J. Mater. Sci.*, 30:2299, 1995.

R. Weil and A. Siat. Occurrence of calcium-carbonate monohydrate in an old gallery mine near sainte-marie-aux-mines(haut-rhin). *Comptes Rendus Hebdomadaires Des Seances De L Academie Des Sciences Serie D*, 280:689, 1975.

S. Weiner and L. Addadi. Design strategies in mineralized biological materials. *J. Mater. Chem.*, 7:689, 1997.

S. Weiner and PM. Dove. *In Biomineralization. Reviews in Mineralogy and Geochemistry.*, chapter 1: An overview of biomineralization processes and the problem of the vital effect, page 1. 54, 2003.

S. Weiner and L. Hood. Soluble protein of the organic matrix of mollusk shells: a potential template for shell formation. *Science*, 190(4218):987, 1975.

S. Weiner and W. Traub. X-ray diffraction study of the insoluble organic matrix of mullusk shel. *FEBS Lett.*, 111:311, 1980.

S. Weiner and W. Traub. Macromolecules in mollusk shells and their function in biomineralization. *Philos. Trans. R. Soc. Lond. Biol. Sci.*, 304:425, 1984.

S. Weiner, Y. Talmon, and W. Traub. Electron diffraction of mollusc shell organic matrices and their relationship to the mineral phase. *Int. J. Biol. Macromol.*, 5:325, 1983a.

S. Weiner, W. Taub, and HA. Lowenstam. *Biomineralization and Biological Metal Accumulation*, page 205. Reidel, Dordrecht, 1983b.

BS. Welinder. Crustacean cuticle i: studies on composition of cuticle. *Comp. Bioch. Physio.*, 47 (2-A):779, 1974.

HR. Wenk. Eine photographische roentgengefügeanalyse. *Schweiz. mineral. petrog. Mitt.*, 45:518, 1965.

HR. Wenk and F. Heidelbach. Crystal alignment of carbonated apatite in bone and calcified tendon: Results from quantitative texture analysis. *Bone*, 24:361, 1999.

HR. Wenk and P. Van-Houtte. Texture and anisotropy. *Rep. Prog. Phys.*, 67:1367, 2004.

WC. Williamson. On some histological fea turesin the shells of the crustacea. *Quart. J. Micr. Sci.*, 8:35, 1860.

SB. Yi. *Investigation on the deformation behavior and the texture evolution in magnesium wrought alloy AZ31*. PhD thesis, TU Clausthal, 2005.

CM. Zaremba, AM. Belcher, M. Fritz, S. Mann Y. Li, PK. Hansma, DE. Morse, JS. Speck, and GD. Stucky. Critical transitions in the biofabrication of abalone shells and flat pearls. *Chem. Mater.*, 8(3):679, 1996.

M. Zhang, A. Haga, H. Sekiguchi, and S. Hirano. Structure of insect chitin isolated from beetle larva cuticle and silkworm (bombyx mori) pupa exuvia. *Intl J Bio Macrom*, 27:99, 2000.

A. Ziegler. Ultrastructure and electron spectroscopic diffraction analysis of the sternal calcium deposits of porcellio scaber latr. (isopoda, crustacea). *J. Struc. Biol.*, 112 (2):110, 1994.

Ali Al-Sawalmih

Personal Information:

Date of Birth: 1975.11.22 Marital status: Married (no children) Nationality: Jordanian

Education:

01.2004- 11-2007 Max-Planck-Institute f. Iron Research Düsseldorf
PhD materials science- RWTH Aachen
Texture of α-chitin biological nanocomposites using synchrotron x-ray diffraction, Prof. Dr. D. Raabe.

01.2002- 12.2003 Max-Planck-Institute f. Solid State Res. Stuttgart
MSc (March 2004)- Solid State physics - University of Stuttgart
X-Ray investigations of multi- and single-layer systems (Prof. Dr. Bernard Keimer)

07.1993- 07.1997 University of Mosul Mosul, Iraq
BSc- Physics – Solid State Physics.

Experience:

01.2007 till now Max-Planck-Institute f. Colloids and Intrfaces Potsdam
Postdoc – Department of Biomaterials. Scanning microbeam WAXS & SAXS texture and microstructure analysis of biological materials . SAXS tomography.

1999- 2001 Teachers Colleges – Dept of Physics Saudi Arabia
Teaching Assistant.

1997- 1999 Al-Ansary School Aqaba-Jordan
Teacher of Physics- Ministry of Education-Jordan

Conferences:

- Talk+Poster: 1st School and Workshop on X-Ray Micro and Nanoprobes (July 2007), Erice-Italy.
- Talk: Minerva School on Biological and Bioinspired Materials (May 2007) Berlin.
- Talk+Poster: International Syposium on Scanning Microbeam, BESSY-Berlin, 6th December 2006. Small- and Wide- Angle Scattering of Hierarchically Structured Materials Using Microbeam.
- Talk: EUROMAT2005, Prague.
- Poster (Dierk Raabe): MRS Spring Meeting 2005, USA.

Publications and Proceedings:

- Discovery of a honeycomb structure in the twisted plywood patterns of fibrous biological nanocomposite tissue. D. Raabe, P. Romano, C. Sach, **A. Al-Sawalmih**, HG. Brokmeier, SB. Yi, G. Servos and HG. Hartwig. JOURNAL OF CRYSTAL GROWTH 283 (1-2): 1-7 SEP 15 (2005).

- Structure and crystallographic texture of arthropod bio-composites, D. Raabe, **A. Al-Sawalmih**, P. Romano, C. Sach, HG. Brokmeier, SB. Yi, G. Servos and HG. Hartwig. ICOTOM 14: MATERIALS SCIENCE FORUM 495-497: 1665-1674, Part 1&2 (2005).
- Microstructure and crystallographic texture of the chitin-protein network in the biological composite material of the exoskeleton of the lobster Homarus americanus. D. Raabe, P. Romano, C. Sach, H. Fabritius, **A. Al-Sawalmih**, SB. Yi, G. Servos and HG. Hartwig. MATERIALS SCIENCE AND ENGINEERING A 421 (1-2): 143-153 Sp. Iss. SI APR 15 (2006).
- Mesostructure of the exoskeleton of the lobster Homarus americanus. D. Raabe, P. Romano, **A. Al-Sawalmih**, C. Sachs, G. Servos, HG. Hartwig. MATERIALS RESEARCH SOCIETY SYMPOSIUM PROCEEDINGS. Vol. 874, 155-160 (2005).
- The small-angle and wide-angle x-ray scattering setup at beamline BL9 of DELTA. C. Krywka, C. Sternemann, M. Paulus, N. Javid, R. Winter, **A. Al-Sawalmih**, SB. Yi, D. Raabe and M. Tolan. JOURNAL OF SYNCHROTRON RADIATION 14, 244–251 (2007).
- Preferred crystallographic textures of a-chitin and calcite as a joint microscopic composite design and macroscopic biological construction principle of the exoskeleton of the lobster Homarus americanus. D. Raabe, **A. Al-Sawalmih**, S-B. Yi, and H. Fabritius. ACTA MATERIALIA, Accepted.
- Investigation of the orientation relationship between alpha-chitin and calcite in crustacean cuticle using synchrotron x-ray diffraction. **A. Al-Sawalmih**, H. Fabritius, S.B. Yi and D. Raabe. To be submitted to "Advanced Materials"

Learning:

- **Marie-Curie Summer School 2006**
  Polyphase and Composites Materials
  Alvdalen-Sweden, August 13-23, 2006
- **Basic Course on Crystallographic Textures (TEXMAT2006)**
  Texture Analysis in Materials Science
  Clausthal University of Technology
  Calusthal-Zellerfeld,-Germany, April 10-12, 2006.
- **4th European Winter School (NESY2005)**
  Research with Neutron and Synchrotron Radiation
  Austrian Academy of Science
  Sportheim Planneralm- Austrea, March 7-12 2005.
- **4th Summer School on Condensed Matter Research**
  Magnetism.
  Paul Scherrer Institute PSI - Switzerland.
  Zuoz- Switzerland, August 14-21, 2002.

Invited talks:

- **ANKA Users' Meeting 2006**
  Forschungszentrum Karlsruhe, ANKA Synchrotron Facility, 09-10.10.2006
- **Seminar at Dept of Exp. Physics- Dortmund University**, Prof. Dr. Metin Tolan, 02.05.2006
- **DELTA Users' Meeting 2005**
  DELTA Synchrotron Facility-Dortmund
  30.11.2005